Topological Bubble Nucleation

Saquib Hassan

Linacre College

University of Oxford

A thesis submitted for the degree of

Doctor of Philosophy in Theoretical Physics

Trinity Term 2024

Abstract

Sidney Coleman's study of false vacuum decay, in which a metastable state tunnels to a state of lower energy, remains one of the most fascinating aspects of semi-classical methods in non-perturbative quantum field theory. The Schwinger effect is the decay of a background electric field into charged particle-antiparticle pairs, their energy coming from screening the electric field. After reviewing essential background material, this thesis applies the techniques of false vacuum decay to axion electrodynamics, a theory of a photon and a hypothetical neutral pseudo-scalar particle, the axion, interacting through a topological term in the action. Remarkably, a mechanism similar to the celebrated Schwinger effect emerges, in which a background electromagnetic field can decay through the nucleation of bubbles, except for the perplexing point that in axion electrodynamics there are no charged particles in the spectrum. This mechanism naturally leads to a parallel process in brane nucleation, and equipped with the lessons of false vacuum decay in axion electrodynamics, we immediately obtain decay rates for branes in background electric fields. We then propose relations between quantities such as brane tension and interaction strength to cosmological quantities such as the Hubble parameter, generalizing the recent Festina Lente conjecture for massive charged particles.

Contents

For my family, especially my late grandfather.

Acknowledgements

I am forever grateful to John March-Russell for being a phenomenal supervisor. His vast, encyclopedic knowledge encompassing diverse branches of physics has been a lighthouse of guidance throughout my research, and his kindness and compassion are calming in even the most strenuous circumstances. I am fortunate to have met Georges Obied and together we have collaborated on multiple ideas. Moreover, I am thankful to have had a second supervisor, Prateek Agrawal, as well as a college advisor, Subir Sarkar, who have mentored me during my time here at Oxford. Jim Alexander and Yuval Grossman were wonderful advisors during my undergraduate course at Cornell University, and I have benefited immensely from them, especially during difficult times.

Aside from academic pursuits, it has been a privilege for me to serve as Junior Dean at Oxford, first at Mansfield College, and subsequently at Linacre College. I am honored that Gail Leckie and Jane Hoverd entrusted me with such responsibilities.

Most of all, I thank my parents for the many years of love, time, and effort that they have invested in me.

Finally, I would not be here were it not the the extremely generous financial support of the Prime Minister Fellowship, Prime Minister's Office, Dhaka, Bangladesh, as well as a grant from G-Research, London, in addition to support from the Particle Theory Group, Theoretical Physics, University of Oxford, United Kingdom.

Statement of Originality

This thesis is based on research and contains no material that has already been accepted, or is concurrently being submitted, for any degree or diploma or certificate or other qualification in this university or elsewhere. To the best of my knowledge and belief this thesis contains no material previously published or written by another person, except where due reference is made in the text.

Saquib Hassan

2024

Chapter 1

Introduction

1.1 Motivation and Overview

The *axion* remains one of the most well motivated and searched for proposed particles in high energy physics. Its existence would resolve a great many mysteries in theoretical physics. For instance, phenomenological models of the axion can solve the strong CP problem of the standard model [1, 2, 3] and axions may constitute portions of dark matter [4, 5].

Axion-Maxwell theory, or axion electrodynamics, is the theory of an Abelian gauge field, or photon, interacting with a neutral (pseudo)scalar field, or axion, via an anomaly term. Such an interaction is an extremely peculiar one: it is called a *Chern-Simons* interaction. It is formally independent of the metric tensor, making it topological in a sense, and it is unusual in that it drastically modifies Maxwell's equation leading to a richer theory of electrodynamics. The phenomenological implications are profound: for instance, magnetic monopoles acquire electric charge, becoming dyons, in the presence of a constant background axion field [6, 7]. Moreover, due to this topological operator, electric charges and currents are assigned

to regions of space in which the axion field varies.

Parallel to the above is the study of non-perturbative effects in quantum field theory. The vast majority of calculations in quantum field theory are done at the perturbative level, where one typically has an exact solution, with corrections involving a small parameter, and correlation functions are computed as a series in that small parameter. However, non-perturbative processes exist in quantum field theory, which cannot be expressed as an analytic expansion in that small parameter. One such process is *false vauum decay* in quantum field theory [8, 9, 10, 11]. In essence, a field could be at a local minimum of a potential profile, known as a false vacuum. Such a configuration is typically unstable, and can decay into a lower energy energy state, through quantum tunneling of the field past the potential barrier. This phenomenon is the subject of a myriad of research, some of which are [12, 13, 14, 15, 16, 17, 18].

One particular application of great interest to us is *Schwinger pair production* [19, 20]. Here, one sees that a background electric field is unstable and can decay through the nucleation of pairs of charged particles, say electrons and positrons. As we will review, the pair nucleation rate per volume is

$$\Gamma/V \sim \exp\left(-\frac{\pi m^2}{eE}\right), \tag{1.1}$$

where E is the background electric field, which decays into pairs of particles of mass m and charges $\pm e$. This process is manifestly non-perturbative. Indeed, if one were to approximate the decay rate as a function, $\Gamma/V = f(e)$, of the small parameter e, then presumably one could write $f(e) \approx f(0) + ef'(0) + e^2 f''(0)/2 + \cdots$ but every single derivative of eq. (1.1) with respect to e, as well as $f(e)$ itself, vanishes at $e = 0$. Therefore, we will not be able to see this result at any finite order of the

expansion parameter in perturbation theory.

One of the main results of this thesis is to show that non-perturbative false vacuum decay occurs in axion electrodynamics, in the presence of background electromagnetic fields. More specifically, we will argue that metastable states of axion electrodynamics can decay to more stable ones through nucleating *bubbles*. Furthermore, we will illustrate that this process is highly reminiscent of Schwinger pair production.

What is remarkable is that whereas in the Schwinger effect the background electric field could decay only due to the existence of light charged particles, in axion electrodynamics we do not consider any charged particles at all, only the photon and the axion. We will argue that this is only made feasible by a Chern-Simons term. In essence, our work lies at the intersection of Chern-Simons theories, and the theory of false vacuum decay.

The results we have found are sufficiently intriguing that they naturally lend themselves to applications in other areas of theoretical physics, such as black holes, swampland conjectures, and constraints in string theory and D-branes. The swampland program consists of the effort to elucidate the boundary between effective field theories that appear to be viable theories of low energy physics but which *cannot* be UV completed to a theory of quantum gravity (the swampland), versus theories that are good descriptors of low energy phenomenology and *can* be completed to a theory of quantum gravity (the landscape). As such, a further motivation is the application of false vacuum decay in axion electrodynamics towards understanding restrictions on the sprectrum of strings and branes in quantum gravity. In exploring this exiting avenue, we will find that there are indeed restrictions on branes and

strings in de Sitter. More specifically, we will find connections between quantities that are string-y and brane-y, such as brane tension and Wess-Zumino coupling coefficient, and the Hubble parameter which is cosmological. We will then proceed to extend these findings to higher dimensional spacetimes, and higher dimensional branes.

1.2 Outline

This thesis is structured as follows. Chapter 2 provides a brief overview of two key subjects that are important for the main content of this thesis. First, we look at instantons and bounces, with a focus towards their applications in false vacuum decay. Moreover, we present Schwinger pair production in the language of bubble nucleation in false vacuum decay. Doing so allows for a natural progression towards applying these techniques in axion electrodynamics. Second, we also review the swampland conjecture, choosing to focus on those select few that are most relevant to this thesis. Importantly, we review the vital pieces of the recent Festina Lente conjecture. We subsequently review the basics of string theory and branes, before moving on to Chern-Simons theories. In Chapter 3 we present an expanded version of the material in [21] discussing our recent findings of a false vacuum decay process in axion electrodynamics. In Chapter 4 we study the nucleation of branes in electric field backgrounds, and extend the results of the Festina Lente conjecture to branes. We find an intriguing connection between branes with Wess-Zumino couplings and domain walls in axion electrodynamics. This work is largely based on an upcoming paper with John March-Russell and Georges Obied. Finally, we conclude with Chapter 5, including a discussion of possible exciting directions moving forward.

Chapter 2

Essential Ingredients

In this chapter, we briefly review the key ingredients necessary for the subsequent chapters. The first section provides key material regarding instantons, which are certain interesting solutions of the equations of motions in Euclidean time. In particular, our focus will be on deriving an expression for the decay rate of a metastable minimum (or false vacuum) of a potential in quantum field theory, which is analogous to barrier penetration in quantum mechanics. We start by introducing solitons, which are static solutions of field equations, and then proceed to quantum tunneling. We then put these ingredients together with the aim of introducing false vacuum decay, with a special focus on the thin wall limit. This coverage is largely based upon the seminal papers [8, 9, 10], as well as *Aspects of Symmetry* by Sidney Coleman [11], and textbook resources [22, 23, 24].

Having built up the machinery of instantons, we will then review the Schwinger effect [19, 20] that we outlined in the previous chapter, but using the worldline instanton solution [25, 26], which immediately has the interpretation of a false vacuum decay problem. Such an interpretation lends itself to a natural extension in axion-Maxwell theory, which is the subject of Chapter 3. Moreover, the worldline approach to false

vacuum decay offers a generalization to brane nucleation using worldvolume actions, which we explore in Chapter 4. The Schwinger effect is the subject of extensive research, for instance [27, 28, 29, 30, 31, 32].

Once we have reviewed instantons and the Schwinger effect, we will then move on to reviewing (some of) the *Swampland Conjectures*. The Swampland program consists of a series of conjectures relating low energy effective field theories to quantum gravity. More specifically, low energy effective field theories that may seem to be consistent possible descriptions of nature may not actually be consistent with quantum gravity under UV completion. Theories that are seemingly reasonable descriptions of nature at low energy scales but are impossible to reconcile with quantum gravity are said to be in the *swampland*. Theories that can be rendered consistent with essential requirements of quantum gravity are said to be in the *landscape*. The *swampland program* describes a set of conjectures that elucidate the boundary between the swampland and the landscape. Recent reviews include the comprehensive resources [33, 34, 35, 36, 37, 38]. Sharpening these conjectures - and obtaining phenomenological implications - is the subject of recent exciting work such as [39, 40, 41, 42, 43].

Here too, we can only cover a few key topics. Our main focus will be on conjectures pertaining to conducting thought experiments in particle physics, especially Hawking radiation and the Schwinger effect, around black holes. The most important topic for us is the recent and exciting "Festina Lente" conjecture [44, 45] which is believed to apply to de Sitter universes. What is astonishing is that this conjecture connects a charged particle's mass and charge with Hubble size, something cosmological. We will generalize this conjecture in Chapter 4 by finding an analogous connection for branes in de Sitter.

2.1 Solitons and Kinks

Before proceeding to false vacuum decay, we will require some elementary background in solitons. These objects are time-independent solutions of the equations of motion of a quantum field theory. Consider the following action for a real scalar field $\Phi(t, x)$ in $(1+1)d$:

$$I = \int d^2x \; \mathcal{L}(\Phi), \;\; \text{with} \;\; \mathcal{L}(\Phi) = -\frac{1}{2}\partial_\mu \Phi \partial^\mu \Phi - U(\Phi), \tag{2.1}$$

where we denote a potential $U(\Phi)$ that respects $\mathbb{Z}_2$ symmetry in Φ, and contains no derivatives in Φ. Explicitly, let us choose the potential

$$U(\Phi) = \frac{\lambda}{2}\Big(\Phi^2 - \frac{\mu^2}{\lambda}\Big)^2, \tag{2.2}$$

where μ^2 and λ are both separately positive and real parameters. Let us, for

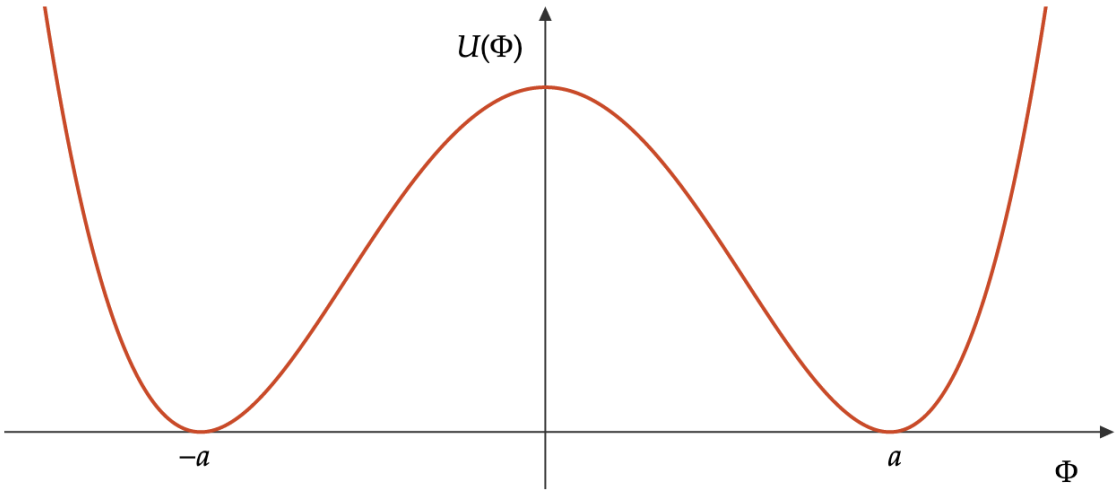

Figure 2.1: The potential $U(\Phi) = \frac{\lambda}{2}(\Phi^2 - a^2)^2$.

convenience, call $\mu/\sqrt{\lambda} = a$. Another useful example, that will play a role in Chapter 3 is the sine-Gordon potential

$$U_{\text{SG}}(\Phi) = \frac{\alpha}{\beta^2}\Big(1 - \cos(\beta\Phi)\Big). \tag{2.3}$$

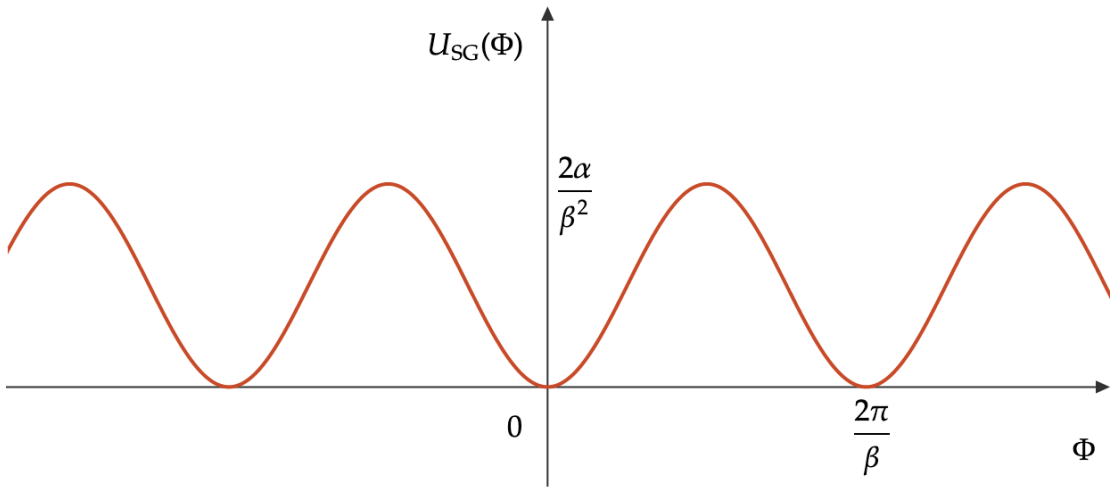

Figure 2.2: The sine-Gordon potential $U_{\mathrm{SG}}(\Phi) = \frac{\alpha}{\beta^2}\Big(1 - \cos(\beta\Phi)\Big)$.

In any case, let us return to the action of eq. (2.1). The momentum conjugate to Φ is given by

$$\Pi_\Phi = \partial_t \Phi, \tag{2.4}$$

from which one obtains the Hamiltonian density by a Legendre transformation

$$\mathcal{H} = \Pi_\Phi \partial_t \Phi - \mathcal{L}. \tag{2.5}$$

The Hamiltonian is then given by

$$H = \int dx\ \mathcal{H} = \int dx\ \left(\frac{1}{2}\Pi_\Phi^2 + \frac{1}{2}(\partial_x \Phi)^2 + U(\Phi)\right). \tag{2.6}$$

Let us now look for field configurations Φ that minimize H and are static, i.e. $\Phi(t,x) = \Phi(x)$. Then $\Pi_\Phi = 0$, and the Hamiltonian to minimize is

$$H = \int dx\ \mathcal{H} = \int dx\ \left(\frac{1}{2}(\partial_x \Phi)^2 + U(\Phi)\right). \tag{2.7}$$

Varying this expression with respect to $\Phi(x)$ gives

$$\partial_x^2 \Phi = \frac{dU}{d\Phi}. \tag{2.8}$$

Note that we could have obtained this same equation by seeking constant time solutions of the equations of motion that follow from varying eq. (2.1), in which case we would have

$$-\partial_t^2 \Phi + \partial_x^2 \Phi = \frac{dU}{d\Phi}. \tag{2.9}$$

Either way, it stands to reason that a constant value of Φ that minimizes the potential U will be a solution. In the case of the potential in eq. (2.2), such solutions are $\Phi = \Phi_\pm = \pm a$. But we would like a non-trivial static solution. By direct verification, we see that

$$\Phi(x) = a \tanh(\mu x) \tag{2.10}$$

is such a solution, known as a *kink*. See Fig. 2.3.

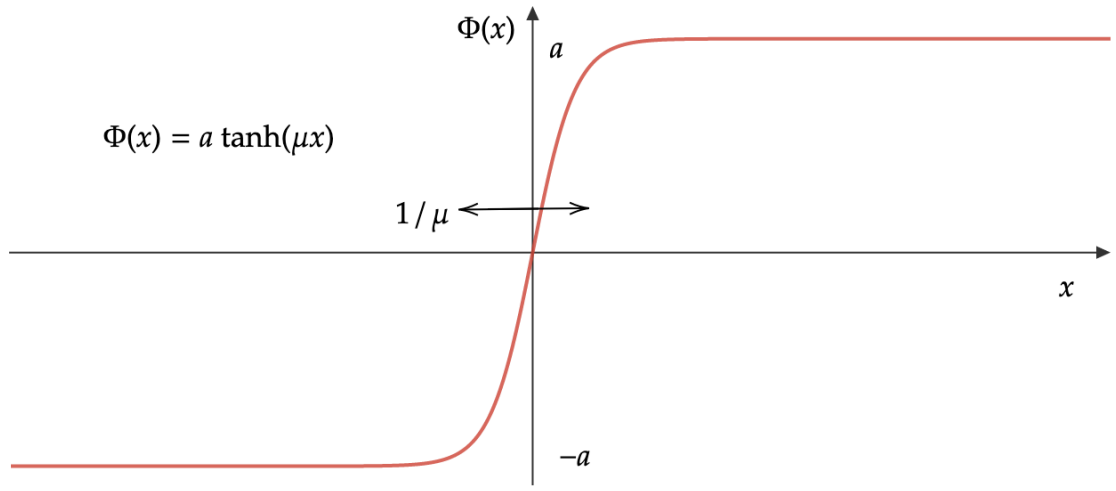

Figure 2.3: A kink solution.

Moreover, as $x \to \pm\infty$, $\Phi(x) \to \pm a$, which is to say that a kink is a solution that

interpolates between two different solutions, which are themselves minima of the potential $U(\Phi)$. Higher dimensional analogs of this are called *domain walls*.

Using the integral expression for the Hamiltonian eq. (2.6), we see that the mass of a kink is

$$M = \frac{4\mu^3}{3\lambda}. \tag{2.11}$$

This expression is finite owing to the fact that the potential vanishes far away[1], and the derivative energy is sharply localized in a region of width $\sim \mathcal{O}(\mu^{-1})$ centered at $x = 0$, which is the only region over which the kink solution appreciably changes. Outside this region, the kink exponentially approaches its asymptotic values. Due to the $\mathbb{Z}_2$ symmetry, $-\Phi$ is also a solution, called an *anti-kink*, which interpolates between $\mp a$ at $x = \pm\infty$. Note that a kink and anti-kink have a distinguishing feature. Indeed, the current

$$j^\mu = -\frac{1}{2a}\epsilon^{\mu\nu}\partial_\nu\Phi \tag{2.12}$$

satisfies $\partial_\mu j^\mu = 0$, and the conserved quantity associated with a spatial integral of the time component of this current is

$$Q = \int dx\ j^0 = \frac{1}{2a}\Big(\Phi(x=\infty) - \Phi(x=-\infty)\Big) \tag{2.13}$$

depends only on the asymptotic values of the field Φ. In particular, for a kink, we see that $Q = 1$ whereas for an anti-kink $Q = -1$. Kinks and anti-kinks can interact and annihilate, due to non-linear interactions in the potential, while preserving the total Q. We can also get a moving kink of speed v by boosting a static solution:

$$\Phi(t,x) = a\tanh\Big(\mu\gamma(x-vt)\Big),\ \text{where}\ \ \gamma = \frac{1}{\sqrt{1-v^2}}. \tag{2.14}$$

[1]Actually the field approaches a value that minimizes the potential far away, but we have taken the minimum value of the potential to vanish.

When λ is perturbatively small, which we have been assuming throughout, note that the soliton mass M can be considerably larger than the mass of the elementary particle excitation in the spectrum, which would appear to be $\sim \mu$.

A similar configuration arises in the case of the sine-Gordon potential of eq. (2.3) where constant minima configurations are $\Phi = 2\pi n/\beta$, where n is an integer. A kink solution will interpolate between two adjacent minima. For instance, a kink interpolating between $\Phi = 0$ and $\Phi = 2\pi/\beta$ is

$$\Phi(x) = \frac{4}{\beta} \arctan\Big(\exp\big(\sqrt{\alpha}x\big)\Big). \tag{2.15}$$

We see once more that as $x \to \infty$, $\Phi \to 2\pi/\beta$, and as $x \to -\infty$, $\Phi \to 0$, with changes in Φ being localized near $x = 0$. As such, the mass of this soliton is

$$M = \frac{8\sqrt{\alpha}}{\beta^2}. \tag{2.16}$$

2.2 Instanton Magic

Quantum Tunneling and False Vacuum Decay

Consider a spinless particle in one spatial dimension, with the following Hamiltonian:

$$H = \frac{p^2}{2m} + V(x). \tag{2.17}$$

Recall that the path integral computes the transition amplitude of a particle; in Euclidean signature,

$$\langle x_2| \exp(-HT) |x_1\rangle = \int \mathcal{D}x \ \exp\Big(-I_{\mathrm{E}}[x]\Big). \tag{2.18}$$

Here, T is a positive number and the left hand side is the amplitude for a particle starting at x_1 at time $t = -T/2$ propagating to x_2 at time $t = T/2$.[2] Inserting a complete set of energy eigenstates, we see that

$$\langle x_2| \exp(-HT) |x_1\rangle = \sum_n \exp(-E_n T) \langle x_2|n\rangle \langle n|x_1\rangle , \tag{2.19}$$

where the sum is over energy eigenstates. It follows from the sum over exponentially weighted functions that only the ground state - or first term - contributes significantly at late times. The Euclidean action is

$$I_{\rm E} = \int_{-T/2}^{T/2} d\tau \left(\frac{\dot{x}^2}{2} + V(x) \right). \tag{2.20}$$

The positive sign in front of the potential is due to the Euclidean time derivative. It is this sign difference that renders solutions of the Euclidean action akin to real time solutions in an inverted potential $-V(x)$, as shown in Fig. 2.5. Solutions to Euclidean equations of motion are called instantons.

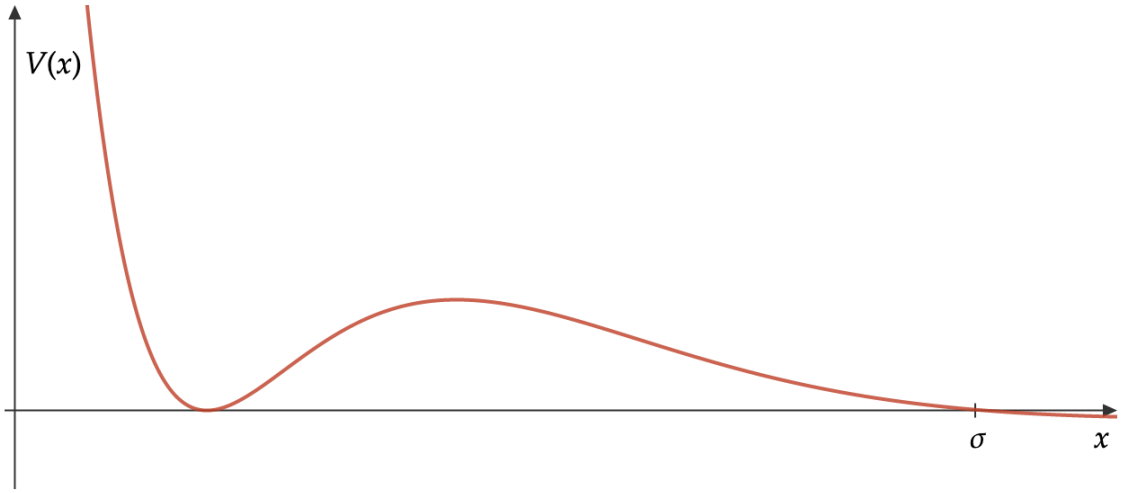

Figure 2.4: A potential profile with a metastable minimum, followed by a lower energy profile for $x > \sigma$.

[2]Or from time $t = 0$ to T. That is a choice of convention.

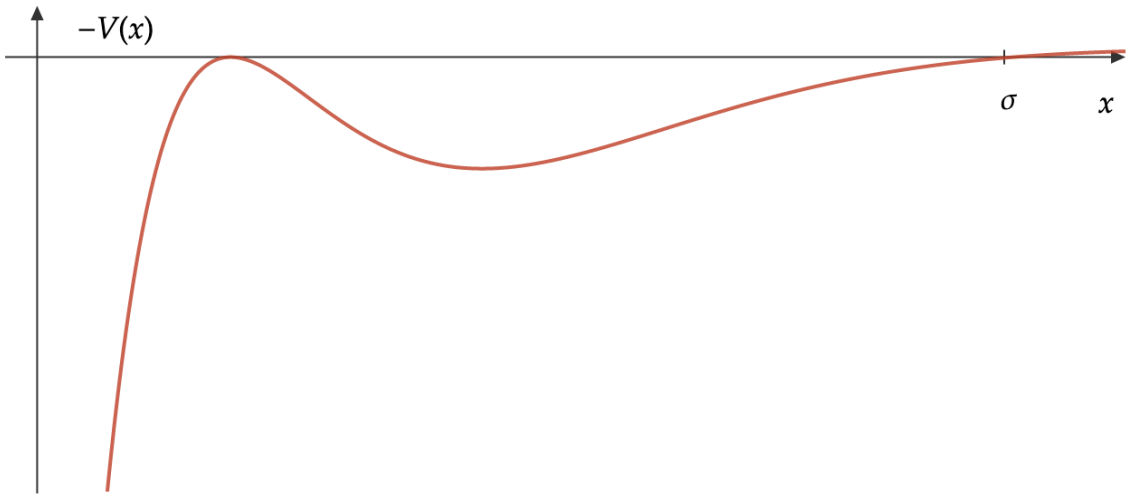

Figure 2.5: The inverted potential which admits solutions in Euclidean time.

Consider the harmonic oscillator with $V(x) = \omega^2 x^2/2$. Plugging the above action eq. (2.20) into the right hand side of the path integral relation in eq. (2.18) we infer with a Gaussian integral that the transition amplitude for propagation from $x = 0$ back to itself in time T is given by the formal expression

$$\mathcal{A} \sim \left(\mathrm{Det}\Big(-\frac{d^2}{d\tau^2} + \omega^2 \Big) \right)^{-1/2} . \tag{2.21}$$

We would like to know what this amplitude looks like at late times. We know that the ground state wavefunction of a harmonic oscillator is $\langle x|0\rangle = (\omega/\pi)^{1/4} \exp(-\omega x^2/2)$, with corresponding energy eigenvalue $E_0 = \omega/2$. Then it follows from eq. (2.19) that

$$\mathcal{A} \sim \left(\frac{\omega}{\pi}\right)^{1/2} \exp(-\omega T/2). \tag{2.22}$$

for late times. We then equate these two expressions above for $\mathcal{A}$.[3]

In order to evaluate the path integral, we may consider a saddle point approximation

[3]This derivation has been quick. It suffices for our purposes but a derivation applicable for more general boundary conditions is in [46].

about a stationary point of the action. That is to to say, we seek a solution $\bar{x}(\tau)$ for which

$$\frac{\delta I_{\rm E}}{\delta x} = 0, \tag{2.23}$$

which yields the equation of motion: $x = \bar{x}(\tau)$. Then differences of the action from its minimum come from paths that deviate from $\bar{x}$. Call the path

$$x(\tau) = \bar{x}(\tau) + \sum_n c_n u_n(\tau), \tag{2.24}$$

where the $\{u_n\}$ are a set of orthonormal functions, in the sense that

$$\int_{-T/2}^{T/2} d\tau \; u_m(\tau) u_n(\tau) = \delta_{mn}. \tag{2.25}$$

Also, $u_n(\pm T/2) = 0$. Recall that in the path integral approach, one inserts a space integral at every infinitesimal time slice so that the measure $\mathcal{D}x$ is actually a product of dx at infinitesimally separated values of τ. Then the parametrization eq. (2.24) may be viewed as a change of variables, with integration over c_n. In essence, $\mathcal{D}x \sim \Pi_n dc_n$, where once again we neglect the precise numerical value of the Jacobian factor.

Now a saddle point approximation of the amplitude gives

$$\langle x_2 | \exp(-HT) | x_1 \rangle \sim \exp(-I_{\rm E}(\bar{x})) \times \left({\rm Det} \Big(-\frac{d^2}{d\tau^2} + \frac{d^2 V}{dx^2}(\bar{x}) \right)^{-1/2} \tag{2.26}$$

where the first term comes from the minimum action, and the second factor comes from a Gaussian integral over the c_n terms which appear quadratically[4], with the understanding that the determinant is a product of eigenvalues $\{\lambda_n\}$, which are found

[4]We only get terms like c_n^2 and not $c_n c_m$ (where $n \neq m$) due to orthonormality of u_n functions.

from

$$\frac{d^2u_n}{d\tau^2} + V''(\bar{x})u_n = \lambda_n u_n. \tag{2.27}$$

Suppose now we seek the amplitude for a particle to travel from $x = 0$ back to itself. A trivial solution would be $x = 0$ for eternity. However, the particle may move from the top of the hill, rolling to $x = \sigma$ in Fig. 2.5, and subsequently returning to $x = 0$. This trajectory is called a bounce solution. Indeed, there could be multiple such bounces as the particle briefly stabilizes at the top and bounces once more, or many times for that matter. If these bounces are well separated in time, then the amplitudes will multiply; this is called the *dilute instanton gas* approximation. If the bounce solution is sharply localized in time, but then the particle stabilizes at the hill top for longer, then the amplitude is simply a contribution from the bounce, say K occuring n times, times the amplitude for a harmonic oscillator which is a good approximation near an extremum:

$$\left(\frac{\omega}{\pi}\right)^{1/2} \exp(-\omega T/2) K^n. \tag{2.28}$$

One must also integrate over the times at which the bounces occur in sequence:

$$\int_{-T/2}^{T/2} d\tau \int_{-T/2}^{\tau_1} d\tau_2 \cdots \int_{-T/2}^{\tau_{n-1}} d\tau_n = \frac{T^n}{n!}. \tag{2.29}$$

Multiplying this factor to the above expression, and summing over all possible bounces $n \geq 0$, we obtain the amplitude

$$\left(\frac{\omega}{\pi}\right)^{1/2} \exp\Big(-\omega T/2 + K \exp(-I_{\rm E})T \Big). \tag{2.30}$$

Interpreting the exponent as $-ET$, where $E = E_0 - i\Gamma/2 = \omega/2 - K\exp(-I_{\rm E})$, it immediately follows that when K is imaginary[5], there is a decay channel with decay width $\Gamma \sim \mathrm{Im}(K)\exp(-I_{\rm E}(\bar{x}))$.[6] From this point onward, let us only consider the exponent[7], whose value only requires evaluating the classical action on a Euclidean solution, so that

$$\Gamma \sim \exp(-I_{\rm E}(\bar{x})). \tag{2.31}$$

What is pleasing to see though, is that this is the same exponent one would expect to find from the WKB approximation in non-relativistic quantum mechanics.

The extension of this result to field theory is natural. Consider a scalar field Φ with potential profile as in Fig. 2.6.

Take the Euclidean action

$$I_{\rm E}[\Phi] = \int d^4x \left(\frac{1}{2}\partial_\mu\Phi\partial^\mu\Phi + V(\Phi)\right). \tag{2.32}$$

A solution is at $\Phi = \Phi_0$, but we see from Fig. 2.6 that this is a metastable solution. If at some large negative Euclidean time $\tau = -T$ the solution is at $\Phi = \Phi_0$, let us look for a solution that at $\tau = 0$ gives a field profile with $V(\Phi) < 0$. We would also like that as $|\mathbf{x}| \to \infty$, $\Phi \to \Phi_0$ so that $V \to 0$ in order to keep the integral over space finite. Both of these requirements are satisfied by seeking solutions of the form

[5]This occurs due to one of the eigenvalues in $\{\lambda_n\}$ being negative. An explicit computation of eigenvalues in [9] shows exactly one negative eigenvalue. Upon Gaussian integration, this will yield an imaginary term due to a square root in eq. (2.26). Indeed, this makes K pure imaginary and that is precisely why the decay process occurs, which we can see immediately by a Wick rotation of eq. (2.30) to real time.

[6]On a technical note, there is also a vanishing eigenvalue which follows from the equation of motion itself. Upon Gaussian integration, the square root of this zero eigenvalue will appear as an infinite pre-factor for the decay rate (eq. (2.26)), reflecting the fact that there is a time translation symmetry for infinite time T. This formally infinite term is rendered finite by using a collective coordinate (see [11]) change of variables. In the field theory case, there will also be a volume term appearing due to a space translation symmetry. We do not consider these details here due to our focus being exclusively on the bounce exponent for all future calculations in this thesis.

[7]This is justified when the quadratic correction is small, i.e. when the logarithm of the determinant gives a small correction to the action. In essence, we require $I_{\rm E} \gg 1$.

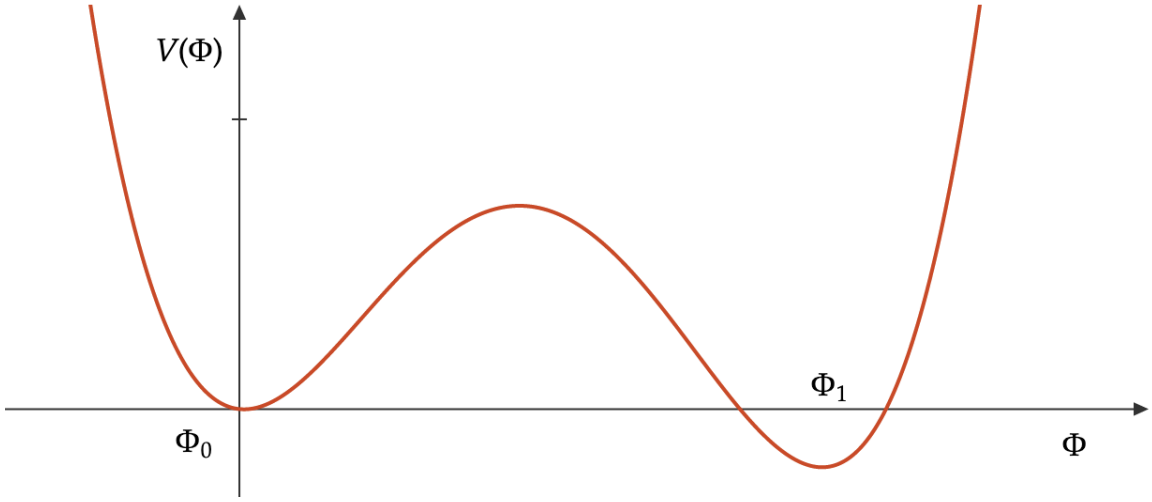

Figure 2.6: A potential profile for Φ with a metastable minimum $V = 0$ at $\Phi = \Phi_0$, followed by a lower energy profile for $\Phi = \Phi_1$.

$\Phi = \Phi(\rho)$ where $\rho^2 = \tau^2 + |\mathbf{x}|^2$. This is the $O(4)$ symmetric ansatz.

Now, the equation of motion becomes

$$\frac{d^2\Phi}{d\rho^2} + \frac{3}{\rho}\frac{d\Phi}{d\rho} = \frac{dV}{d\Phi}. \tag{2.33}$$

This equation of motion is that of a particle - if one is to view Φ as such - in an inverted potential, along with a friction term that decays with "time" ρ. Note that we also impose Neumann boundary conditions so that

$$\frac{d\Phi}{d\rho} \to 0 \text{ as } \rho \to 0, \tag{2.34}$$

to prevent singular behavior at the origin. Requiring the field be at its false vacuum value far away, along with the Neumann boundary condition at the origin, we have enough information to numerically integrate the above, generating a solution for the field profile, $\bar{\Phi}(\rho)$. Putting this solution in the Euclidean action gives the nucleation

rate

$$\Gamma/V \sim \exp\bigl(-I_{\rm E}(\bar{\Phi})\bigr). \tag{2.35}$$

Note the shape of the solution here: every slice of constant τ has a spatial spherical symmetry and so the bubble is is born a sphere at some critical size. Upon Wick rotating back to real time, we see that $\rho \to \sqrt{|\mathbf{x}|^2 - t^2}$, which means that the spherical bubble expands outwards in a hyperbolic trajectory in spacetime, asymptotically approaching the speed of light.

While in practice this equation is extremely difficult to solve analytically, there are special cases in which wherever the height of the potential barrier is large compared to the difference in energies of the false and true minima; these cases lead to analytic solutions called thin wall solution. In the next chapter we will explicitly show some of these. Other analytic approaches involve approximating the potential as a sequence of straight lines stitched together [13], which generalizes a previous result of [12].

The Schwinger Effect

The worldline action of a single particle of mass m and electric charge e is

$$I = -m\int_{\rm WL} ds + e\int_{\rm WL} A, \tag{2.36}$$

where the abbreviation WL denotes an integral over the particle's worldline. The first term on the right hand side gives the integral over the length of the worldline. The one-form gauge field is $A = A_\mu dx^\mu$. For a constant electric field E, we may gauge fix $A_1 = 0$, and $A_0 = Ex$. Consider now the problem of charged particle pair production by strong background electric fields in $(1+1)d$. Then in Euclidean signature, the

worldline action for the production of an electron positron pair[8] in a background electric field E is given by the effective single particle action

$$I_{\mathrm{E}} = \int d\tau \Big(m\sqrt{1+\dot{x}^2} + m - eEx \Big), \tag{2.37}$$

where the separating distance between the pair is x and an overdot indicates derivative with respect to Euclidean time τ. The momentum conjugate to x is

$$p = \frac{m\dot{x}}{\sqrt{1+\dot{x}^2}}. \tag{2.38}$$

The potential $m - eEx$ is sharply taken to vanish when the separation length x vanishes, i.e. we can view this setup as a barrier penetration problem where the effective single particle begins at the origin where the potential vanishes. It then tunnels through a potential barrier of linear slope until it has accumulated energy $2m$ from the electric field (figure 2.7), emerging as a pair of oppositely charged particles. This process will lead to pair creation such that the pair can now be accelerated away

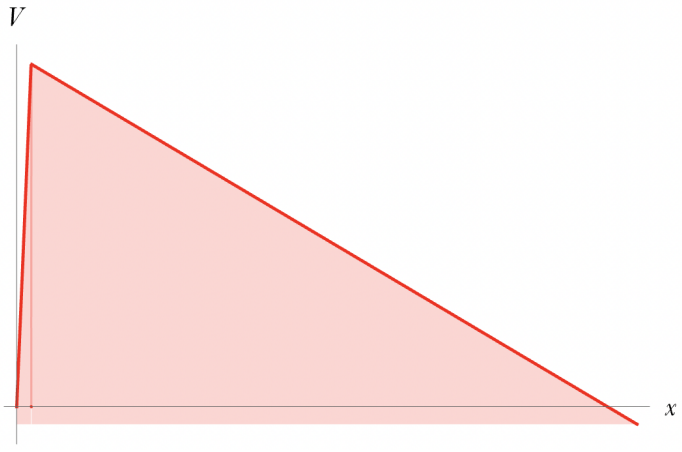

Figure 2.7: The effective potential for barrier penetration resulting in Schwinger pair production.

by the electric field. There is a screening of the electric field in the intermediate

[8]The situation is more complicated when there are multiple pairs [47].

region of space between the particles by the newly formed pair, but if the background electric field is sufficiently strong and the charges sufficiently weak, we may neglect this screening effect. Varying the action (eq. (2.37)) with respect to x gives the equation of motion

$$\frac{d}{d\tau}\Big(\frac{\dot{x}}{\sqrt{1+\dot{x}^2}}\Big) + \frac{eE}{m} = 0. \tag{2.39}$$

One may attempt an $O(2)$ symmetric ansantz to solve this differential equation, and indeed the instanton that solves it is the following:

$$x^2 + \tau^2 = x_*^2, \tag{2.40}$$

where the constant $x_* = 2m/eE$, and it is fully fixed by the above equation; it is not an independent parameter. Physically, x_* is the separation length at which the pairs emerge[9]. Putting this solution in eq. (2.37) gives the pair nucleation rate per unit volume

$$\Gamma/V \sim \exp\left(-\frac{\pi m^2}{eE}\right), \tag{2.41}$$

which is the same result Schwinger derived [19, 20]. We have neglected a pre-factor, focusing only on the exponent. Notice that upon nucleation, the particles follow a hyperbolic trajectory in space-time since the equation of motion is now $x^2 - t^2 = x_*^2$ thereby asymptotically approaching the speed of light as they are accelerated away by the external electric field. Viewing pair nucleation as a false vacuum decay problem will directly lead us to bubble nucleation in axion electrodynamics.

2.3 Swampland Conjectures

Several conjectures can be motivated by considering thought experiments involving black holes, and semi-classical particle physics in black hole backgrounds. We state

[9]There is a hierarchy of scales: one assumes that the critical length is larger than the Compton wavelength for one of the particles. This amounts to requiring $m^2 \gtrsim eE$.

a few such conjectures, emphasizing those that are closely related to this thesis.

Weak Cosmic Censorship Conjecture

Perhaps the earliest of the swampland conjectures is the Weak Cosmic Censorship Conjecture (WCCC) of Penrose [48]. Intuitively, it states that physical singularities originating from gravitational collapse (such as $r = 0$ of a Schwarzschild black hole) are hidden from external observers by an event horizon (at $r = 2G_{\rm N}M$ for Schwarzschild black holes). Immediately, interesting consequences follow from the WCCC for Reissner-Nordstrom black holes, which are non-rotating black holes of mass M and electric charge Q in an asymptotically flat background. Such a black hole has the line element

$$ds^2 = -h(r)dt^2 + h(r)^{-1}dr^2 + r^2 d\theta^2 + r^2 \sin^2\theta d\phi^2, \tag{2.42}$$

$$h(r) = 1 - \frac{2G_{\rm N}M}{r} + \frac{G_{\rm N}Q^2}{r^2}, \tag{2.43}$$

where the singularity at $r = 0$ is physical and cannot be removed by a coordinate transformation.

Inspecting the $h(r)^{-1}$ in the metric, the radial coordinates of the horizons are determined by $h(r_\pm) = 0$, from which we see that

$$r_\pm = G_{\rm N}M \pm G_{\rm N}\sqrt{M^2 - \frac{Q^2}{G_{\rm N}}}, \tag{2.44}$$

label the inner and outer horizons. It reduces to $r = 2G_{\rm N}M$ as $Q \to 0$ as anticipated. However, real solutions only exist provided that $\sqrt{G_{\rm N}}M \geq Q$, or else the horizons no longer exist and one finds a naked singularity at $r = 0$. Therefore, the WCCC

conjecture asserts that there should not be physical black holes for which $\sqrt{G_{\rm N}}M < Q$.

We should also note the classification of the solutions as Q varies. When $\sqrt{G_{\rm N}}M > Q$, the black hole is subextremal and the horizons are apart. When $\sqrt{G_{\rm N}}M = Q$, the horizons coincide at $r = G_{\rm N}M$ and the solution is said to be extremal. Finally, when $\sqrt{G_{\rm N}}M < Q$, we have superextremal solution with no horizons (we may view it as the horizons crossing as Q is increased from subextremality towards superextremality), which WCCC forbids. Indirect evidence for WCCC also exists; for instance, Boulware has argued [49] that for a thin shell to collapse forming a naked singularity, the energy density of the shell has to be negative.

No Global Symmetries Conjecture

The no global symmetries conjecture (NGSC) [50] states that there are no global symmetries in quantum gravity, and any symmetry is either broken or gauged [33].

We can motivate this conjecture using semi-classical arguments based on Hawking radiation [51, 52]. See also [53, 54]. Consider a Schwarschild black hole with line element

$$ds^2 = -h(r)dt^2 + h(r)^{-1}dr^2 + r^2 d\theta^2 + r^2 \sin^2\theta d\phi^2, \tag{2.45}$$

$$h(r) = 1 - \frac{2G_{\rm N}M}{r}. \tag{2.46}$$

The black hole has no hair [55], which is to say in this case that the only variable parameter that the black hole possesses is its mass M.[10] One important point to

[10]More generally, all stationary black hole solutions of the Einstein-Maxwell-Hilbert action can be characterized by three externally observable parameters: mass, charge, and angular momentum [56].

note is that this is an eternal black hole solution, at least classically. How it was born - whether from a collapsing star or in a thermal bath - is unimportant. The metric is the same whether or not we construct it from, say, neutrons, neutrinos, photons, etc. In particular, there are global symmetries such as the accidental $U(1)$ symmetries of the Standard Model, lepton number and baryon number. We could make the black hole purely from an equal number protons and electrons. However, the only parameter in question once the black hole is formed is M, and no semblance of baryon or lepton number remains. We could just as well have made it out of neutrons, which have baryon number only and no lepton number.

In either case, the black hole will radiate by emitting Hawking radiation. This radiation will cause the black hole to lose its mass, simultaneously raising its temperature, and decreasing the area of the horizon. However, this radiation from the horizon is not sensitive to global charge, since it only depends on M. As such, baryon and lepton number symmetry are violated by the black hole since either of the above two methods of creation will lead to the same outcome. This thought experiment illustrates that quantum gravity does not preserve global symmetries.

On the other hand, suppose we were to construct a subextremal Reissner-Nordstrom black hole with protons and neutrons, then the resulting metric will depend on the mass M and charge Q of the black hole, although not the baryon number. Now the Hawking radiation is sensitive to the emission of charged particles. In practice, it will attempt to radiate towards neutrality by disproportionately emitting positively charged particles [57] such as positrons. This behavior is owing to the conservation of electric charge, which is a global piece of a $U(1)$ gauge invariance that quantum gravity does appear to preserve.

Let us also briefly consider an argument associated with *remnants*[11]. These objects are the final states of Hawking radiation of black holes carrying global charge. One presumes that such a remnant, unlike a black hole, is no longer describable semi-classically, and that it has a mass of $\mathcal{O}(M_{\rm Pl})$. Now, if we construct a black hole using a large number of charged particles, then when the mass of the black hole is of $\mathcal{O}(M_{\rm Pl})$ after considerable Hawking evaporation, we are left with a highly charged object with a mass of $\mathcal{O}(M_{\rm Pl})$. This state is now stable since it no longer possesses enough mass to radiate away its charge. We can repeat this argument with a different range of initial charges. Ultimately, we are left with an infinite number of remnants. If we ask that there should not be an infinite number of remnants [58], then global symmetry should be broken by quantum gravity.

Weak Gravity Conjecture

The weak gravity conjecture (WGC) [59] states that in a theory of gravity weakly coupled to a $U(1)$ gauge theory with gauge coupling g, there exists at least one particle of mass m and charge qg satisfying $qg \gtrsim m/M_{\rm Pl}$.

Arguments exist based upon string theory [60], but let us use more elementary arguments based on black holes [61, 62]. Consider an electrically charged black hole. According to the WCCC, we should not have superextremal solutions since those would possess naked singularities. But an extremal black hole solution satisfies $Q = M/M_{\rm Pl}$. Hawking radiation is turned off since the black hole has vanishing temperature[12]. It would then appear we have a stable state despite not having a symmetry protecting it[13]. Nevertheless, extremal Reissner-Nordstrom black holes

[11] See also [34] for a discussion of this point.
[12] The fact that charged black holes have lower temperature was argued in [52]
[13] Indeed, no such symmetry should even exist due to the NGSC.

have background electric fields and so the Schwinger effect can occur, semi-classically producing charged particles. Imagine such particle-antiparticle pairs nucleating spontaneously. If at least one particle species carries charge and mass, qg and m, respectively with $qg \gtrsim m/M_{\rm Pl}$ then the gravitational attraction force on the positively charged particle will be $F_{\rm G} = -(Mm/M_{\rm Pl}^2)r^{-2}$, and the electric repulsion force will be $F_{\rm E} = (Mqg/M_{\rm Pl})r^{-2}$ since $Q = M/M_{\rm Pl}$. It follows that this positively charged particle will escape to infinity, allowing the extremal black hole to decay. In the deep infrared, corrections to this linear inequality have been computed [63].

Festina Lente Conjecture

We are now ready to briefly summarize the recent Festina Lente conjecture (FLC) [44, 45]. Just as the extremal Reissner-Nordstrom black hole was the key object of interest in the WGC, here the key object will be extremal black holes in de Sitter backgrounds. Explicitly, the line element is the following:

$$ds^2 = -h(r)dt^2 + h(r)^{-1}dr^2 + r^2 d\theta^2 + r^2 \sin^2\theta d\phi^2, \tag{2.47}$$

with lapse function

$$h(r) = 1 - \frac{2G_{\rm N}M}{r} + \frac{G_{\rm N}Q^2}{r^2} - \frac{r^2}{l^2}, \text{ where } l^2 = \frac{3}{\Lambda}, \tag{2.48}$$

where Λ is the cosmological constant and l is the de Sitter length. In addition to the two black hole horizons, there is also a new root of $h(r)$ corresponding to the cosmological horizon, say at $r = r_{\rm C}$. Extremal solutions are those in which two, or all three, horizons coincide. We review these extremal spacetimes in Appendix A.

What is interesting is the case in which the black hole outer horizon and the

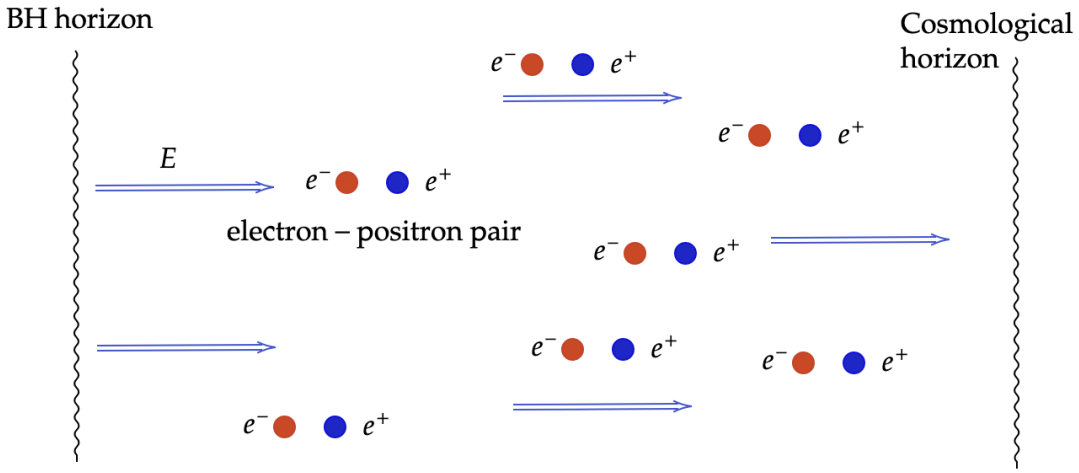

Figure 2.8: Schematic diagram showing pair nucleation - such as electrons and positrons - in a background electric field E, on the Nariai branch.

cosmological horizon coincide (Nariai branch), as well as when all three horizons coincide (ultracold point); details are in Appendix A. A coordinate change (see Appendix A) shows that the near horizon geometry of a freely falling observer on the Nariai branch is $\mathrm{dS}_2 \times S^2$ and at the ultracold point $\mathrm{Mink}_2 \times S^2$, where the curvature scale of the S^2 is $R \sim l \sim H^{-1}$, along with a background electric field in the spatial direction of Mink_2 of magnitude $E \sim M_{\mathrm{Pl}} H$.[14] This feature is analogous to the background electric field seen by a freely falling observer in an extremal Reissner-Nordstrom black hole, whose near horizon geometry is $\mathrm{AdS}_2 \times S^2$. In any case, the background electric field is able to decay via Schwinger pair production of charged particles (see Fig. 2.8), with $\Gamma \sim \exp(-\pi m^2/qE)$.

Let us first consider the case in which $m^2 \gg qE$. It has been shown [44] that all configurations within the shark fin diagram (Appendix A) evolve to empty de Sitter, consistent with previous arguments on the evolution of black holes in de Sitter [64]. However, when $m^2 \ll qE$, nucleation is fast, although the semi-classical approximation breaks down. One can consider a sudden approximation in which

[14] This value diminishes as one goes lower down the Nariai branch (see Fig. A.1)

the electric field rapidly discharges by pair nucleation, although the background geometry has not yet back-reacted. The particle pairs annihilate with one another forming photons which dissipate away (see Fig. 2.9). Everywhere on the Nariai

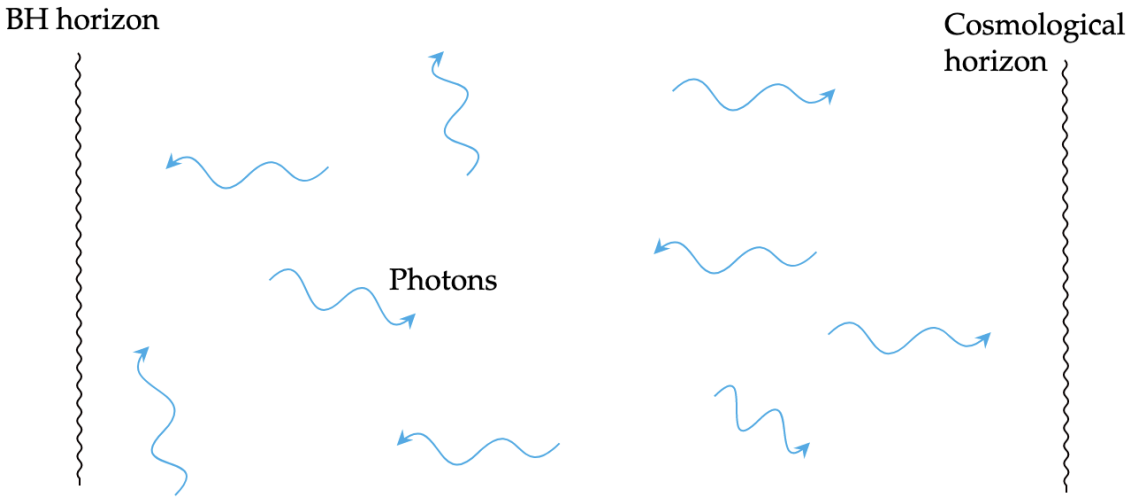

Figure 2.9: Rapid pair nucleation leads to annihilation, forming photons.

branch, up to the ultracold point (see Appendix A), a transition in which the electric field, and by extension Q rapidly falls leads to a transition from extremal to superextremal solution (see Fig. A.1). This pathology would be analogous to the inner and outer horizons of a Reissner-Nordstrom black hole crossing. One difference here is that by *lowering* the electric field rapidly one gets an extremal configuration if the starting point is the Nariai branch. The opposite behavior is true on the upper branch (see Fig. A.1). In fact it was shown in [44] that this evolution leads to a big crunch singularity. The argument of the FLC is that this outcome must be avoided, which is guaranteed by taking $m^2 \gg qE$. Since $E \sim M_{\rm Pl}H$, the condition is that

$$m^2 \gtrsim qM_{\rm Pl}H. \tag{2.49}$$

Notice the direction of the inequality, which is different from the WGC. In some sense, this is a strong gravity conjecture. What is even more interesting is that the inequality must apply to every single charged particle in the spectrum, for if *even*

a single particle (pair) violated it, then that particle would nucleate at a fast rate, leading to a superextremal configuration.

Throughout the remainder of this thesis, we will accept the argument of [44, 45] and *assume* that the Festina Lente conjecture is true. We emphasize though, that unlike the WGC, the FLC has no evidence supporting it from string theory.

2.4 On Strings and Branes

Recall the worldline action of a charged particle interacting with a photon,

$$I = -m \int ds + e \int A, \tag{2.50}$$

where the electromagnetic gauge field is $A = A_\mu dx^\mu$. Let us momentarily disregard the second term and focus on the first. The first integral is over the length of the worldline of the particle in spacetime. Here, $-ds^2 = g_{\mu\nu} dx^\mu dx^\nu = (-\dot{t}^2 + \dot{\mathbf{x}}^2) d\tau^2 = d\tau^2$, where the spacetime coordinates are parameterized by the particle's proper time τ, and overdots indicate derivatives with respect to τ. There is an explicit reparameterization invariance of the action under $\tau \to f(\tau)$. The generalization to extended objects is a natural extension of the worldline action; indeed, if a point sweeps out a worldline, then a string would sweep out a worldsheet. Its action would be

$$I = -T \int d^2\xi \sqrt{-h}. \tag{2.51}$$

The integral gives the worldsheet area, while the prefactor T denotes the string tension. Explicitly, h_{ab} is the induced metric on the worldsheet:

$$h_{ab} = g_{\alpha\beta} \frac{dX^\alpha}{d\xi^a} \frac{dX^\beta}{d\xi^b}, \tag{2.52}$$

where just as τ previously parameterized the worldline, the coordinates $\{\xi^a\}$ now parameterize the worldsheet. This expression in eq. (2.51) is the famous Nambu-Goto action [65, 66] [15]. An immediate generalization to higher dimensional extended objects is clear; for an object with p spatial dimensions, the action is

$$I = -T \int d^{p+1}\xi \sqrt{-h}. \tag{2.53}$$

Formally, extended objects of p spatial dimensions upon which the endpoints of open strings may end are known as Dp branes, and they are dynamical objects in their own right [78].

The (Dirac)-Born-Infeld Action

There may also be intrinsic gauge fields living on the brane. Indeed, there is a non-linear generalization of Maxwell theory known as the Born-Infeld action:

$$I_{\text{BI}} = -T \int_{\text{Brane}} d^{p+1}\xi \sqrt{-\text{Det}(\eta_{ab} + 2\pi\alpha' F_{ab})}. \tag{2.54}$$

We can observe that when $\alpha' F_{ab} \ll 1$, the determinant can be expanded out using the standard relation $\text{Det}(\exp(M)) = \exp(\text{Tr}(M))$. The action then reduces to

$$-T \int_{\text{Brane}} d^{p+1}\xi \left(1 + \pi^2 \alpha'^2 F_{ab} F^{ab} + \cdots \right). \tag{2.55}$$

The leading non-trivial term in Maxwell theory, and the ellipses contain non-linear corrections to Maxwell theory, suppressed by higher powers of α'. We may also be interested in considering interactions of the gauge field with fluctuations of the brane,

[15] While we cannot provide an elaborate review of string theory and branes here, comprehensive resources are available: [67, 68, 69, 70, 71, 72, 73, 74, 75, 76, 77].

in which case a generalization of the above is the Dirac-Born-Infeld action:

$$I_{\rm DBI} = -T \int_{\rm Brane} d^{p+1}\xi \sqrt{-{\rm Det}(h_{ab} + 2\pi\alpha' F_{ab})}, \tag{2.56}$$

where one takes into account the pull-back formula for the intrinsic brane metric:

$$h_{ab} = \eta_{\mu\nu} \frac{\partial X^\mu}{\partial \xi^a} \frac{\partial X^\nu}{\partial \xi^b}. \tag{2.57}$$

For clarity, $\{X^\mu\}$ and $\{\xi^a\}$ are the bulk and brane coordinates respectively[16]. Moreover, one may also incorporate a $(p+1)$ form field by adding $C_{(p+1)}$ to the Lagrangian which charges the brane.

The Wess-Zumino Term

A natural interaction is of the form

$$I_{\rm WZ} = \gamma \int_{\rm Brane} \exp(2\pi\alpha' F) \wedge A, \tag{2.58}$$

which is known as the Wess-Zumino interaction, and A is a one-form Ramond-Ramond field[17]. The exponential is a formal expression indicating the fact that one takes the number of field strength tensors such that those, combined with A, match the dimension of the worldvolume of the brane so that the integration makes sense[18]. It

[16] One should also consider the anti-symmetric two form gauge field B_{ab} for closed string theories, but in this thesis we will exclusively consider backgrounds involving a $U(1)$ gauge field and our solutions in subsequent chapters will not require additional fields. We assume throughout the dilaton that should be present is stabilized, so that it is merely a constant absorbed into the definition of the tension T.

[17] We will only consider one form fields, but in type IIA string theory we could also have three form, etc. In type IIB we would instead have zero-form, two form, etc. As such, more general Wess-Zumino interactions are possible. Nevertheless, the backgrounds that we consider only involve a non-vanishing one form field.

[18] Note for clarity that F in eq. (2.58) is the field strength corresponding to a gauge field intrinsic to the brane. It is *not* the field strength corresponding to the Ramond-Ramond field.

is interactions of this form that will play a key role in studying brane nucleation in Chapter 4. In particular, note the curious special case of the D0 brane, or particle. Then the only term in the expansion of exponential that matters is unity, i.e. the zeroth order term, which is simply the same as the second term in (2.50). We have seen that this term induces pair nucleation in two dimensions, and so it is actually suggestive that the Wess-Zumino term may induce brane nucleation in higher dimensions.

Chapter 3

Nucleation of Bubbles in Chern-Simons Theories

We will derive a process in axion electrodynamics that, in the presence of parallel background electric and magnetic fields, leads to bubble nucleation.

3.1 Bubbles in $(1+1)d$

Before proceeding to the main problem of finding a new instanton of axion electrodynamics in $(3+1)d$, let us first consider the analogous problem in $(1+1)d$. In this low dimensional problem, axion electrodynamics vacuum decay is very similar to Schwinger pair production and we will emphasize these similarities in this section. Much of the material in this section is analogous to the $(3+1)d$ process we consider below, and these analogies will guide us in the main problem, although there are significant differences as well which we will elaborate on afterwards.

The Lorentzian signature action for $(1+1)d$ axion electrodynamics is

$$I = \int d^2x \left(-\frac{1}{4} F_{\mu\nu} F^{\mu\nu} - \frac{1}{2} \partial_\mu \theta \partial^\mu \theta - \left(\frac{m}{N}\right)^2 \Big(1 - \cos(N\theta)\Big) + \frac{Ke}{2\pi} \theta \epsilon_{\mu\nu} F^{\mu\nu} \right), \quad (3.1)$$

where $F_{\mu\nu}$ is the Maxwell field strength for the photon A_μ, and the pseudoscalar θ is the axion field. Moreover, e is the electromagnetic coupling; the integers N and K are the domain wall number and anomaly coefficient, respectively. The antisymmetric symbol is $\epsilon_{\mu\nu}$, with $\epsilon_{01} = +1$. The field θ is periodic with the gauge identification $\theta \sim \theta + 2\pi$. In (1+1)$d$, there is only one independent component of the Maxwell tensor which is the electric field $E = F_{10}$. Varying the action (3.1) with respect to A_μ and θ, we obtain the following equations of motion for the fields:

$$\partial_x E = -\frac{Ke}{\pi} \partial_x \theta, \quad \partial_t E = -\frac{Ke}{\pi} \partial_t \theta, \text{ and,} \quad (3.2)$$

$$\frac{1}{m^2} \partial^2 \theta = \frac{1}{N} \left(\sin(N\theta) - KN \frac{eE}{\pi m^2} \right). \quad (3.3)$$

There is no Bianchi identity in $(1+1)d$ since the antisymmetric symbol has only two indices. From eq.(3.3) constant θ local extrema are given by

$$\theta = \frac{1}{N} \arcsin\left(\frac{KNeE_0}{\pi m^2} \right), \quad (3.4)$$

where $KNeE_0/\pi m^2 \leq 1$, with subsequent minima $2\pi/N$ units apart. We now discuss tunneling between these minima.

Previous work [79] has considered how solitons can lead to decays of excitations. We would instead like to consider how charged domain wall pairs nucleate leading to electric field screening, akin to the Schwinger effect. Consider the theory of eq. (3.1) with a constant background electric field E_0. Using eq. (3.2), we see that the effective electric charge density is proportional to the spatial derivative of the axion field

value and vanishes when the axion is constant. It is then easy to see that a pair of domain walls, of opposite orientation can screen the background electric field. This configuration can be nucleated from the vacuum in the presence of an electric field and is exactly analogous to the Schwinger pair production process with the domain walls playing the role of the electron-positron pair. The screening effect of these domain walls facilitates the decay of the background electric field. We describe this process in the thin and thick wall limits.

Thin Wall

Let us start by solving the system above (i.e. eq. (3.2) and eq. (3.3) in the presence of a background electric field E_0) in a convenient limit where we take $Ke \ll E_0$. Then we can neglect the back-reaction of the axion profile on the electric field. More precisely, we take $E/m \to \infty$ and $e/m \to 0$, but keeping their product fixed. This limit ensures that the right hand sides of both expressions of eq. (3.2) vanish, while the term proportional to eE in the eq. (3.3) remains relevant. The implication here is that we can treat $E = E_0$ as a constant that solves the first two equations of (3.2). From the last of eq. (3.2), we see that the axion field evolves in the potential

$$V(\theta)/m^2 = \frac{1}{N^2}\Big(1 - \cos(N\theta)\Big) - K\frac{eE_0}{\pi m^2}\theta \ . \tag{3.5}$$

So far, we have not assumed any thin wall limit. If we also take $KNeE_0/m^2 \ll 1$, the subsequent minima will not be of significantly different energy, and the barrier height will be relatively large. In such a scenario, the thin wall approximation is applicable and can be used to describe the tunneling process and calculate its rate [8].

Differentiating eq. (3.5) with respect to θ, one can find the minima. The first

minimum is at

$$\theta_0 \approx \frac{KeE_0}{\pi m^2}, \tag{3.6}$$

with a subsequent lower energy minimum at $\theta_0 + 2\pi/N$. Physically, when a transition occurs, a bubble forms in such a way that in the bubble interior, $\theta = \theta_0 + 2\pi/N$ and in the bubble exterior $\theta = \theta_0$. Note that this is true in the thin wall limit; when one considers a thick wall bubble, the bubble interior will be at an intermediate value of θ rather than at a minimum, after which the field classically rolls to the minimum. Then the energy density in the interior is lower than in the exterior. A domain wall pair - with opposite orientations of the two walls - constitutes the boundary of the bubble and interpolates between these two minima. Because of the opposite orientations of the two walls eq. (3.2) indicates that they carry opposite charges as expected. Moreover, this is a screening orientation: the right wall is positively charged and the left wall is negatively charged (see figure 3.1). Let us now calculate the bubble

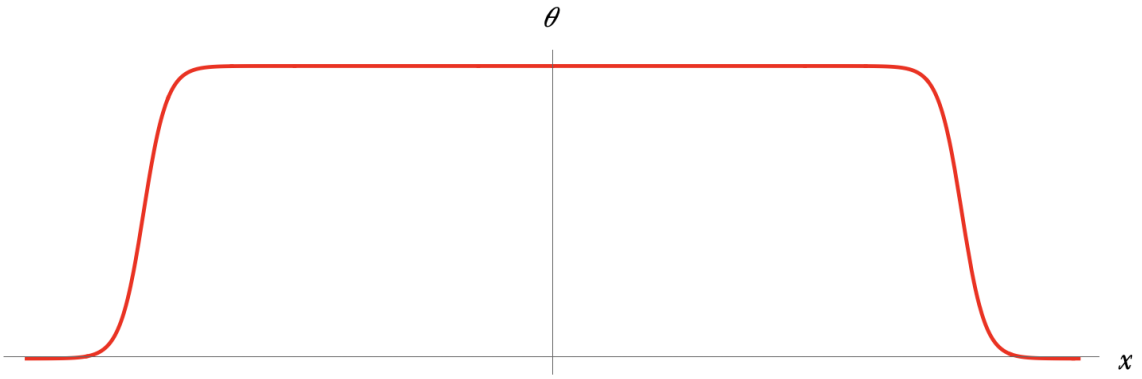

Figure 3.1: Schematic outline of the bubble profile for θ in the (1+1)d thin-wall example.

structure and the decay rate. Under a Wick rotation $it = \tau$ and the identification

$-I_{\rm E} = iI$, the Euclidean action corresponding to eq. (3.1) is

$$I_{\rm E} = \int dx d\tau \left(\frac{1}{4} F^{(\rm E)}_{\mu\nu} F^{(\rm E)}_{\mu\nu} + \frac{1}{2} (\partial_\mu \theta)^2 + \left(\frac{m}{N}\right)^2 \Big(1 - \cos(N\theta)\Big) - i \frac{Ke}{2\pi} \theta \epsilon^{\mu\nu} F^{(\rm E)}_{\mu\nu} \right), \tag{3.7}$$

where the superscript denotes Euclidean fields $F^{(\rm E)}_{\mu\nu} = \partial_\mu A^{(\rm E)}_\nu - \partial_\nu A^{(\rm E)}_\mu$, with $iA^{(\rm E)}_\tau = A_0$; also note that $\epsilon_{1\tau} = 1$ whereas previously in Lorentzian signature $\epsilon_{01} = 1$. The equations of motion, upon varying with respect to $A^{(\rm E)}$ and θ, are

$$\partial_\mu F^{(\rm E)\mu\nu} = i \frac{Ke}{\pi} \epsilon^{\mu\nu} \partial_\mu \theta, \quad \text{and} \quad \partial^2 \theta = m^2 \left(\frac{\sin(N\theta)}{N} - i \frac{Ke}{2\pi m^2} \epsilon^{\mu\nu} F^{(\rm E)}_{\mu\nu} \right). \tag{3.8}$$

From now on we drop the superscript denoting Euclidean fields to avoid clutter, although the context should make it unambiguous.

First we search for an instanton when $KNeE_0/m^2 \lesssim 1$, and $Ke/N \ll E_0$. Then the screening effect of the electric field by the domain wall is small. In essence, we take the right hand side of the first of eq. (3.8) to be vanishingly small, so that the electric field is effectively constant. Then the photon just serves as a background field. Analogous to the Schwinger effect, we attempt an $O(2)$ symmetric ansatz, taking $\theta = \theta(\rho)$ where we define the dimensionless length $\rho = m\sqrt{\tau^2 + x^2}$. Then the equation of motion for the axion becomes

$$\frac{d^2 \delta\theta}{d\rho^2} + \frac{1}{\rho} \frac{d\delta\theta}{d\rho} = \frac{1}{N} \sin(N\delta\theta) + \mathcal{O}(\theta_0), \tag{3.9}$$

where $\delta\theta(\rho) = \theta(\rho) - \theta_0$. In the thin wall limit where $\theta_0 \ll 1$ we may drop the $\mathcal{O}(\theta_0)$ term, as well as the friction term on the left hand side, which means (3.9) is solved

by the sine-Gordon soliton

$$\theta(\rho) = \theta_0 + \frac{2\pi}{N} - \frac{4}{N}\arctan\Big(\exp(\rho - \rho_*)\Big). \tag{3.10}$$

The wall thickness is therefore $\mathcal{O}(m^{-1})$, and the wall is situated at $x = m^{-1}\rho_*$ upon nucleation. We may find ρ_* by substituting this solution in eq. (3.7), and minimizing[1] to obtain the radius of the critical bubble. We find

$$\rho_* \approx \frac{4m^2}{NKeE_0}. \tag{3.11}$$

This expression is in good agreement with numerical solutions in the regime of validity of the thin wall approximation. Moreover, a solution with this critical radius has Euclidean action

$$I_{\mathrm{E}} = \frac{32\pi m^2}{N^3 KeE_0} \tag{3.12}$$

Already, we see a resemblance with the Schwinger tunnelling exponent $I_{\text{Schwinger}} = \pi\mu^2/qE$, with μ the particle's mass. To understand this point better, it is helpful to know the energy momentum tensor in order to compute the domain wall mass. The Hilbert energy momentum tensor is

$$T^{\mu\nu} = F^{\mu\lambda}F^{\nu}{}_{\lambda} + \partial^{\mu}\theta\partial^{\nu}\theta - \eta^{\mu\nu}\left(\frac{1}{4}F_{\alpha\beta}F^{\alpha\beta} + \frac{1}{2}(\partial\theta)^2 + \left(\frac{m}{N}\right)^2\Big(1 - \cos\left(N\theta\right)\Big)\right), \tag{3.13}$$

which agrees with the canonical energy-momentum tensor upon Belinfante improvement; note the absence of the topological term. Actually even under Belinfante improvement, the canonical energy momentum tensor will appear to have terms arising from the topological Chern-Simons operator in the action, but one can

[1] Recall that we are keeping the electric field constant in this approximation. We will drop this condition in an example momentarily.

show that such terms actually cancel, and we are left with the Hilbert form. It is tempting to infer from this observation that the Chern-Simons term is immaterial, but such a conclusion is misleading: the equations of motion, and their solutions θ and A_μ, depend on the topological term and so ultimately the energy-momentum tensor does too when evaluated on a solution. Alternatively, one can rewrite the energy momentum tensor in terms of canonically conjugate momenta, and then the Chern-Simons term will reappear.

Using eq. (3.13), we find that the mass of the domain wall is $m_{\rm DW} \approx 8m/N^2$. Here again, the thin wall approximation is necessary. The domain wall charges are $Q_{\rm DW} = \pm 2eK/N$ from integrating the first of eq. (3.2). Using these results in eq. (3.12), it then follows that the decay rate is

$$\Gamma/V \sim \exp\left(-\frac{\pi m_{\rm DW}^2}{Q_{\rm DW} E_0}\right). \tag{3.14}$$

The exponent of the nucleation rate is similar to that in the Schwinger effect of charged particles, except with the particle's mass and charge replaced by those of the domain wall. This similar scaling behavior demonstrates that axion domain wall nucleation is a type of Schwinger process.

There are a few points that we wish to emphasize here. First, in the case of the Schwinger effect, one nucleates a pair of charged particles. Here, one instead nucleates from the vacuum a pair of extended objects - domain walls - which have an effective electric charge. In $(1{+}1)d$ the domain wall is a $(0{+}1)d$ object and this process is thus very similar to particle production in the Schwinger effect. In higher dimensions this conceptual difference becomes more important as the domain walls can no longer be thought of as particles. Importantly, this process can happen even in the absence of charged particles in the spectrum.

Moreover, as we stated earlier, the magnitude of the charge on the wall is $2eK/N$, yet we have neglected the change in the electric field. However, in practice the interior electric field is now $E = E_0 - 4eK/N$, and after the walls have propagated outwards, the new background electric field is $E_0 - 4eK/N$, and the expectation value of the axion is $\theta = N^{-1} \arcsin\left(KNe(E_0 - 4eK/N)/m^2\right)$. We only considered cases for which $E_0 \gg eK/N$ so that the screening of the electric field is small for each individual bubble that is nucleated. This approximation is not essential. Nevertheless it leads to an important matter regarding bubble expansion in real time after nucleation. We may understand the outward expansion as being caused by the pressure difference between the interior and the exterior. In particular, from the energy momentum tensor in eq. (3.13) the pressure P in a region where the axion is not varying significantly is

$$P \approx -\frac{E^2}{2} - \left(\frac{m}{N}\right)^2 \Big(1 - \cos\left(N\theta\right)\Big). \tag{3.15}$$

This applies in the interior and exterior regions, but not on the wall itself. This expression need not hold in the thick wall limit in which the interior axion field is not constant. As θ changes by $2\pi/N$ between the exterior and the interior, the second term in the expression for the pressure does not change. However, the electric field is screened on the inside and the pressure is therefore less negative (i.e. higher) inside the bubble. This pressure difference leads to an outward force on the wall which causes expansion, ultimately leading to a hyperbolic trajectory in real time.

Thick Wall

Now, we may study processes in which the thin wall approximation is no longer valid. In this case, we consider the scenario in which the difference in energies of the

two minima is no longer small compared to the barrier height. To add to this, we do not assume that the electric field is unchanged, and we incorporate the screening effect of the domain wall. Then the axion will begin rolling in the inverted potential subject to the (Euclidean) time dependent friction. This will lead to a thick wall profile for which one must numerically integrate the equations of motion to obtain the instanton solution. Substituting this solution in the Euclidean action gives the bounce.

There is subtle point that we should clarify before proceeding. This point stems from the fact that for a dynamical electric field we have to treat the action, in particular the boundary terms, carefully [14]. Typically, when we vary the action with respect to the fields, it is assumed that the field configurations are fixed on the boundary. This allows us to drop boundary terms. Then requiring a stationary action immediately yields the equations of motion. In our case, we would like the fields θ and $F_{\mu\nu}$ (or E) to be fixed at the boundary. The standard procedure however assumes that A_μ is fixed at the boundary rather than $F_{\mu\nu}$. We can see this by varying eq. (3.1) with respect to A_μ; note that the boundary term contains δA_μ which one typically assumes vanishes[2]. We may rectify this issue by adding a total derivative $\partial_\mu((F^{\mu\nu} - Ke\theta\epsilon^{\mu\nu}/\pi)A_\nu)$ to the Lagrangian of eq. (3.1). This addition amounts to a Legendre transformation at the level of δI, since $Ke\theta\epsilon^{\mu\nu}/\pi - F^{\mu\nu}$ is the momentum conjugate to A_ν. Varying the new action, one can show that the surface term only contains $\delta F_{\mu\nu}$ now, and not δA_μ. This procedure does not alter the equations of motion since we are merely adding a total derivative. Therefore, solutions, in particular bubble configurations, remain unchanged. Nevertheless, quantities that depend not only on the functional form of the action *but also its numerical value* -

[2]Actually, the component of A_μ tangential to the boundary is required to be fixed on the boundary.

such as decay rates - may be altered. Explicitly, the new action I' is

$$I' = \int d^2x \left(\frac{1}{4} F_{\mu\nu} F^{\mu\nu} - \frac{1}{2} (\partial\theta)^2 - \left(\frac{m}{N}\right)^2 (1 - \cos(N\theta)) \right) + \int d^2x \left(A_\nu \partial_\mu \left(F^{\mu\nu} - \frac{Ke}{\pi} \theta \epsilon^{\mu\nu} \right) \right). \tag{3.16}$$

Varying this action with respect to the fields gives the correct equations of motion, with the requirement that $\delta\theta$ and $\delta F_{\mu\nu}$ vanish on the boundary. One can Wick rotate eq. (3.16) to compute the decay rate. The second line vanishes on the equations of motion. Note that the topological term no longer explicitly appears in the first line – which is the line that contributes to the decay rate – despite playing a crucial role in the decay process. Let us now return to the problem of computing bubble nucleation rates for arbitrary walls.

First we will assume an $O(2)$ symmetric ansatz for our fields, so that $\theta = \theta(\rho)$ as before, and $A = A_\rho(\rho) d\rho + A_\phi(\rho) d\phi$. where ϕ is the angular coordinate in the τx-plane. Moreover, we gauge fix $A_\rho = 0$. This gauge choice is consistent with the $O(2)$ ansatz under which the gauge fields and transformation parameters do not depend on ϕ either. For instance, we may not have been able to consistently require A_ϕ to vanish in general by gauge choice. Then it automatically follows that $E = E(\rho)$ since now $E = i\rho^{-1} \partial_\rho A_\phi(\rho)$. We will apply a similar strategy to dynamics in $(3+1)d$ in section 3.2. Varying eq. (3.7), subject to the boundary condition at infinity, $\theta_0 = N^{-1} \sin^{-1}(NKeE_0/\pi m^2)$, we find the following equation for $\delta\theta$:

$$\frac{d^2\delta\theta}{d\rho^2} + \frac{1}{\rho} \frac{d\delta\theta}{d\rho} - \frac{1}{N} \left(\sin(N\theta_0 + N\delta\theta) - \sin(N\theta_0) \right) - \left(\frac{Ke}{\pi m} \right)^2 \delta\theta = 0, \tag{3.17}$$

where we must also require that the derivative of $\delta\theta$ vanishes at the origin. Note that we have integrated the first of eq. (3.8) and substituted the result into the second. Then numerical integration gives the axion profile. As an example, consider the case

in which $E_0/m = 3$, and $e/m = N = K = 1$. Numerical integration of eq. (3.17) shows that at the center of the bubble, $\theta - \theta_0 \approx 1.955$ and figure 3.2 explicitly shows the thick wall bubble profile. Substituting this profile in eq. (3.16) gives the decay rate

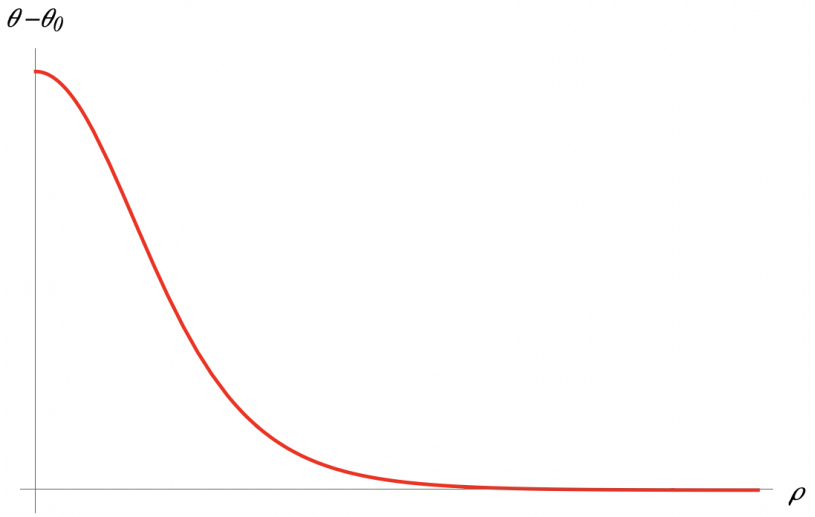

Figure 3.2: Bubble profile for $\theta - \theta_0$.

$\Gamma/V \sim \exp(-I_{\rm B})$, with $I_{\rm B} \approx 5.416$. This is a reasonably fast decay process since the exponent is approaching unity. Note though, that when $I_{\rm B} \lesssim 1$, we do not trust the semi-classical analysis but intuitively the decay is also fast for $I_{\rm B} \lesssim 1$. An important aspect of this decay process is that even when we included the back-reaction of the electric field, the $O(2)$ ansatz was still valid. In section 3.2 we will find that in $(3+1)d$, incorporating the back-reaction of the gauge field drastically reduces the symmetry group of the solution.

3.2 Bubbles in Axion-Maxwell Theory

Our focus will be on axion electrodynamics with an action:

$$I = \int d^4x \left(-\frac{1}{4} F_{\mu\nu} F^{\mu\nu} - \frac{f^2}{2} \partial_\mu \theta \partial^\mu \theta - V(\theta) + \frac{K\alpha}{8\pi} \theta \epsilon_{\mu\nu\rho\sigma} F^{\mu\nu} F^{\rho\sigma} \right), \tag{3.18}$$

where $F_{\mu\nu} = \partial_\mu A_\nu - \partial_\nu A_\mu$ is the Maxwell field strength corresponding to the photon A_μ, $\theta \equiv a/f$ where a is the neutral pseudo-scalar axion field with periodicity $a \sim a + 2\pi f$, f is the mass-dimension one axion decay constant and $\alpha = e^2/4\pi$ is the $U(1)$ fine structure constant. The integer K specifies the Chern-Simons interaction term between the gauge field and the axion. Note that $\epsilon_{\mu\nu\rho\sigma}$ is the totally antisymmetric symbol with $\epsilon_{0123} = +1$.

Since we are mainly interested in the physically most motivated case of a massive axion we also include a non-zero axion potential, $V(\theta)$. Our conclusions will apply to any $V(\theta)$ that is a periodic function. This includes the case where $V(\theta)$ has a sub-periodicity $V_{\rm N}(\theta) = V_{\rm N}(\theta + 2\pi/N)$ corresponding to a $\mathbb{Z}_{\rm N}$ global symmetry of the theory with N degenerate local minima.[3] In phenomenological studies of the QCD axion, the integer $N \geq 1$ is known as the domain wall number and is typically determined by anomalies of the UV theory. For concreteness we will consider a simple potential of the "one-instanton" form (although we emphasize that our conclusions apply to more general periodic potentials [80]):

$$V(\theta) \equiv V_{\rm N}(\theta) = \left(\frac{mf}{N}\right)^2 \Big(1 - \cos(N\theta)\Big), \tag{3.19}$$

where we have chosen the normalization of $V_{\rm N}(\theta)$ so that the parameter m is the mass of the axion around any one of the minima of $V_{\rm N}(\theta)$. The theory is thus specified by the two integers K, N, the dimensionless coupling α and the dimensional parameters m, f.

The action eq. (3.18) can be thought of as arising from a UV theory of the

[3]When UV completed to a theory including gravity we expect that this $Z_{\rm N}$ global symmetry to be explicitly broken. The size of this symmetry breaking can be exponentially smaller than the non-perturbative effects that give rise to $V_{\rm N}(\theta)$, and we can work in the approximation where this breaking is sub-leading to the effects of the background gauge fields.

axion interacting with the photon in the presence of heavy $U(1)$-charged fermions which transform chirally under the continuous global shift symmetry $a(x) \to a(x) + c$ for $c \in \mathbb{R}$ a constant. These fermions determine the integer K in the Chern-Simons topological coupling through their anomaly coefficient. In addition the axion is coupled to a sector with non-perturbative dynamics that generates a potential for the axion breaking the continuous shift symmetry $a(x) \to a(x) + c$ down to a $\mathbb{Z}_{\mathrm{N}}$ subgroup. See also [81] for a review of these effects. We will not need to specify the exact form of these dynamics as long as it takes place at energy scales much higher than m, in other words, well above the low-energy effective field theory regime containing the axion and the photon degrees of freedom.

We are mostly interested in the case where there are parallel background electric and magnetic fields. In this situation, $\epsilon_{\mu\nu\rho\sigma} F^{\mu\nu} F^{\rho\sigma} = 8\mathbf{E} \cdot \mathbf{B} \neq 0$, which leads to a monodromy (see for example [82]) breaking of the discrete shift symmetry in θ. Then, moving between adjacent minima can change the energy in the electromagnetic fields and there are transitions from one vacuum to another of lower energy. We will compute the nucleation rate of such processes both in the thin wall and thick wall limits.

First we consider the Witten and Sikivie effects in section 3.3. These are the effects that will be responsible for screening the electromagnetic fields. Then in section 3.4 we describe domain wall nucleation without taking into account this screening. This will be done by taking an appropriate 'no back-reaction' limit. This analysis gives the correct leading order expression for the decay rate (up to an overall $\mathcal{O}(1)$ coefficient in the thick wall case that we comment on). However, in order to pin down the symmetries and time evolution of the domain wall, we have to include back-reaction due to the Witten and Sikivie effects. We do this in section 3.5.

3.3 The Witten and Sikivie Effects

The equations of motion for the axion and photon fields are obtained by varying the action of eq. (3.18), with $V_{\rm N}(\theta)$ given in eq. (3.19). These equations are:

$$-\partial_t^2\theta + \partial_i^2\theta = m^2\left(\frac{1}{N}\sin(N\theta) - K\frac{\alpha}{8\pi}\left(\frac{1}{mf}\right)^2\epsilon^{\mu\nu\rho\sigma}F_{\mu\nu}F_{\rho\sigma}\right), \tag{3.20}$$

$$\partial_\mu F^{\nu\mu} = -\frac{K\alpha}{2\pi}\epsilon^{\mu\nu\rho\sigma}\partial_\mu(\theta F_{\rho\sigma}), \tag{3.21}$$

$$\epsilon^{\mu\nu\rho\sigma}\partial_\nu F_{\rho\sigma} = 0, \tag{3.22}$$

where the last equation is the Bianchi identity. For constant electromagnetic and θ fields, eq. (3.21) and eq. (3.22) are automatically satisfied. If so, we can also satisfy eq. (3.20) by ensuring that its right hand side vanishes (when the term involving the electromagnetic fields has magnitude smaller than $1/N$). Such values of θ label the minima and maxima of an "effective" potential for constant electric and magnetic field backgrounds. The extrema of this potential are given by solutions to the equation:

$$\sin(N\theta) = \frac{NK\alpha}{\pi}\frac{\mathbf{E}\cdot\mathbf{B}}{(mf)^2}. \tag{3.23}$$

In particular, in a setup with constant $\mathbf{E}$ and $\mathbf{B}$ fields oriented along the $+z$-axis the $F\tilde{F}$ term is non-zero and the axion field is displaced from the origin, also acquiring a non-zero value. In this background, with the axion in a local minimum of its potential, we are interested in discussing a process that corresponds to the tunneling of the axion field under the potential barrier [8]. As usual, the tunneling event results in the creation of a bubble inside which the axion is different from (and in our case larger than) its asymptotic value in the local minimum. The boundary of this bubble is an axion domain wall that interpolates between the value of the axion inside the bubble and its value in the local minimum. This domain wall bubble is nucleated

at rest so all time derivatives vanish initially[4]. However, as the axion field varies in space, it induces effective current and charge densities in the Maxwell equations due to the Chern-Simons term on the right hand side of equation (3.21). These effects will modify the electromagnetic fields inside and around the bubble. We may compute corrections to the electric and magnetic fields by integrating eq. (3.21) subject to the Bianchi identity of eq. (3.22). In vector component form, eq. (3.21) reads

$$\nabla \cdot \mathbf{E} = -\frac{K\alpha}{\pi}\nabla \cdot (\theta \mathbf{B}), \quad \text{and} \quad \nabla \times \left(\mathbf{B} - \frac{K\alpha}{\pi}\theta \mathbf{E}\right) = \partial_t \left(\mathbf{E} + \frac{K\alpha}{\pi}\theta \mathbf{B}\right), \quad (3.24)$$

and the Bianchi identity remains the same as in Maxwell electrodynamics. Since all time derivatives vanish on the initial time slice that we are focusing on, we can use the Bianchi identities to reduce equations (3.24) to the simple form:

$$\nabla \cdot \mathbf{E} = -\frac{K\alpha}{\pi}\nabla\theta \cdot \mathbf{B}, \quad \text{and} \quad \nabla \times \mathbf{B} = \frac{K\alpha}{\pi}\nabla\theta \times \mathbf{E}. \quad (3.25)$$

We can view the first equation in eq. (3.25) as a modified Gauss Law, with $\rho_E \sim -\mathbf{B} \cdot \nabla\theta$. The fact that axion gradients parallel to magnetic fields behave like effective electric charges is a manifestation of the Witten effect [6, 7]. More precisely, with a monopole present $\nabla.B \neq 0$, and $\rho_{\rm E} \sim -\alpha\nabla.(\theta\mathbf{B})$, indicating that an integral over a two sphere would demonstrate that the monopole has picked up electric charge in a constant θ background. In our case, this equation implies that the axion domain wall carries electric charge in a transverse background **B**-field, and we do not consider monopoles. In particular, when the magnetic field is oriented along the $+z$ direction as in our setup, the axion domain wall on the initial time slice acquires an effective electric charge density $\rho_{\rm E} \propto \cos\sigma$ where σ is the polar angle measured from the $+z$-axis. The sign of the electric charge is positive in the

[4]The fields are nevertheless evolved non-trivially in Euclidean time, where a bubble emerges from the vacuum at negative Euclidean time, and upon reaching critical radius at Euclidean time $\tau = 0$, then proceeds to expand in real time. Section 3.5 automatically incorporates this point.

northern hemisphere and negative in the southern hemisphere so as to produce an electric field that (partially) screens the original electric field inside the bubble. This is similar to what happens in Schwinger pair production [19]. That said, just outside the poles of the bubble, we expect the electric field to be enhanced compared to its original background value. Finally, we note that the induced charge is proportional to the magnetic field rather than the electric field as happens when polarizing a material.

Similarly, the second of eq. (3.25) is a modified Ampère's law where the cross product on the right hand side represents an effective current density. This effect, whereby axion domain walls carry currents in the presence of parallel background electric fields, has been described a while ago by Sikivie [83, 84] and we will refer to this phenomenon as the Sikivie effect or anomalous Hall effect. Since our background electric field is aligned along the $+z$-axis, the cross product means that the effective current density is of the form $\mathbf{j} \propto \sin\sigma\hat{\varphi}$ where φ is the azimuthal angle in $3d$ space and $\hat{\varphi}$ is the unit vector in the direction of increasing φ. This Hall current is localised on the domain wall and has a magnitude that peaks on the equator. This current is always in the $\hat{\varphi}$-direction and leads to an anti-screening (enhancement) of the magnetic field inside the bubble. The same current, however, leads to a screening of the magnetic field just outside the bubble and near the equator. Again, we note that the value of the current is proportional to the electric field value in the background.

The qualitative discussion above shows that, once back-reaction is taken into account, the electromagnetic fields inside and around the bubble are modified from their original background values. It is then easy to see that this would affect the axion bubble solution itself by considering eq. (3.20) for example. Of course, the equations (3.20), (3.21) and (3.22) should all be solved simultaneously, and we will do this below, but let us first briefly comment on what we would expect from such a

solution. This discussion will be heuristic but helpful in understanding the nature of the solution we get.

Going back to the initial time slice, the pattern of (anti-)screening of the electric/magnetic fields discussed above leads to the following observations. First note that the effective charge (current) density leads to a uniform electric (magnetic) field inside the bubble. This is easy to see by analogy with elementary problems in electrodynamics: The distribution of the effective charge density is similar to that of a dielectric sphere in a background electric field which is known to give a uniform electric field inside the sphere. Similarly, the current density is like that of a charged spherical shell rotating at constant angular velocity which gives a uniform magnetic field inside the shell. Deep inside the bubble, the electric and magnetic fields are then constant and so is the value of the axion field which is set by eq. (3.23).

Now imagine moving from the center of the bubble towards the north pole. All fields remain constant until we get close to the bubble wall. We know that the electric field is larger outside the bubble above the north pole. As such, we expect the axion value to be larger above the north pole. Heuristically one can again see this using eq. (3.23) although this is only heuristic because we are ignoring all derivatives. Conversely, we can imagine moving from the center of the bubble towards the equator. All fields are again constant but once we get close to the bubble wall, the magnetic field starts to decrease. The same heuristic argument, using eq. (3.23), now tells us that the axion field should be lower around the equator of the bubble. These two effects, i.e. larger axion field values just outside the poles and smaller field values around the equator, means that bubble is elongated along the $+z$-axis (recall that the inside of the bubble has a larger field value than the outside). We now turn to a more quantitative analysis of this bubble nucleation process.

3.4 Bubble Nucleation with the $O(4)$ Ansatz

In this section we study axion domain wall nucleation in the limit where we can ignore the back-reaction on electromagnetic fields. This is the first iteration of the solution describing the nucleation process and we will improve this in the following section by including back-reaction effects. Said differently, the Witten and Sikivie effects discussed in the previous section that lead to screening of the electromagnetic fields and elongation of the nucleated bubbles are ignored. As mentioned previously, we will calculate the (thin-wall) bubble nucleation rate and the critical bubble radius in this approximation which is sufficient to get the correct parametric dependence and provide an analytic understanding of the process. These limits will be made more precise below.

We will use Coleman's Euclidean prescription [8] to calculate the domain wall nucleation rate and the critical bubble size. As such, we first Wick rotate the action (3.18) to Euclidean signature (taking $\tau = it$) to get:

$$I_{\rm E} = \int d^4x \left(\frac{1}{4} F_{\mu\nu} F^{\mu\nu} + \frac{f^2}{2} \partial_\mu \theta \partial^\mu \theta + V_{\rm N}(\theta) - i \frac{K\alpha}{8\pi} \theta \epsilon_{\mu\nu\rho\sigma} F^{\mu\nu} F^{\rho\sigma} \right), \tag{3.26}$$

where $\epsilon_{123\tau} = +1$ (note the difference from the Lorentzian signature in eq. (3.18)). Also, $iA_\tau = A_0$, so the components of $F_{\mu\nu}$ here are not the same as in Lorentzian signature.

With this action, the equations of motion become:

$$\partial_\tau^2 \theta + \partial_i^2 \theta = m^2 \left(\frac{1}{N} \sin(N\theta) - iK \frac{\alpha}{8\pi} \left(\frac{1}{mf} \right)^2 \epsilon^{\mu\nu\rho\sigma} F_{\mu\nu} F_{\rho\sigma} \right), \tag{3.27}$$

$$\partial_\mu F^{\nu\mu} = i \frac{K\alpha}{2\pi} \epsilon^{\mu\nu\rho\sigma} \partial_\mu (\theta F_{\rho\sigma}), \tag{3.28}$$

$$\epsilon^{\mu\nu\rho\sigma} \partial_\nu F_{\rho\sigma} = 0. \tag{3.29}$$

Once more, these equations are easy to satisfy with constant electromagnetic and θ fields and these solutions correspond to, when rotated back to Lorentzian signature, the solutions we discussed in section 3.3. In Euclidean signature, the field strength tensor has imaginary electric field components and real magnetic field components.

We will consider the case where the electromagnetic fields are identically constant. More precisely, we take a limit where we can ignore the back-reaction of the axion field on the electromagnetic fields. This can be done by taking $\alpha \to 0$ and $F_{\mu\nu} \to \infty$ keeping the product $\alpha \epsilon^{\mu\nu\rho\sigma} F_{\mu\nu} F_{\rho\sigma}$ finite, or more precisely, keeping $\sqrt{\alpha} F_{\mu\nu}$ finite. In this limit, the right hand side of eq. (3.28) vanishes but the term in eq. (3.27) arising from the Chern-Simons interaction remains relevant. We can then study axion electrodynamics in the presence of non-dynamical background electromagnetic fields which we now do. We will show in section 3.5 that this limit is a consistent leading order solution.

For concreteness, we orient our coordinate system such that the background electric and magnetic fields are $\mathbf{E} = E\hat{\mathbf{z}}$ and $\mathbf{B} = B\hat{\mathbf{z}}$ respectively. Since the parallel background electric and magnetic fields spontaneously break the shift symmetry in θ, the potential when we are ignoring the dynamics of the electromagnetic field is

$$\frac{V(\theta)}{m^2 f^2} = \frac{1}{N^2}\Big(1 - \cos(N\theta)\Big) - K\frac{\alpha E B}{\pi m^2 f^2}\theta. \tag{3.30}$$

The extrema are given by solutions to the equation:

$$\sin(N\theta) = NK\frac{\alpha E B}{\pi m^2 f^2}, \tag{3.31}$$

where we will study the case in which the right hand side has magnitude less than unity so that there are static non-rolling solutions. There is then a transition process

in which the false vacuum at one minimum of the potential tunnels to a lower minimum. In this process, a background value of θ exists in space, and bubbles of higher values of θ with lower potential are spontaneously nucleated. We now solve for the bubble profile and compute the nucleation rate in the special case of the thin wall limit.

To work in the thin wall regime, we consider parameters where $NK\alpha EB/m^2f^2 \ll 1$ and $N\theta \ll 1$ (while still working in the limit of negligible back-reaction). Then a minimum exists at $\theta = \theta_0$ which is given by a solution of eq. (3.31)

$$\theta_0 \approx K\frac{\alpha EB}{\pi m^2 f^2}, \tag{3.32}$$

with a subsequent minimum at $\theta = \theta_0 + 2\pi/N$. Following [10], we expect that the solution with highest symmetry has the lowest action and therefore dominates the nucleation process. As such, we look for an $O(4)$ symmetric instanton solution for the axion so that $\theta = \theta(u)$ with $u = m\sqrt{\tau^2 + x^2 + y^2 + z^2}$ the dimensionless radial coordinate. Then eq. (3.20) becomes approximately

$$\frac{d^2\delta\theta}{du^2} + \frac{3}{u}\frac{d\delta\theta}{du} = \frac{1}{N}\sin(N\delta\theta) + \mathcal{O}(\theta_0) \tag{3.33}$$

where we have defined $\delta\theta = \theta(u) - \theta_0$ and expanded the right hand side in the limit $\theta_0 \ll 1$ as follows from eq. (3.32). This gives the equation of motion for a particle rolling in a potential with dimensionless time u in the presence of a damping force inversely proportional to u. Neglecting the friction term in the thin wall limit, we find that the sine-Gordon soliton is an appropriate solution:

$$\theta(u) = \theta_0 + \frac{2\pi}{N} - \frac{4}{N}\arctan\Big(\exp(u - u_*)\Big). \tag{3.34}$$

The wall thickness is therefore $\mathcal{O}(m^{-1})$ and the wall is situated at $x = m^{-1}u_*$. We may find u_* by substituting this solution in (3.26) and minimizing to obtain the critical bubble size:

$$u_* \approx \frac{12m^2 f^2}{\alpha KNEB}. \tag{3.35}$$

Moreover, using the critical radius we can compute the value of the Euclidean action which directly gives the nucleation rate for such a thin-wall bubble:

$$\Gamma/V \sim \exp\left(-\frac{6912\pi^2 m^4 f^8}{(\alpha KEB)^3 N^5}\right). \tag{3.36}$$

Let us also compare this result with eq. (1.1). The large numerical factor is largely geometric in origin, in that it comes from ratios of volume and area elements - raised to the fourth power - in higher dimensions. It is expected that as m increases, tunneling become more difficult since the wall tension is $T \sim mf^2/N^2$, and therefore there is a greater action, and energy, cost to nucleating a heavier wall. The same argument holds for f. As α becomes smaller, the process is more suppressed since the bubble size scales as $u_* \sim 1/KN\alpha EB$, and therefore a larger critical bubble must be nucleated, mandating a larger action cost. The same argument holds for the background electric and magnetic fields. Increasing N makes the tunneling faster since it effectively decreases the wall tension; increasing K also speeds up the rate since it effectively increases the coupling α. One can also infer the same conclusion by observing eq. (3.35), since increasing K or N simply means that a smaller critical bubble gets nucleated, which certainly has a lower action cost.

3.5 Back-Reaction and the $O(2) \times O(2)$ Solution

We now turn to the fully back-reacted solution. Due to the directionality of the background fields, and as per the discussion in section 3.3, we should not expect the fully back-reacted instanton to be $O(4)$-symmetric as in the case without back-reaction. The back-reaction we find only preserves an $O(2) \times O(2)$ subgroup of the full $O(4)$: the first factor rotates the τz-plane, and the second rotates the xy-plane. To be more precise, we can certainly expect, based upon the parallel electric and magnetic field background, there is a rotational symmetry corresponding to rotations in the xy plane; the assumption of an additional rotational symmetry in the τz plane is purely an ansatz, and we will show this holds by explicitly obtaining a solution[5]. This is the instanton we will look for in this section. As we will see, knowing this symmetry helps inform our coordinate and gauge choices making the problem more tractable.

Assuming that the back-reacted instanton solution preserves this $O(2) \times O(2)$ symmetry, we define dimensionless radial coordinates in the xy- and τz-planes:

$$r = m\sqrt{x^2 + y^2}, \quad \rho = m\sqrt{\tau^2 + z^2}. \tag{3.37}$$

In this coordinate system, the fields in Euclidean signature are simply $\theta = \theta(\rho, r)$, and $A = A_\mu dx^\mu = A_\rho(\rho, r)d\rho + A_\sigma(\rho, r)d\sigma + A_r(\rho, r)dr + A_\phi(\rho, r)d\phi$. We use σ and ϕ to denote the angular coordinates in the τz- and xy- planes respectively and all fields are independent of (ϕ, σ) by symmetry. We now have the $O(2)\times O(2)$ ansatz.

It is easier to solve for the gauge fields rather than the field strength directly.

[5]However, note that we do not prove that this ansatz gives the lowest Euclidean action configuration, and finding a solution does not necessarily exclude the possibility of there existing a lower action solution with a different symmetry group.

The Bianchi identity is now $\nabla_\nu(\epsilon^{\mu\nu\alpha\beta}F_{\alpha\beta}) = 0$, and if the gauge field depends only on the radial coordinates, then we can see that the Binachi identity is automatically satisfied. In fact, we may re-express it as

$$[\mu\nu\alpha\beta]\partial_\mu\partial_\alpha A_\beta = 0, \tag{3.38}$$

and the contraction of the anti-symmetric symbol with two symmetric partial derivatives manifestly vanishes. A point to note here is that due to the coordinates, the anti-symmetric symbol is now $[\mu\nu\alpha\beta]$, and $\epsilon_{\mu\nu\alpha\beta} = \sqrt{h}[\mu\nu\alpha\beta]$, along with $\epsilon^{\mu\nu\alpha\beta} = [\mu\nu\alpha\beta]/\sqrt{h}$ in Euclidean signature. It is $\epsilon_{\mu\nu\alpha\beta}$ that transforms as a tensor. Previously in Cartesian coordinates, we did not need to make this distinction.

In addition, we have the freedom to pick a convenient gauge choice. Our ansatz above already assumes that the gauge fields are independent of the angular coordinates so that we may no longer perform gauge transformations that depend on the angular coordinates since these spoil the ansatz. That said, we may still consider $A \to A + d\Lambda(\rho, r)$.

We now pick $\Lambda(\rho, r)$ such that A_r vanishes. This gauge choice eliminates one of the field components; we can still perform gauge transformations that depend on ρ only, but let us check that this is enough to eliminate $A_\rho(\rho, r)$. Consider an equation of motion, eq. (3.28):

$$\nabla_\mu F^{\nu\mu} = i\frac{K\alpha}{\pi}\epsilon^{\mu\nu\alpha\beta}\partial_\mu\theta\partial_\alpha A_\beta. \tag{3.39}$$

Since the derivatives on the right hand side must be either ρ or r, but not simultaneously both, it follows that if ν were picked to be one of these two coordinates, then the right hand side would necessarily vanish due to repeated

indices on the Levi-Civita tensor. The covariant derivative is important here due to our coordinates. The left hand side of eq. (3.39) can be evaluated using the $\nabla_\mu F^{\nu\mu} = \partial_\mu F^{\nu\mu} + \Gamma^\mu_{\mu\sigma} F^{\nu\sigma} + \Gamma^\nu_{\mu\sigma} F^{\sigma\mu} \to \partial_\mu F^{\nu\mu} + \Gamma^\mu_{\mu\sigma} F^{\nu\sigma}$ since $F_{\mu\nu}$ is anti-symmetric. Furthermore, the remaining Christoffel symbol can be expanded to give $\nabla_\mu F^{\nu\mu} = h^{-1/2}\partial_\mu(h^{1/2}F^{\nu\mu})$ where h is the determinant of the metric $h_{\mu\nu} = \mathrm{diag}(1, r^2, 1, \rho^2)$ in the $O(2) \times O(2)$ adapted coordinate system.

Upon inspecting the $\nu = \rho$ and r components of eq. (3.39), we find that $A_\rho(\rho, r)$ must satisfy

$$\partial_\rho(r\rho\partial_r A_\rho) = 0, \text{ and } \partial_r(r\rho\partial_r A_\rho) = 0, \tag{3.40}$$

implying that $r\rho\partial_r A_\rho$ is constant, from which it follows that

$$A_\rho = \frac{k}{\rho}\log r + f(\rho), \tag{3.41}$$

where k is an integration constant and $f(\rho)$ is an arbitrary function of ρ. Requiring non-singular behavior at either $r = 0$ or $\rho = 0$ compels us to choose $k = 0$. But then A_ρ is a function of ρ only, which we happily gauge away since carrying out a gauge transformation of the type $A \to A + d\Lambda(\rho)$ will not alter the other components. This is another piece of the gauge field that now vanishes. Therefore, we may obtain the entirety of the information regarding the electric and magnetic fields by solving for θ, A_ϕ, and A_σ.

We will be calculating in the weak coupling limit in which $\alpha \ll 1$. It is useful to organize the equations in powers of α. To this end, we rescale $A_\mu \to \sqrt{\alpha}A_\mu/m$. The

Euclidean equations of motion (3.27) and (3.28) are now:

$$\partial_\rho^2\theta + \frac{\partial_\rho\theta}{\rho} + \partial_r^2\theta + \frac{\partial_r\theta}{r} - \frac{\sin(N\theta)}{N} + \frac{iK}{\pi r\rho}\left(\frac{m}{f}\right)^2 (\partial_\rho A_\sigma \partial_r A_\phi - \partial_r A_\sigma \partial_\rho A_\phi) = 0, \tag{3.42}$$

for the axion, as well as:

$$\partial_\rho^2 A_\sigma - \frac{\partial_\rho A_\sigma}{\rho} + \partial_r^2 A_\sigma + \frac{\partial_r A_\sigma}{r} - \frac{iK\alpha}{\pi}\frac{\rho}{r}(\partial_r\theta\partial_\rho A_\phi - \partial_\rho\theta\partial_r A_\phi) = 0, \tag{3.43}$$

$$\partial_\rho^2 A_\phi + \frac{\partial_\rho A_\phi}{\rho} + \partial_r^2 A_\phi - \frac{\partial_r A_\phi}{r} - \frac{iK\alpha}{\pi}\frac{r}{\rho}(\partial_r\theta\partial_\rho A_\sigma - \partial_\rho\theta\partial_r A_\sigma) = 0. \tag{3.44}$$

for the gauge boson.

We now have a system of non-linear coupled partial differential equations, and in general we do not expect analytic solutions. The last two equations encapsulate the Witten and Sikivie effects. As a sanity check, let us first consider the familiar small back-reaction limit which is the limit $\alpha \to 0$ in the above equations. We may neglect the non-linear $\mathcal{O}(\alpha)$ terms in equations (3.43) and (3.44). Then the background configurations of constant electric and magnetic fields - E_0 and B_0 respectively - solve these two equations; i.e.

$$i\tilde{A}_\sigma = \frac{\tilde{E}_0\rho^2}{2m^2}, \quad \text{and} \quad \tilde{A}_\phi = \frac{\tilde{B}_0 r^2}{2m^2}. \tag{3.45}$$

where we have denoted $\tilde{E}_0 = \sqrt{\alpha}E_0$ and $\tilde{B}_0 = \sqrt{\alpha}B_0$. We may then substitute these expressions in eq. (3.42), which reduces to

$$\partial_\rho^2\theta + \frac{\partial_\rho\theta}{\rho} + \partial_r^2\theta + \frac{\partial_r\theta}{r} - \frac{\sin(N\theta)}{N} + \frac{K}{\pi}\left(\frac{m}{f}\right)^2 \frac{\tilde{E}_0\tilde{B}_0}{m^4} = 0. \tag{3.46}$$

This is readily solved by the $O(4)$ symmetric ansatz [10]: if one takes $\theta(\rho, r) = \theta(\sqrt{\rho^2 + r^2})$, then it follows that

$$\partial_\rho^2\theta + \rho^{-1}\partial_\rho\theta + \partial_r^2\theta + r^{-1}\partial_r\theta \to \partial_u^2\theta + 3u^{-1}\partial_u\theta, \tag{3.47}$$

where now $u = \sqrt{\rho^2 + r^2}$. We therefore obtain

$$\frac{d^2\theta}{du^2} + \frac{3}{u}\frac{d\theta}{du} - \frac{\sin(N\theta)}{N} + \frac{K}{\pi}\left(\frac{m}{f}\right)^2 \frac{\tilde{E}_0\tilde{B}_0}{m^4} = 0, \tag{3.48}$$

at $\mathcal{O}(\alpha^0)$ which we may solve numerically, or with a phenomenological approximation to the wall profile, or with the thin wall approximation under appropriate circumstances. We call this $O(4)$ symmetric solution $\tilde{\theta}(u)$. It is by solving this expression that we may obtain the bounce exponent in $\Gamma/V \sim \exp(-I_B)$, such as in section 3.4.[6] Incorporating back-reaction effects should then give $\mathcal{O}(\alpha)$ corrections to the exponent. It is also now clear why the procedure of section 3.4 was justified: the regime in which $\alpha \ll 1$, but $\tilde{E}_0$ and $\tilde{B}_0$ are held fixed (eq. (3.45)), gives a critical size to the bubble which depends only on $\tilde{E}_0\tilde{B}_0 = \alpha E_0 B_0$, as we see in eq. (3.35). Back-reaction effects are corrections on top of this $\mathcal{O}(\alpha^0)$ profile. Typically, we can only solve the set of equations (3.42), (3.43) and (3.44) numerically subject to specific boundary conditions, as we now discuss.

In order to do that, we have to impose appropriate boundary conditions on the fields. Far away from the origin (i.e. when $\rho \to \infty$ or $r \to \infty$), all fields must match on to their asymptotic values. These are the ones given in eqs. (3.45) for A_ϕ and A_σ. For the axion field θ, it should match to a value θ_0 given by a solution to eq. (3.23). In addition, all fields must obey vanishing Neumann boundary conditions

[6] We note that numerical solutions show that even thick wall cases possess the same bounce exponent as in eq. (4.2) up to an overall $\mathcal{O}(1)$ multiplicative factor. Nevertheless, an $\mathcal{O}(1)$ reduction in the exponent can lead to a significant enhancement of the nucleation rate.

at $r = 0$ or $\rho = 0$ to avoid spurious singularities. Finally, we also impose the Dirichlet conditions $A_\phi = 0$ at $\rho = 0$ and $A_\sigma = 0$ at $r = 0$ since these determine components of the **E** and **B** fields that vanish by the symmetry of the problem. We show two examples of the solutions to these equations in the next subsection. Note the presence of the features discussed in section 3.3, i.e. the elongation of the instanton solution and the (anti-)screening of the electric and magnetic fields.

The interaction of the axion with the gauge field will induce changes in both these fields. Concretely, we denote these changes through the following perturbations: $\theta(\rho, r) = \tilde{\theta}(u) + \alpha\delta\theta(\rho, r)$, $A_\phi(\rho, r) = \tilde{A}_\phi(\rho) + \alpha\delta A_\phi(\rho, r)$, and $A_\sigma(\rho, r) = \tilde{A}_\sigma(r) + \alpha\delta A_\sigma(\rho, r)$, with the expansion truncated to first order in α.

It then follows from eq. (3.43) and eq. (3.44) that the gauge field perturbations satisfy the following differential equations at $\mathcal{O}(\alpha)$:

$$\partial_\rho^2 \delta A_\sigma - \frac{\partial_\rho \delta A_\sigma}{\rho} + \partial_r^2 \delta A_\sigma + \frac{\partial_r \delta A_\sigma}{r} = -\frac{iK}{\pi}\frac{\tilde{B}_0}{m^2}\frac{\rho^2}{\sqrt{\rho^2 + r^2}}\frac{d\tilde{\theta}}{du}, \tag{3.49}$$

$$\partial_\rho^2 \delta A_\phi + \frac{\partial_\rho \delta A_\phi}{\rho} + \partial_r^2 \delta A_\phi - \frac{\partial_r \delta A_\phi}{r} = \frac{K}{\pi}\frac{\tilde{E}_0}{m^2}\frac{r^2}{\sqrt{\rho^2 + r^2}}\frac{d\tilde{\theta}}{du}. \tag{3.50}$$

Note that the terms on the right hand sides of both equations above show that the varying axion profile sources the change in the electric and magnetic fields from their unperturbed background values. We also find that at corrections linear in α, the components of the gauge field perturbation effectively decouple. In general though, gauge field components will not decouple order by order with higher powers of α. We must now numerically integrate these equations, subject to the requirements above.

We may also compute the change in the bubble profile due to these back-reactions

of the electromagnetic field. From eq. (3.42), at $\mathcal{O}(\alpha)$,

$$\partial_\rho^2 \delta\theta + \frac{\partial_\rho \delta\theta}{\rho} + \partial_r^2 \delta\theta + \frac{\partial_r \delta\theta}{r} = \delta\theta \cos\tilde{\theta} - \frac{1}{\pi}\left(\frac{m}{f}\right)^2 \left(\frac{\tilde{E}_0}{m^2} \frac{\partial_r \delta A_\phi}{r} + \frac{\tilde{B}_0}{m^2} \frac{\partial_\rho \delta A_\sigma}{\rho} \right), \quad (3.51)$$

which upon integrating subject to the same Neumann boundary conditions as above, we obtain a modified bubble profile, which incorporates $O(2) \times O(2)$ corrections to the leading order $O(4)$ solution.

3.6 Example Solutions

We will now, utilizing some toy choice of parameters, demonstrate both thin wall and thick wall critical bubble solutions at nucleation and explore some of their features. We will also discuss the subsequent real time evolution of the nucleated bubbles.

Thin wall

Consider the choice $\alpha = 0.1, m/f = 0.1$, with anomaly coefficient and domain wall number set $K = N = 1$, as well as the background fields $E_0/m^2 = B_0/m^2 = 30$. The asymptotic value of the axion is $\theta_0 \approx 0.291$, while its interior value is $\theta_0 + 2\pi$. For the leading order $O(4)$ symmetric profile, we must solve eq. (3.48). In this regime the thin wall approximation is applicable since using eq. (3.35) one finds $u_* \approx 13.3 \gg 1$, and as shown in Fig. 3.3, the numerical solution is very well approximated by the thin wall solution from eq. (3.34).

We then use this leading solution in eqs. (3.42)-(3.44) to compute the back-reaction of the electric and magnetic fields, as well as the correction to the axion profile. Obtaining these solutions for the gauge field components, we then directly compute the electric and magnetic field perturbations. We take the $\tau = 0$ slice so $\rho \to z$, and by rotational symmetry, set $y = 0$ so that $r \to x$. See Fig. 3.5. Notice, given the

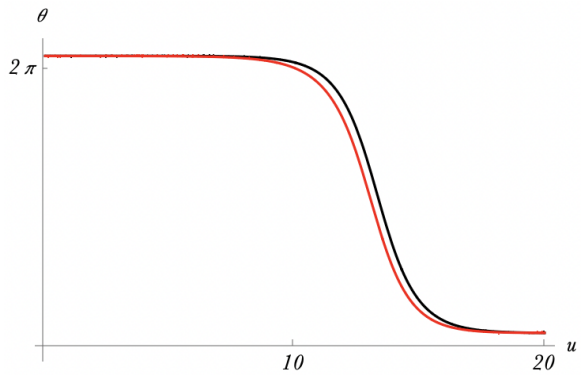

Figure 3.3: Bubble profile for $\tilde{\theta}(u)$ at leading order. The red curve denotes the numerical solution, and the black curve denotes the thin wall approximation (see text).

bubble profile, the electromagnetic field pattern is intuitively what we expect based upon the discussion in section 3.3. The modified axion profile is shown in Fig. 3.6.

We would also like to observe the energy density distribution in the xz -plane. The wall will carry positive energy due to a varying axion profile of course, but we would like to see where this energy is sourced from. To that end, we use the Hilbert energy momentum tensor:

$$T^{\mu\nu} = F^{\mu\lambda}F^{\nu}_{\ \lambda} + f^2\partial^\mu\theta\partial^\nu\theta - \eta^{\mu\nu}\left(\frac{1}{4}F_{\alpha\beta}F^{\alpha\beta} + \frac{f^2}{2}(\partial\theta)^2 + \left(\frac{mf}{N}\right)^2\Big(1-\cos\left(N\theta\right)\Big)\right), \tag{3.52}$$

where we remark that the Chern-Simons term does not explicitly contribute[7]. Evaluating T^{00}, we find that the bubble interior has, to leading non-trivial order, *the same energy density as the far exterior*! In contrast, we see that the region of lower energy density is actually *outside* the bubble, like a doughnut - or torus - about the equatorial plane (see Fig. 3.4 and Fig. 3.7). This energy distribution is in stark

[7]The same arguments we made earlier carry through here; in particular, this stress tensor agrees with the canonical version despite seeming not to due to Chern-Simons terms that appear in the canonical form. Those terms cancel when simplified, giving agreement with the Hilbert form.

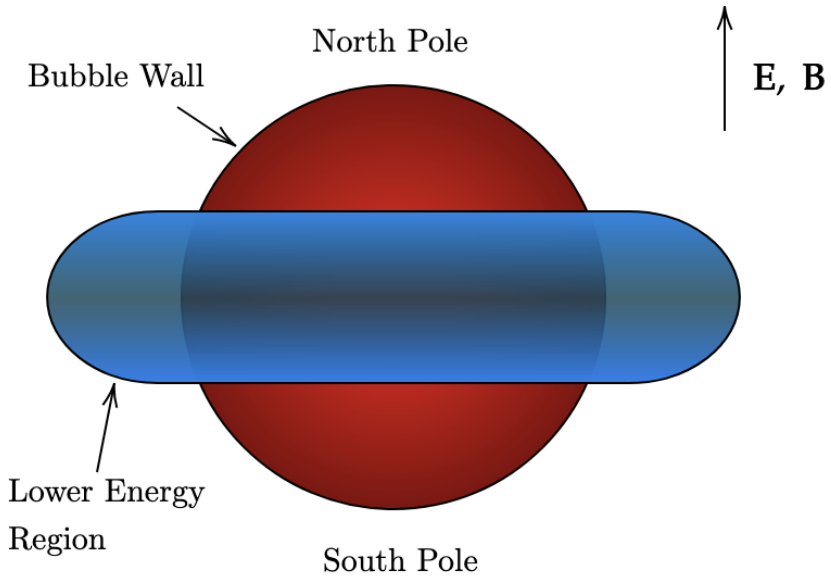

Figure 3.4: Cartoon of energy distribution, showing the bubble wall (red) and a region of lower energy density (blue), relative to the background, *outside* the bubble.

contrast to the usual version of false vacuum decay in which the interior contains lower energy density, as in [8] for instance. Moreover, it is different from even the $(1+1)d$ version. As far as we are aware, such a configuration is unlike anything else existing in the literature.

To explain this energy distribution, note that from eq. (3.52), the θ-dependent piece changes on the wall and gives positive energy density as anticipated. However, the bizarre energy distribution stems from the electromagnetic part. From Fig. 3.5, above the north pole, both electric and magnetic fields actually enhance the background electric and magnetic fields respectively. In the interior, the electric field is screened and the magnetic field is anti-screened, so the change in energy density cancels at this order, giving the same energy density as the far away false vacuum. Just outside the bubble, about the equatorial plane, Fig. 3.5 shows that *both* the electric and magnetic fields are screened, however. It is precisely this zone that has

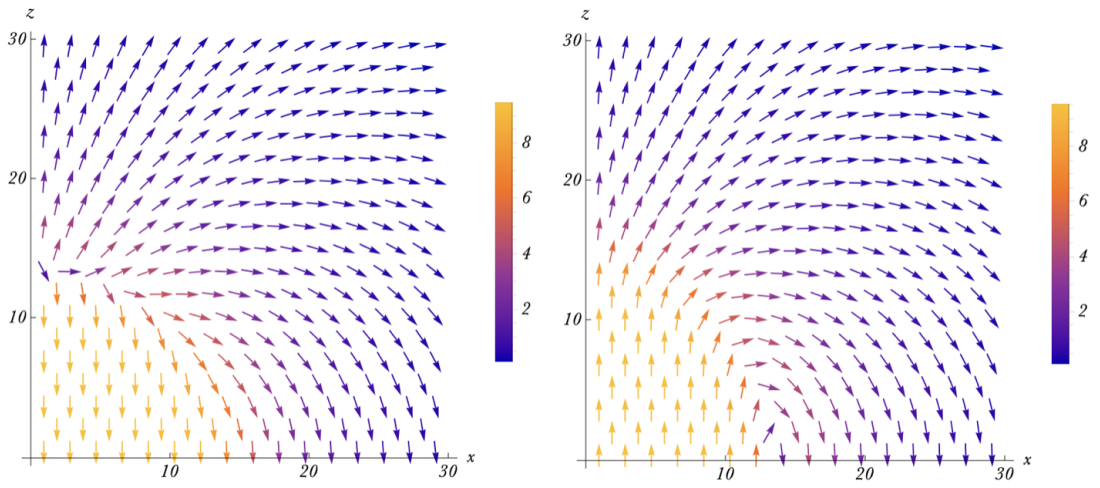

Figure 3.5: The left panel shows the electric field sourced by the nucleated axion domain wall; similarly the right panel shows the magnetic field induced by the domain wall currents (both fields divided by α). The constant $\hat{\mathbf{z}}$-directed background $\mathbf{E}$ and $\mathbf{B}$ fields are not shown. The induced fields partially screen the background $\mathbf{E}$ field inside the domain wall and less so outside around the equator, while anti-screening the $\mathbf{E}$ field outside the poles. The $\mathbf{B}$ fields are anti-screened inside the domain wall and somewhat less so outside the poles of the domain wall, but screened significantly in a torus shaped equatorial region outside the wall.

lower energy relative to the background. Despite initial appearances, this region actually has a large volume, which one can picture by rotating the diagrams around the z axis. So there is a torus-shaped region of lower energy density outside the prolate bubble.

Thick wall

Now consider the following choice of parameters: as before, $N = K = 1$, but now we set $\alpha = 0.1\pi$, $m/f = 1/\sqrt{2}$, $E_0/m^2 = 7$, $B_0/m^2 = 2$. The background value of the axion field is $\theta_0 \approx 0.775$. We find the leading order solution, given by numerically integrating eq. (3.48). The interior value of $\tilde{\theta}(u) - \theta_0$ as $u \to 0$ is

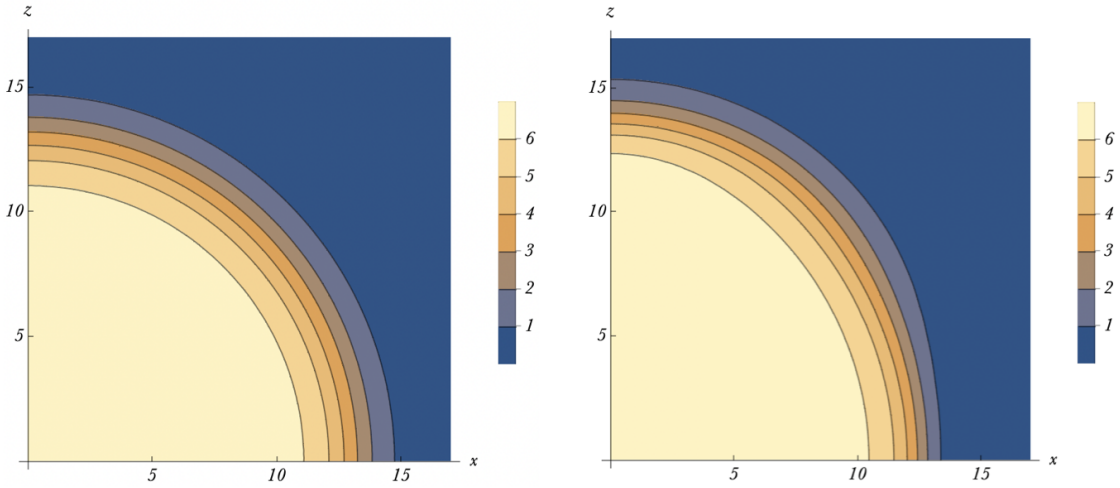

Figure 3.6: Left panel shows the leading-order O(4)-symmetric bubble profile $\tilde{\theta}(u)$, so not including back-reaction effects from the domain-wall-generated electric and magnetic fields. Contour lines indicate the value of the axion field varying from exterior value θ_0 to interior value $\theta_0 + 2\pi$ (we have taken $N = 1$). Right panel shows the bubble profile including leading-order back-reaction effects $\tilde{\theta}(u) + \alpha\delta\theta(\rho, r)$. The bubble has become slightly prolate.

approximately 5.71. In fact, as the field tunnels, it does not even reach a subsequent minimum, but emerges instead at some intermediate value, from which it will then classically roll in real time. We consider the real time evolution of this bubble below. Again, using these leading solutions, we can compute the back-reaction effects, which modify the shape of the bubble, using eq. (3.42) - eq. (3.44). Incorporating these effects in eq. (3.52) gives the energy density (with the background value subtracted), shown on the right hand side of Fig. 3.8. The dark blue region is the region of lower energy density.

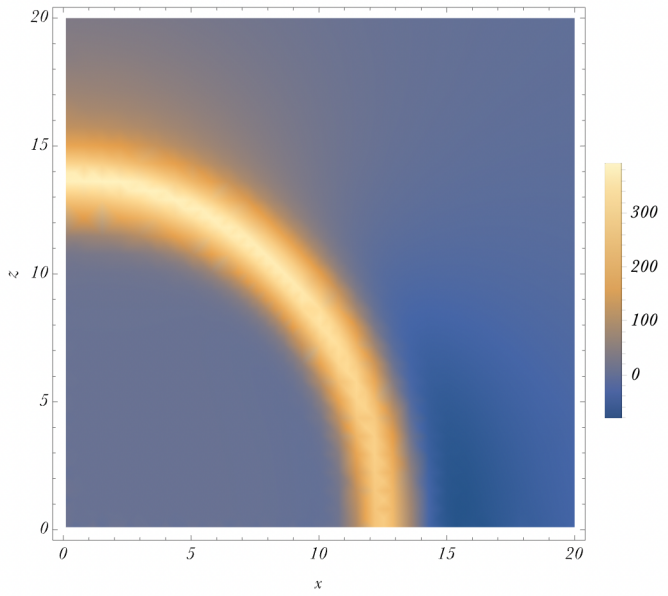

Figure 3.7: Energy density with the uniform background value subtracted. The bright yellow represents the wall. The pale blue in the bubble interior and far in the exterior indicate the same energy density at this order. The region of lower energy density is dark blue, just outside the bubble near the x axis. The pale yellow just above the north pole represents anti-screening (see text). The dark blue region dominates the volume-integrated change in energy upon rotating the figure about the z axis to obtain the full three dimensional picture.

3.7 Evolution in Real Time

The Euclidean evolution that we have been using prepares an initial state on the $t = 0$ time slice in Minkowski space. We will argue qualitatively why the bubble now expands, despite the fact that the lower energy density is now in the bubble exterior. We also look at numerical time evolution using the Lorentzian signature (classical) equations of motion in section 3.8. In this case, we find that it is numerically more efficient to track the electric and magnetic fields (and the axion) directly since these equations have single time derivatives. The equations we use are the Maxwell equations in eq. (3.24), the usual electromagnetic Bianchi identities and the axion

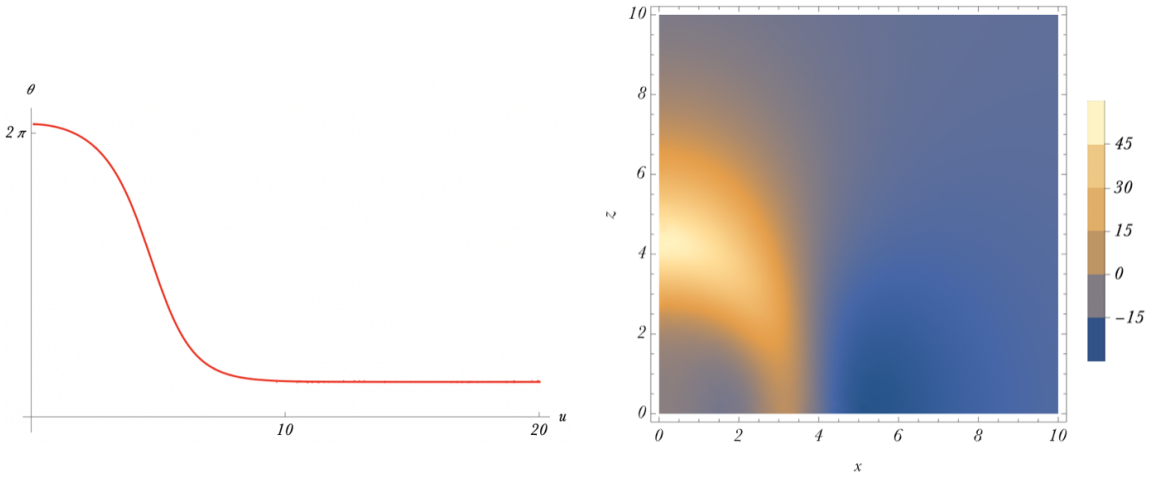

Figure 3.8: The left panel shows the thick wall bubble profile for $\tilde{\theta}(u)$ at leading order and at the instant of nucleation. The right panel shows the full energy distribution, including the back-reacted field profiles computed using $\tilde{\theta}(u)$, at nucleation. Observe again that the lower energy density region is outside the equator of the domain wall in a toroidally shaped region, rather than on the inside.

equation of motion in eq. (3.20).

Pressure differences on the bubble wall

We can intuitively understand the expansion of the bubble by studying the pressures on either side of the wall. To that end, we use the Hilbert energy momentum tensor eq. (3.52). It is convenient, though not essential, to have the thin wall profile of section 3.5 in mind (see also Fig. 3.9). We require the spatial components,

$$T_{ij} \approx \frac{1}{2}(E^2 + B^2)\delta_{ij} - (E_i E_j + B_i B_j). \tag{3.53}$$

Notice that since we are in the thin wall regime, the terms depending on axion derivatives are negligible away from the wall so we do not include them above. Furthermore, to leading non-trivial order in the α-expansion, the axion changes by

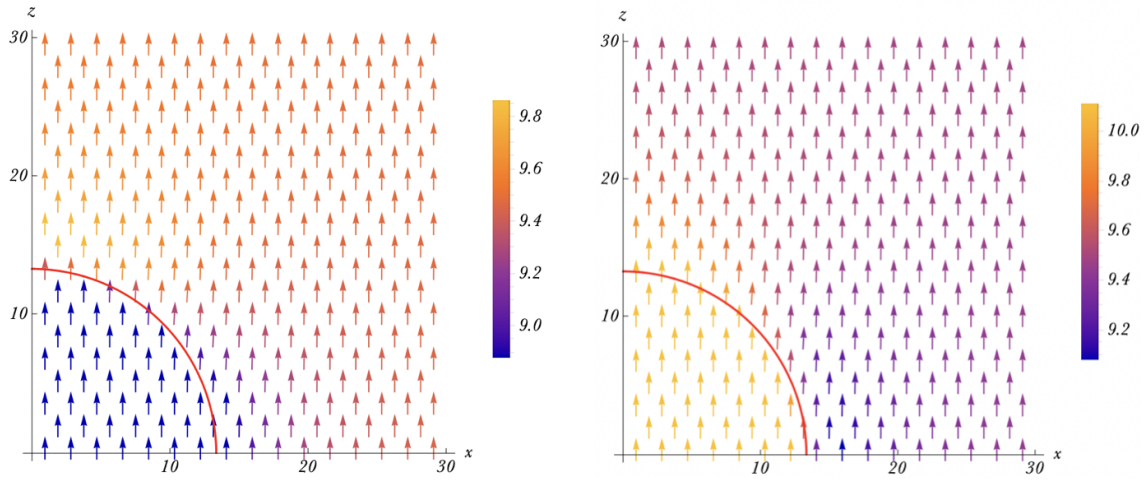

Figure 3.9: The left panel shows the back-reacted electric field from Fig. 3.5 superimposed on the background $\tilde{E}_0/m^2$. Similarly, the right panel shows the back-reacted plus the background magnetic field. The red line indicates the wall position (see section 3.5).

2π from one side of the wall to the other (here again we specialize to the $N = 1$ case, though similar statements are true for $N > 1$ as well), so we can drop the $\cos\theta$ potential term when computing pressure differences across the wall. As such, only the electromagnetic fields are important for this discussion.

Let us start by comparing the pressures along the z-axis on either side of the bubble wall near the north pole, i.e. with T_{zz}. Just outside the north pole, the electric field is anti-screened (enhanced) and the magnetic field is also enhanced. On the other side of the domain wall, i.e. just inside the bubble near the north pole, the magnetic field is still anti-screened, but the electric field is screened. A quick computation of $T_{zz} \approx -(E_z^2 + B_z^2)/2$ shows that the pressure is higher (i.e. less negative) inside the bubble causing a force in the $+z$-direction (see Fig. 3.9). So we infer an outward force along the north pole. A similar argument - due to the $O(2) \times O(2)$ symmetry - indicates that there is an outward force along the south

pole as well. Next, consider the pressure differences near the equator of the bubble in Fig. 3.9. For this, consider T_{rr} (in cylindrical coordinates). Just outside the bubble wall, along the x-axis or equatorial plane for that matter, E_x, E_y, B_x, and B_y all vanish by symmetry so only the z-components contribute to $T_{rr} \approx (E_z^2 + B_z^2)/2$ (the sign difference relative to T_{zz} is important here). Along the equator, slightly outside the bubble, both E_z and B_z are screened. On the other hand, just inside, only E_z is screened whereas B_z is enhanced (in fact, $E_z^2 + B_z^2$ inside is the same as the asymptotic exterior upto and including $\mathcal{O}(\alpha)$ corrections). Using these to compute T_{rr} shows that the pressure inside is a larger positive number than that outside, implying that there is an outward force along the equator. We may therefore understand the bubble evolution by considering pressure gradients associated with these semi-classical solutions.

3.8 A Russian Doll Instanton

As a concrete example, let us study the real time evolution of the thick wall bubble of section 3.5. On the initial time slice, we see the nucleated oblong bubble (right hand side of Fig. 3.8; Georges Obied has written the real time evolution code). The bubble wall interpolates over the potential barrier and the axion field inside the bubble lies on the other side of this potential potential barrier. Since this is a thick wall profile, the axion field tunnels from the false vacuum to some intermediate value between the false vacuum and true vacuum. Subsequently, in real time, the field rolls to the true vacuum. In fact, from Fig. 3.10, we see the axion traverses its field range three times before stabilising. In short, there is an initial quantum tunnelling, followed by two additional cascades from classical rolling. These give the domain wall an interested foliated structure that could lead to distinct observational signatures. We will study the phenomenology of these cascading decays in a more

general setting in future work.

Another feature of the back-reacted time evolution is the (anti-)screening of the electromagnetic fields. In the initial configuration, the fields have values that are different from the asymptotic background although not by much. By the time the bubble has expanded, the majority of the electric field inside the bubble has been screened. The magnetic field inside the bubble is larger than its initial value but in return it is screened in a larger volume around the bubble. By integrating the energy density inside and around the bubble, we can clearly see the nucleation and evolution of the axion domain wall leads to a lower energy configuration. This is yet another piece of evidence supporting our claim that parallel $\mathbf{E}$ and $\mathbf{B}$ fields will spontaneously nucleate axion domain walls as this process leads to a lower energy state. A striking feature of the axion domain wall profile is its lopsided oblong shape. In fact, we see that this asymmetry becomes more pronounced as the domain wall evolves in time.

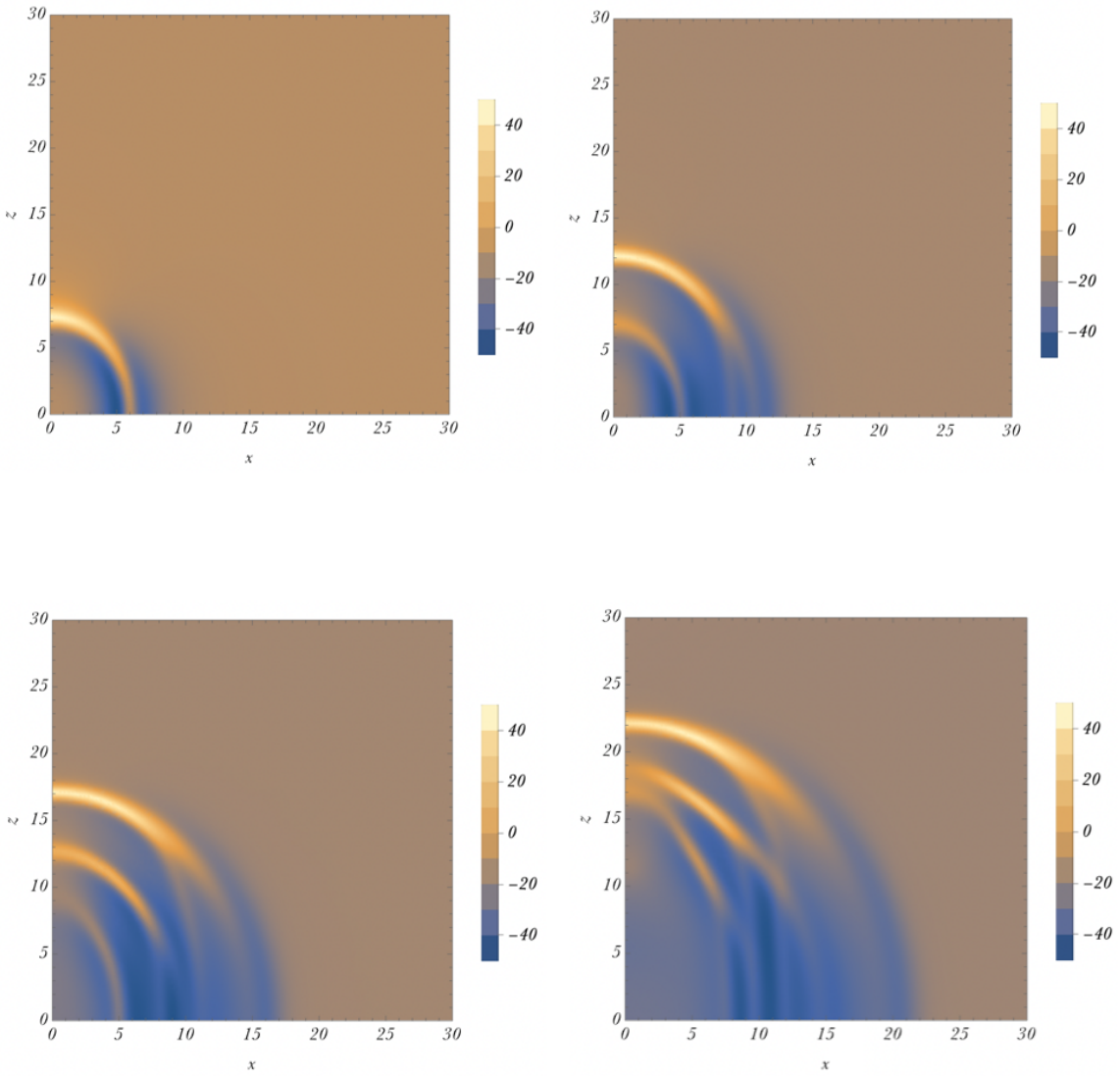

Figure 3.10: Real time evolution of the bubble energy density (in units of m^4, with background subtracted) for the thick wall bubble. The top left (right) is at $t = 20$ (40); the bottom left (right) is at $t = 60$ (80), in units of m^{-1}. The initial energy density at $t = 0$ is given by Fig. 3.8. Notice in this figure that the lower energy (dark blue) region is growing in time as the bubble expands.

Chapter 4

Bounds for Branes in de Sitter

In this chapter, we study the nucleation of branes in the presence of background electric fields.

The motivating purpose of this exploration is to extend the Festina Lente swampland conjecture to incorporate not just massive charged particles, but also branes. In particular, we are especially interested in branes that have a Wess-Zumino term on their worldvolume action. These operators appear naturally in string theory, and we will see that they are closely related to the axion domain wall nucleation problem - in the presence of background electric and magnetic fields - that we have so far considered. Notice a key point: axion domain walls in background electric and magnetic fields will be immensely helpful in finding the nucleation rate of branes, in the presence of only electric fields and not magnetic fields. It is a bound on this decay rate that remarkably relates brane tension, coupling, Planck mass, and Hubble size.

4.1 Nucleation with Nambu-Goto action

We would like to generalize the Festina Lente conjecture to branes in $(3+1)d$. First we will consider D2 branes, with a Wess-Zumino type worldvolume interaction[1]. We will show that this solution follows immediately from the (seemingly unrelated) Schwinger-like bubble nucleation process in axion-Maxwell theory that we have recently shown in the previous chapter. There, we showed that in the presence of parallel background electric and magnetic fields, the axion field can decay via bubble nucleation with energy coming from the screening the elctromagnetic field. Crucially, a topological Chern-Simons term, $\theta\epsilon_{\mu\nu\rho\sigma}F^{\mu\nu}F^{\rho\sigma}$, was responsible for assigning electric charges and currents to the bubble walls [6, 7, 83, 84], which allowed the decay to proceed.

Now we would like to first reformulate this result with a Nambu-Goto type action for thin walls. This procedure will then generalize to branes, and the axion will be a guiding light to deriving key results.

Chern-Simons Bubble Nucleation with Worldvolume Action

In the previous chapter we showed that in the presence of parallel background electric and magnetic fields, bubble nucleation occurs by the formation of axion domain walls. In the thin wall case the critical bubble size is

$$r_* = \frac{12mf^2}{\alpha EB}, \tag{4.1}$$

[1]Although we call these objects Dp branes, the form of the actions we will take will be fairly general and may apply to other such branes.

which must be larger than m^{-1} for consistency. We showed that the decay rate per unit volume is

$$\Gamma/V \sim \exp(-I_{\rm B}), \text{ with } I_{\rm B} \approx \frac{6912\pi^2 m^4 f^8}{(\alpha KEB)^3 N^5}. \tag{4.2}$$

Let us focus on the special case in which the nucleated bubble size is much larger than the wall thickness, i.e. the domain wall that is a boundary for the bubble is effectively two dimensional in space. Then the nucleation, and subsequent expansion, process should be describable with a woldvolume effective field theory, akin to how one realizes the Schwinger effect for point particles [19, 20] with an equivalent worldline action [14, 26] rather than the full Euler-Heisenberg action.

Concretely, we should have an action resembling a Nambu-Goto action with additional terms that lead to the nucleation of axion domain walls. Such as action is the following:

$$I = \int_{\rm Bulk} d^4x \left(-\frac{1}{4} F_{\mu\nu} F^{\mu\nu} \right) - T \int_{\rm WV} d^3\xi \sqrt{-h} + g \int_{\rm WV} d^3\xi \sqrt{-h} \epsilon^{abc} A_a F_{bc} \tag{4.3}$$

where the abbreviation WV denotes a worldvolume integral; ξ_a is an intrinsic brane coordinate and h_{ab} is the induced metric on the brane. T denotes the brane tension. The worldvolume indices are related to the bulk indices in the follwing way: for a tensor on the brane

$$S_{abc\ldots} = S_{\alpha\beta\gamma\ldots} e^\alpha_a e^\beta_b e^\gamma_c \ldots \tag{4.4}$$

where the projection tensor,

$$e^\alpha_a = \frac{\partial x^\alpha}{\partial \xi^a}, \tag{4.5}$$

denotes a projection of the (flat) bulk indices to the brane. For instance, we obtain the worldvolume metric from the bulk spacetime metric via

$$h_{ab} = \eta_{\alpha\beta} e^{\alpha}_{a} e^{\beta}_{b}. \tag{4.6}$$

Then the length of a line element on the worldvolume will match in both bulk and brane coordinates. We can infer the parameters of this action based on considering the thin wall case, a special class of solutions of eq. (3.20), in which the axion is of the form[2] $(\theta - \theta_0) \sim 2\pi(1 - H(r - r(t)))$, where H is the Heaviside function and θ_0 is the asymptotic value of the axion field. Then integrating by parts, the term $\theta F \wedge F \sim d\theta \wedge A \wedge F$ in eq. (3.18) becomes $A \wedge F$ upon integrating over r, since the derivative of a Heaviside function becomes a delta function in the radial coordinate. Comparing eq. (4.3) with eq. (3.18) indicates that $g \sim \alpha$.

Moreover, since we are considering a spherically symmetric θ profile, a simple scaling argument shows that integration over the derivative term (or potential term) of eq. (3.18) implies that $T \sim mf^2$. Here we have used the fact that the delta function has width $m^{-1} \to 0$, but we emphasize that this limit must be taken in the final step, or else one gets a product of delta functions. If we are solely interested in parametric form and scaling behavior, then we are done here. However, we will also describe an explicit matching procedure below in which we determine the values of T and g, including their numerical prefactors and not just their parametric scaling.

Additionally, on a technical note, the worldvolume action should also be able to describe fluctuations of the wall itself that do not respect spherical symmetry, but nevertheless have negligible wall thickness. The use of spherical symmetry in the above paragraph was merely to match "Wilson coefficients" T and g to

[2]Let us also set $K = N = 1$ for concreteness.

the full axion-Maxwell action, but once we have them we should be able to use the Nambu-Goto action to describe non-spherically symmetric dynamics as well. Previous work has incorporated Nambu-Goto membrane actions - or used arguments invoking them - in describing dynamical evolution of domain walls or bubbles, for instance [85, 86, 87].

In any case, we should be able to compute the bubble size and nucleation rate, and match these outputs with eq. (4.1) and eq. (4.2) respectively, since the action eq. (4.3) contains the brane and electromagnetic degrees of freedom. First let us ignore the back-reaction of the electromagnetic field as before. Then the Euclidean version of eq. (4.3) with $t_{\rm E} = it$ is:

$$I_{\rm E} = \int_{\rm Bulk} d^4x \left(\frac{1}{4} F_{\mu\nu} F^{\mu\nu} \right) + T \int_{\rm WV} d^3\xi \sqrt{h} - ig \int_{\rm WV} d^3\xi \sqrt{h} \epsilon^{abc} A_a F_{bc}. \tag{4.7}$$

Consider now a nucleated $O(4)$ symmetric bubble. On the one hand, the second term on the right hand side of eq. (4.7) is proportional to the worldvolume $\sim R^3$. On the other hand, we can view the final term as a boundary integral over $A \wedge F$, where the boundary here is the worldvolume that separates the bulk into two regions. By Stokes' theorem, we then have a bulk integral over $F \wedge F \sim \mathbf{E}.\mathbf{B}$. So the final term is $\sim R^4 gEB$. Then the Euclidean action that must be minimized has the form $I_{\rm E} \sim TR^3 - gEBR^4$, and so the critical radius of the bubble is $R \sim T/gEB$. The decay rate is

$$\Gamma/V \sim \exp(-I_{\rm B}), \text{ with } I_{\rm B} \sim \frac{T^4}{(gEB)^3}. \tag{4.8}$$

Pleasingly, this scaling matches the decay rate from eq. (4.2), with the parameters g and T identified in accordance with the arguments of the previous paragraphs. To obtain the appropriate numerical factors we should write $T = k_1 m f^2$ and $g = k_2 \alpha$, where the dimensionless numbers k_1 and k_2 are 12π and $1/8$ respectively. This choice

correctly reproduces the results in eq. (4.1) and eq. (4.2).

4.2 An Explicit Solution for D2 Branes

We would like to generalize the worldline picture of Schwinger pair production of D0 branes (particles) [14, 26] to higher dimensional branes. Explicitly, let us consider D2 branes. The background field is - just as in the typical Schwinger effect - a constant uniform electric field in the z direction: $\mathbf{E} = E\hat{\mathbf{z}}$. We consider the following action:

$$I = \int_{\mathrm{WV}} d^3\xi \left(-\frac{1}{4} F^{(\mathrm{B})}_{ab} F^{(\mathrm{B})ab} \right) - T \int_{\mathrm{WV}} d^3\xi \sqrt{-h} + g \int_{\mathrm{WV}} \sqrt{-h} \epsilon^{abc} A_a F^{(\mathrm{B})}_{bc} \qquad (4.9)$$
$$+ \int_{\mathrm{Bulk}} d^4x \left(-\frac{1}{4} F_{\mu\nu} F^{\mu\nu} \right).$$

The corresponding Euclidean action is

$$I_{\mathrm{E}} = \int_{\mathrm{WV}} d^3\xi \left(\frac{1}{4} F^{(\mathrm{B})}_{ab} F^{(\mathrm{B})ab} \right) + T \int_{\mathrm{WV}} d^3\xi \sqrt{h} - ig \int_{\mathrm{WV}} \sqrt{h} \epsilon^{abc} A_a F^{(\mathrm{B})}_{bc} \qquad (4.10)$$
$$+ \int_{\mathrm{Bulk}} d^4x \left(\frac{1}{4} F_{\mu\nu} F^{\mu\nu} \right).$$

Here A_μ, with $F = dA$, indicates the electromagnetic vector potential, and $A^{(\mathrm{B})}_a$, with $F^{(\mathrm{B})} = dA^{(\mathrm{B})}$, being a $U(1)$ gauge potential living on the brane. The constant bulk electric field configuration implies that $F^{tz} = E$, and if we gauge fix A_μ such that only A_t is non-vanishing, then it follows that a solution of the vector potential is $A_\mu = Er \cos\sigma \delta^t_\mu$. Treating this term as a background field, we will now show that a gauge field solution for $A^{(\mathrm{B})}$ exists corresponding to an instanton representing a nucleated bubble.

The equation of motion for the brane gauge field is

$$\partial_a\Big(\sqrt{-h}F^{(\mathrm{B})ab} + 2g[cab]A_c\Big) = 0. \tag{4.11}$$

Here $[abc]$ is the totally anti-symmetric symbol related to[3] $\epsilon^{abc} = -[abc]/\sqrt{-h}$. Physically, this equation states that the background electric field induces charges on the brane, since we can read it as a modified Gauss law. We have written this equation in Lorentzian signature but we can freely translate between Euclidean and Lorentzian signature without ambiguity. To properly fix the conventions, let us now establish a coordinate system compatible with the standard rotationally symmetric ansatz. Following [8, 10, 11] we assume the ansatz

$$r^2 - t^2 = r_*^2, \text{ or } \quad r^2 + t_{\mathrm{E}}^2 = r_*^2, \tag{4.12}$$

with $x^2 + y^2 + z^2 = r^2$ i.e. the $O(4)$ ansatz in Euclidean signature. We take the bulk coordinate system to consist of $\{t, r, \sigma, \phi\}$; in the bubble interior, we take the coordinate system to be $\{\tau, R, \sigma, \phi\}$, and the corresponding line elements are respectively:

$$ds^2 = -dt^2 + dr^2 + r^2 d\sigma^2 + r^2 \sin^2\sigma d\phi^2,$$

$$ds^2 = -d\tau^2 + dR^2 + R^2 d\sigma^2 + R^2 \sin^2\sigma d\phi^2,$$

the latter of which extends up to the bubble[4]. On the bubble, these two line elements must match, forcing $r = R$ and $dR = 0$, as well as

$$\Big(\frac{dr}{d\tau}\Big)^2 - \Big(\frac{dt}{d\tau}\Big)^2 = 1. \tag{4.13}$$

[3]The extra sign is due to Lorentzian signature; it is not present in Euclidean signature, but it is a simple matter to Wick rotate to Euclidean signature.

[4]τ is not to be confused with the Euclidean time here.

This matching procedure is akin to Oppenheimer-Snyder collapse of a thin shell of gravitating matter, except the situation here is simpler since we take the exterior metric to be flat rather than Schwarzschild[5]. A solution compatible with our aforementioned ansatz is

$$r(\tau) = r_* \cosh(\tau/r_*), \text{ and } \quad t(\tau) = r_* \sinh(\tau/r_*). \tag{4.14}$$

It is a choice to have set our clocks such that the initial time $t = 0$ corresponds to $\tau = 0$. Furthermore, we can also Wick rotate to Euclidean signature to reveal that

$$r(\tau_{\rm E}) = r_* \cos(\tau_{\rm E}/r_*), \text{ and } \quad t_{\rm E}(\tau_{\rm E}) = r_* \sin(\tau_{\rm E}/r_*). \tag{4.15}$$

The picture in Euclidean signature is clear: we have an $O(4)$ instanton appearing at $\tau_{\rm E} = 0$, which we continue by Wick rotation to Lorentzian time and match at $\tau = 0$. The nucleated bubble that is born with a critical radius r_* - which we will compute momentarily - then expands in a hyperbolic trajectory which asymptotically approaches a future light cone.

Using the parametrization of eq. (4.15), the projection tensors of eq. (4.5) now have the following components

$$e^t_\tau = \cosh(\tau/r_*), \quad e^r_\tau = \sinh(\tau/r_*), \quad e^\sigma_\sigma = 1, \quad e^\phi_\phi = 1, \tag{4.16}$$

with all other pieces vanishing.

It then follows from eq. (4.6) that the metric on the brane with intrinsic coordinates

[5]For details, see [88, 56, 89, 90]

$\{\tau, \sigma, \phi\}$ is

$$[h_{ab}] = \begin{pmatrix} -1 & 0 & 0 \\ 0 & r(\tau)^2 & 0 \\ 0 & 0 & r(\tau)^2 \sin^2 \sigma \end{pmatrix}. \tag{4.17}$$

We now possess all of the ingredients necessary to solve eq. (4.11). Note that by azimuthal symmetry, we should be able to remove dependence on the equatorial angle ϕ in $A_a^{(\mathrm{B})}$, i.e. $A_a^{(\mathrm{B})} = A_a^{(\mathrm{B})}(\tau, \sigma)$. Therefore, we are free to gauge fix $A_\sigma^{(\mathrm{B})} = 0$; with this symmetry and the given ansatz, we would not have been able to gauge away $A_\phi^{(\mathrm{B})}$. Recalling that $A_\tau = A_t e_\tau^t$ (with other components vanishing), due to the anti-symmetry of the interaction term, $A_\tau^{(\mathrm{B})}$ does not appear. Actually we are being slightly quick here; a solution satisfying $\partial_\sigma A_\tau \sim 1/\sin\sigma$ is possible but such a term gives the brane kinetic piece an infinite Euclidean action, and so only a vanishing constant prefactor is allowed.

Now, we turn to the problem of solving for $A_\phi^{(\mathrm{B})}$, which we have argued is the only non-vanishing component of $A_a^{(\mathrm{B})}$. Setting the free index in eq. (4.11) to ϕ gives the following second order partial differential equation:

$$\partial_\sigma \left(\frac{1}{r_*^2 \cosh^2(\tau/r_*) \sin\sigma} \partial_\sigma A_\phi^{(\mathrm{B})} + 2gEr_* \cosh^2(\tau/r_*) \cos\sigma \right) = \frac{1}{\sin\sigma} \partial_\tau^2 A_\phi^{(\mathrm{B})}. \tag{4.18}$$

It is at this stage that recalling the bubble nucleation process in axion electrodynamics greatly helps.

Let us for a moment look closely and compare the expressions of eq. (4.7) and eq. (4.9). The two are strikingly similar. In the case of the former, we know from the discussion in section 4.1 that an axion bubble nucleates in the presence of parallel electric and magnetic fields. In the present case, we do not have a background magnetic field. Nevertheless, we can see that if we pick $F^{(\mathrm{B})}$ to have

a component mimicking a background magnetic field, then our interaction will resemble a Quantum Hall state on an axion domain wall. That is to say, the Wess-Zumino interaction on the brane will resemble a Chern-Simons interaction on an axion domain wall. In short, we have to get $\mathbf{E}.\mathbf{B}$ in the action for this argument to carry through. The background A_μ already contains the electric piece. A constant magnetic field in the $\hat{\mathbf{z}}$ direction corresponds to having[6]

$$A_\phi^{(\mathrm{B})} = k \cosh^2(\tau/r_*) \sin^2\sigma, \tag{4.19}$$

which is proportional to $x^2 + y^2$, and involves an unkown coeffiecient k. We now use this informed guess in eq. (4.18). Hearteningly, this ansatz is indeed a solution. In principle, one could guess the ansatz and solve eq. (4.18) without any relation to the axion domain wall, but it would be an exceptionally lucky guess. In fact, this step fully fixes the numerical prefactor $k = -gEr_*^3/2$ as well. We emphasize once more for clarity that there is no background magnetic field, just an electric field; the magnetic field is inspirational only, and for the sole purpose of solving for the brane vector potential $A^{(\mathrm{B})}$, which is ultimately what we require.

In summary, we have derived a solution to eq. (4.11) corresponding to a spherical brane bubble nucleation process (see Fig. 4.1). We may also like to ask how the background electric field back-reacts to this nucleation process. As we have briefly mentioned before, the interaction assigns charges to the brane, but as the bubble expands in real time, there will be currents due to its expanding nature, and hence magnetic fields as well. An analogous step occurs in the Schwinger effect when the charges particles accelerate. As such, let us then only focus on the induced charges at nucleation, i.e. at $\tau_{\mathrm{E}} = \tau = t = 0$.

[6]This expression follows from the $O(2) \times O(2)$ ansatz in [21], or Chapter 3.

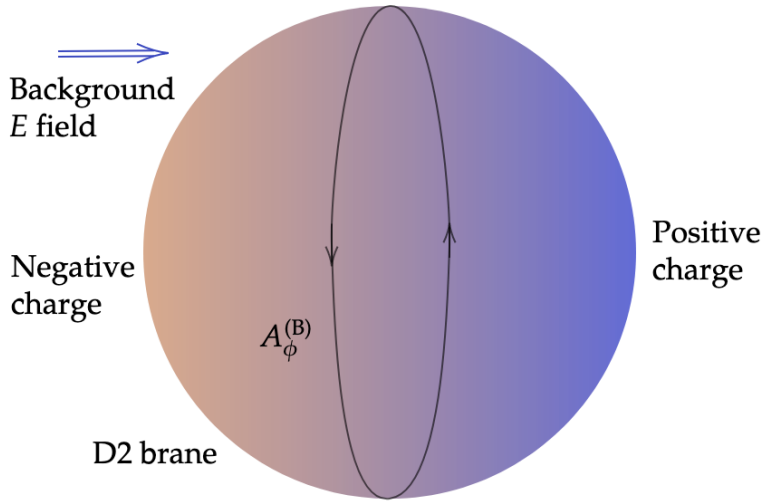

Figure 4.1: Schematic diagram represent brane nucleation. The oppositely colored hemispheres indicate that they are oppositely charged. There is a non-vanishing gauge field $A_\phi^{(\mathrm{B})}$ on the brane.

Looking once again at the action eq. (4.9), we can treat the coeffient of A_a as a source for the electromagnetic gauge field, which is to say that we can treat $g\epsilon^{abc}F_{bc}^{(\mathrm{B})}$ as an electric source current j^a. We can then solve the (sourced) wave equations in the bulk upon converting $j^a \to j^\alpha$ with the projection tensors e_a^α, thereby extracting the back-reaction on the electric field; this effect will be higher order in g, as it must. We find that at $t = 0$, the only non-vanishing component of the current is

$$j^t = 2g^2 E r_* \cos\sigma, \tag{4.20}$$

which we identify as the electric charge density, ρ_{E}. In essence, the brane acquires the charge distribution resembling a conducting shell in a uniform background electric field in the $\hat{\mathbf{z}}$ direction. The northern and southern hemispheres are oppositely charged due to the sign of $\cos\sigma$ changing across hemispheres.

At the moment of birth, the electric field gets screened uniformly in the interior, and the electric potential is proportional to a first order Legendre polynomial,

with radial scaling behavior of the form $\sim r$ and $\sim r^{-3}$ in the bubble interior and exterior respectively. It is this screened electric field that provides the energy for the brane, and the gauge field configuration living on the brane. Upon nucleation, the background electric field pulls apart these two oppositely charged hemispheres, leading the bubble to expand.

We are left with one final task: we must still calculate what r_* actually is! Towards this end, we put the solutions we have obtained so far in the Euclidean action eq. (4.10) and minimize it with respect to r_*, which in turn yields the critical radius of the bubble. We find that

$$r_* \sim \frac{T^{1/2}}{gE}. \tag{4.21}$$

We may now obtain the nucleation rate:

$$\Gamma/V \sim \exp(-I_{\rm B}), \text{ with } I_{\rm B} \sim \frac{T^{5/2}}{(gE)^3}. \tag{4.22}$$

As before, an exponentially suppressed nucleation rate requires $T^{5/2} \gtrsim (gE)^3$.

4.3 A Swampland Condition

At the ultracold point of the Nariai solution, $E \sim M_P H$. If the brane nucleation is too rapid, then the spacetime undergoes a big crunch singularity as outlined in [44, 45]. See Fig. 4.2.

Avoiding this outcome requires the nucleation rate to be exponentially suppressed,

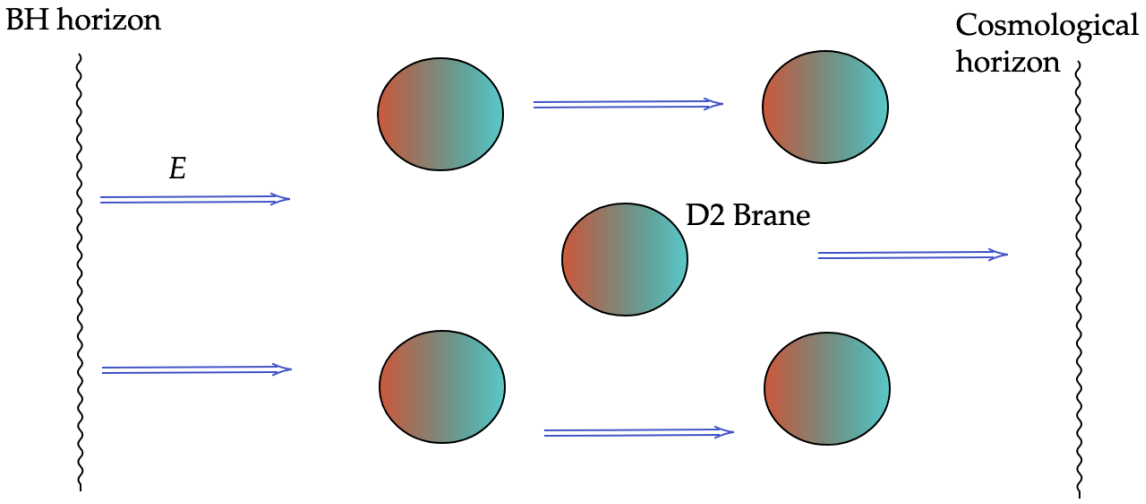

Figure 4.2: Schematic diagram represent brane nucleation. The oppositely colored hemispheres indicate that they are oppositely charged.

which in turn places a lower bound on brane tension. In fact, we require

$$T \gtrsim (gM_{\rm Pl}H)^{6/5}. \tag{4.23}$$

This expression is a striking result: quantum gravity relates brane tension and Wess-Zumino coupling with the size of the Hubble horizon. An assumption here is that the bubble size is less than the characteristic curvature scale of the spacetime geometry, so that the flat space limit is well justified, i.e. $r_* \sim T^{1/2}/gE \ll 1/H$, which is to say $T \ll (gM_{\rm Pl})^2$ on the Nariai branch near the ultracold point. One may interpret a violation of this bound to be an obstruction to nucleation - since a bubble that is too large will not fit - so that the true requirement is

$$T \gtrsim \min\Big((gM_{\rm Pl}H)^{6/5},\ gM_{\rm Pl}^2\Big). \tag{4.24}$$

Having already demonstrated an explicit solution for the brane gauge field in the previous section, we could ask ourselves the following question: if the scaling of eq. (4.22) is all we seek, can we use simpler arguments to extract it?

4.4 Scaling Arguments

Let us attempt to re-derive D2 brane nucleation rates in $(3+1)d$ using scaling arguments alone. On a first note, a significant portion of the above section relied on the thin wall limit, in which the wall thickness is negligible compared to the bubble size, for which the characteristic length scale is r_*. We should look at the scaling behavior of the action with respect to this parameter. Let us schematically rewrite eq. (4.10) in a language more amenable to scaling arguments:

$$I_{\rm E} \sim T \int_{\rm WV} \star 1 + ig \int_{\rm WV} A \wedge F^{(\rm B)} + \int_{\rm WV} F^{(\rm B)} \wedge \star F^{(\rm B)} + \int_{\rm Bulk} dA \wedge \star dA, \qquad (4.25)$$

where once again we disregard numerical factors for simplicity[7].

Since we neglect the back-reaction of the bulk electromagnetic field, let us ignore the final term since it will cancel in the evaluation of the bounce action. The equation of motion of the brane gauge field is

$$d \star F^{(\rm B)} \sim ig\ dA. \qquad (4.26)$$

Knowing that $dA \sim E$, i.e. the background electric field, we infer the scaling behavior of the brane field strength $F^{(\rm B)} \sim gE$. Putting this term in eq. (4.25), and integrating over the bubble worldvolume, we find

$$I_{\rm E} \sim TR^3 + (gE)^2 R^5, \qquad (4.27)$$

[7]The $\star$ symbol is the Hodge dual operator. In d dimensions, it maps a k form to a $d-k$ form of different basis forms. For example, in $d=3$, $\star(dx^2 \wedge dx^3) = dx^1$, mapping a two-form to a one-form. So the integral over $\star 1$ indicates a worldline/wolrdsheet/worldvolume integral. Similarly, one can show that the $dA \wedge \star dA$ is the kinetic piece for the Ramond-Ramond field, A. For additional details on these topics, see [56, 91, 92, 93, 94, 95] for example.

where the power law behavior of R in the second term is fixed by dimensional analysis. We once more obtain, in agreement with eq. (4.21), $r_* \sim T^{1/2}/gE$ by minimizing the above action with respect to R. This result implies again that the bounce action of eq. (4.27) scales as $I_{\rm B} \sim T^{5/2}/(gE)^3$, just as in eq. (4.22).

We reiterate that such scaling arguments cannot give explicit solutions as in section 4.2, and they assume such a solution exists. Nevertheless, a major advantage is immediately clear: a direct scaling argument gives the parametric form of the bounce action. It is this simplification that lends this method viable for extracting the form of the bounce action for branes of different dimensions in higher dimensional spacetimes as well, especially where we are not able to solve for the bounce itself.

4.5 Generalizations to Other Branes and Higher Dimensions

The methods we have outlined above are especially applicable to analogous problems in higher dimensions. In all cases, we assume the dimension of the brane can vary, i.e. we may allow Dp branes with $p \leq n-1$ in $(n+1)d$. We just considered D2 branes in $(3+1)d$. In subsequent examples, we continue to assume only a uniform background electric field, E. We provide specific examples below.

D1 Branes (Strings) in $(3+1)d$

The Euclidean action for strings in $(3+1)d$ is of the form

$$I_{\rm E} \sim T\int_{\rm WS} \star 1 + ig\int_{\rm WS} A\wedge d\theta + \int_{\rm WS} d\theta\wedge\star d\theta + \int_{\rm Bulk} dA\wedge\star dA, \tag{4.28}$$

where the abbreviation WS denotes a worldsheet integral, and θ is a scalar field on the string, whose equation of motion is

$$d \star d\theta \sim ig\ dA. \tag{4.29}$$

Scaling arguments suggest $d\theta \sim gE$ since $dA \sim E$. Using dimensional analysis, we infer

$$I_{\mathrm{E}} \sim TR^2 + (gE)^2 R^4, \tag{4.30}$$

and hence $r_* \sim T^{1/2}/gE$, and $I_{\mathrm{B}} \sim (T/gE)^2$. Exponentially suppressed nucleation requires $T^2 \gtrsim (gE)^2$. This scaling behavior continues to hold for strings in higher dimensions as well.

D6 Branes in $(7+1)d$

As a final example, consider D6 Branes in $(7+1)d$, with action

$$I_{\mathrm{E}} \sim T \int_{\mathrm{WV}} \star 1 + ig \int_{\mathrm{WV}} A \wedge F^{(\mathrm{B})} \wedge F^{(\mathrm{B})} \wedge F^{(\mathrm{B})} + \int_{\mathrm{WV}} F^{(\mathrm{B})} \wedge \star F^{(\mathrm{B})} + \int_{\mathrm{Bulk}} dA \wedge \star dA. \tag{4.31}$$

It follows that

$$d \star F^{(\mathrm{B})} \sim ig\ d(A \wedge F^{(\mathrm{B})} \wedge F^{(\mathrm{B})}), \tag{4.32}$$

and hence $F^{(\mathrm{B})} \sim 1/gE$. The action becomes

$$I_{\mathrm{E}} \sim TR^7 + (gE)^{-2} R^5, \tag{4.33}$$

which is minimized by $r_* \sim (T^{1/2} gE)^{-1}$, with corresponding bounce $I_{\mathrm{B}} \sim T^{-5/2}(gE)^{-7}$. This time, an exponentially suppressed nucleation rate requires $T^{5/2} \lesssim (gE)^{-7}$. Notice that in stark contrast to previous examples, we now get an upper

bound on the brane tension, not a lower bound. This feature is not unique to D6 branes, as the results of the next section show.

4.6 General Cases and the D3/D4 Exceptions

Using similar arguments to those above, we present results for general dimensions in Table 4.1, and we notice the pattern:

$$gE \lesssim T^{\frac{1}{p+1}+\frac{4-p}{4}}, \tag{4.34}$$

when p is even. Observe how instead of getting a lower bound, we get an upper bound on the tension when $p > 4$. When p is odd,

$$gE \lesssim T^{\frac{1}{p+1}+\frac{3-p}{4}}. \tag{4.35}$$

These relations do not apply when $p = 3$, or when $p = 4$. These special cases are somewhat more subtle. Take for instance the action for a D4 brane:

$$\begin{aligned} I_{\mathrm{E}} \sim T \int_{\mathrm{WV}} \star 1 + ig \int_{\mathrm{WV}} A \wedge F^{(\mathrm{B})} \wedge F^{(\mathrm{B})} + \int_{\mathrm{WV}} F^{(\mathrm{B})} \wedge \star F^{(\mathrm{B})} \\ + \int_{\mathrm{Bulk}} dA \wedge \star dA. \end{aligned} \tag{4.36}$$

Varying with respect to $A^{(\mathrm{B})}$ shows that

$$d \star F^{(\mathrm{B})} \sim ig\ dA \wedge F^{(\mathrm{B})}. \tag{4.37}$$

The complication lies in the fact that the equation of motion possesses an accidental dilatation symmetry[8], in the sense that whatever solution we may obtain for $A^{(\mathrm{B})}$, linearity guarantees that $\lambda A^{(\mathrm{B})}$ is also a solution, for some number λ. The action does

[8]Not a scaling of the coordinate, just the field.

	D1	D2	D5	D6	D7	D8
$(3+1)d$	$T^2 \gtrsim (gE)^2$	$T^{5/2} \gtrsim (gE)^3$	-	-	-	-
$(4+1)d$	$T^2 \gtrsim (gE)^2$	$T^{5/2} \gtrsim (gE)^3$	-	-	-	-
$(5+1)d$	$T^2 \gtrsim (gE)^2$	$T^{5/2} \gtrsim (gE)^3$	-	-	-	-
$(6+1)d$	$T^2 \gtrsim (gE)^2$	$T^{5/2} \gtrsim (gE)^3$	$T^2 \lesssim (gE)^{-6}$	-	-	-
$(7+1)d$	$T^2 \gtrsim (gE)^2$	$T^{5/2} \gtrsim (gE)^3$	$T^2 \lesssim (gE)^{-6}$	$T^{5/2} \lesssim (gE)^{-7}$	-	-
$(8+1)d$	$T^2 \gtrsim (gE)^2$	$T^{5/2} \gtrsim (gE)^3$	$T^2 \lesssim (gE)^{-6}$	$T^{5/2} \lesssim (gE)^{-7}$	$T^7 \lesssim (gE)^{-8}$	-
$(9+1)d$	$T^2 \gtrsim (gE)^2$	$T^{5/2} \gtrsim (gE)^3$	$T^2 \lesssim (gE)^{-6}$	$T^{5/2} \lesssim (gE)^{-7}$	$T^7 \lesssim (gE)^{-8}$	$T^8 \lesssim (gE)^{-9}$

Table 4.1: Conditions on Dp brane parameters for exponentially suppressed nucleation rates in $(n+1)d$.

not have this symmetry. This feature is reminiscent of the small amplitude simple pendulum system whose action is

$$I = \int dt \left(\frac{1}{2}\dot{\theta}^2 - \frac{1}{2}\omega^2\theta^2 \right). \tag{4.38}$$

The equation of motion is that of a simple harmonic oscillator:

$$\ddot{\theta} + \omega^2\theta = 0. \tag{4.39}$$

The implication of this accidental dilatation symmetry ($\theta \to \lambda\theta$) at the level of the equation of motion, albeit not the action, is that the frequency of oscillation ω does not fix the amplitude, which remains an independent parameter. In the case of D4 branes, the accidental symmetry implies that the critical size of the bubble is not fixed by the terms in the action so far. We must include an extra piece in the action that breaks this symmetry at the level of the equation of motion. Such a term may arise, for instance, in a higher order expansion of the DBI action. The same issue occurs with D3 branes. There a simultaneous scaling of the brane gauge field as well as the brane scalar field shows an accidental symmetry at the level of the equation of motion.

4.7 Consistency Conditions on Brane Couplings

All throughout, we have been neglecting brane self-interactions, which is to say that we suppose one part of the brane may only very weakly interact with another part of the brane. When this coupling is strong, our results may not hold. For instance, let us look back at the D2 brane action in eq. (4.25). We should append to the action

the following additional piece:

$$\gamma \int_{\rm WV} C_3 + \int_{\rm Bulk} dC_3 \wedge \star dC_3, \tag{4.40}$$

where C_3 is a three-form. When γ is sufficiently large, the brane will self-interact in ways that may negate the computation of the nucleation rates. In that case, we do not trust the computations above. In this specific case, we should require - as a consistency check - that the contribution of these terms to the bounce is negligible on the bounce solution. The additional equation of motion here is

$$d \star dC_3 \sim \gamma \times \delta(\text{Brane}) \tag{4.41}$$

where there is a delta function on the brane woldvolume which must be integrated with a Green's function for a higher dimensional Laplacian. However, we only seek the contribution to the action, and this follows from the scaling behavior $C_3 \sim \gamma$. Dimensional analysis fixes the correct factor of r_*. Explicitly, the action is modified with the addition of $\gamma^2 r_*^4$, up to numerical coefficients. Ultimately, we must require this contribution to the action to be much less than $I_{\rm B}$ in eq. (4.22), calculated previously, for consistency. This requirement is

$$\gamma^2 \ll T^{1/2} g E. \tag{4.42}$$

Similar arguments apply to branes of other dimensions in higher dimensional spacetimes as well, with natural generalizations of eq. (4.41).

We have presented requirements that lead to exponentially suppressed nucleation rates for branes in background electric fields in Table 4.1. The prerequisite conditions on the brane couplings, for these results to be reliable, is that the following additional

piece:

$$\gamma \int_{\rm WV} C_{p+1} + \int_{\rm Bulk} dC_{p+1} \wedge \star dC_{p+1}, \tag{4.43}$$

gives only a small correction relative to the bounce action, when evaluated on the bounce solution. Repeating calculations based upon the same argument above, the conditions for Dp branes in $(n+1)d$ are given by:

$$\gamma^2 \lesssim \frac{T^{1+\frac{1}{4}(4-p)(n-p-2)}}{(gE)^{n-p-2}}, \tag{4.44}$$

for even p and $p \neq 4$, as well as

$$\gamma^2 \lesssim \frac{T^{1+\frac{1}{4}(3-p)(n-p-2)}}{(gE)^{n-p-2}}, \tag{4.45}$$

for odd p and $p \neq 3$. When the above conditions are satisfied, we trust the results of Table 4.1.

Chapter 5

Conclusion and Outlook

In this thesis, we have presented a novel instanton of axion-Maxwell theory, which facilitates the decay of a parallel background electric and magnetic field configuration through the nucleation of bubbles. This result was the key topic of Chapter 3. The structure of the bubble is rich; indeed, the bubble wall is endowed with charges and currents owing to the classical findings of Witten and Sikivie [6, 7, 83, 84] that follow from having a Chern-Simons term in the action. This process mimics the well-known Schwinger effect [19, 20] and opens up an exciting avenue in non-perturbative quantum field theory.

Furthermore, we have found that the real time evolution of the bubble is unusual. At birth, the region of lower energy is outside the bubble itself which is completely at odds with any other similar result anywhere else in the literature, to the best of our knowledge. In all known cases so far, the lower energy density region lies within the interior of the bubble, rather than the exterior. This feature is also a point Sidney Coleman makes in his papers [8, 9, 10, 11, 96], and the bubble that we have found would therefore be an exception. Moreover, as the bubble expands, the lower energy density region gradually migrates to the interior of the expanding

bubble, and we have shown that - for certain configurations - a cascading avalanche of bubbles, stemming from the classical rolling of the fields, may emerge. We have called this nucleation process a Russian doll instanton.

The implications are vast. On the phenomenological frontier, such axion domain walls could have been nucleated and annihilated in the early universe. This is similar to bubble nucleation in a first order phase transition and will produce gravitational wave signals (see for example [97] and references therein) that could be within the reach of near-future gravitational wave detectors such as PTA's (such as IPTA [98]), laser interferometers (such as LIGO/VIRGO [99, 100], aLIGO [101] or LISA[102]) and atom interferometers (such as AION [103] and MAGIS [104, 105]). However, there are several important features that distinguish our lopsided bubbles from those seen in typical phase transitions that are the subject of work in preparation. Since the bubbles are elongated along the direction of the parallel electric and magnetic fields, they have less symmetry. This can allow the evasion of certain theorems that apply to spherical bubbles and prohibit the production of gravitational wave signals [106]. In summary, if one considers the expansion of two nearby spherical bubbles, the $O(2,1)$ symmetry of the system forbids the generation of gravitational waves by an analog of Birkhoff's theorem that applies to $O(3)$ symmetric spacetimes. For our non-spherical bubbles, there is generically no such $O(2,1)$ symmetry and their expansion can evade this theorem. Such structures will influence the gravitational wave signals and can produce sharp peaks that are distinct from the usual broad peaks characteristic of first order phase transitions. The energy density in electromagnetic fields in and around the bubbles also displays an intricate structure that could give additional observational signatures distinct from those seen in typical first order phase transitions. These features will be the subject of work in preparation. Also, the collision of such bubbles could lead to the

formation of primordial black holes [107] and it would be interesting to see if the asymmetry can play a role in enhancing or quenching the black hole formation rate.

On the more formal side, we have seen in Chapter 4 that the structure of the axion domain wall has intriguing similarities with branes possessing Wess-Zumino interactions. We have extended the Festina Lente swampland conjecture [44, 45] - for charged massive particles in de Sitter space - to branes carrying natural Wess-Zumino couplings as well. It is especially important since top-down attempts using string theory at obtaining constraints on de Sitter are extremely difficult [38], and therefore bottom-up approaches, such as non-perturbative particle physics gedankenexperiments in black hole backgrounds, provide an alternative direction. This exploration amounts to a further contribution to the swampland program.

Appendix A

Extremal Black Hole Solutions in de Sitter

We would like to first review the theory of charged black holes in a de Sitter background. Consider the Einstein-Hilbert-Maxwell action including cosmological constant Λ:

$$I = \int d^4x\sqrt{-g}\left(\frac{1}{16\pi G_{\rm N}}\Big(R - 2\Lambda\Big) - \frac{1}{4}F_{\mu\nu}F^{\mu\nu}\right), \tag{A.1}$$

where $F = dA$, and $G_{\rm N} = M_{\rm Pl}^{-2}$ as usual, with the Planck mass $M_{\rm Pl} = 1.22\times10^{19}$GeV. Varying the action with respect to $g_{\mu\nu}$ gives the equation of motion for the metric tensor

$$R_{\mu\nu} - \frac{1}{2}Rg_{\mu\nu} + \Lambda g_{\mu\nu} = 8\pi G_{\rm N}T_{\mu\nu}, \tag{A.2}$$

where we have defined the electromagnetic energy momentum tensor

$$T_{\mu\nu} = \frac{1}{4\pi}\Big(F_{\mu\rho}F_{\nu}{}^{\rho} - \frac{1}{4}g_{\mu\nu}F_{\rho\sigma}F^{\rho\sigma}\Big). \tag{A.3}$$

Moreover, varying the action with respect to A_μ gives the equation of the motion for the vector potential $\nabla_\nu F^{\mu\nu} = 0$. A solution to this system of equations is the

following:

$$ds^2 = -h(r)dt^2 + h(r)^{-1}dr^2 + r^2 d\sigma^2 + r^2 \sin^2\sigma d\phi^2, \tag{A.4}$$

$$h(r) = 1 - \frac{2G_{\rm N}M}{r} + \frac{G_{\rm N}Q^2}{r^2} - \frac{r^2}{l^2}, \text{ where } l^2 = \frac{3}{\Lambda}, \tag{A.5}$$

$$A = A_\mu dx^\mu = -\frac{Q}{r}dt. \tag{A.6}$$

We use σ to denote the polar angle to avoid confusion with the axion field. This line element describes a black hole with mass parameter M and electric charge parameter Q, although we note that the spacetime is not asymptotically flat , but rather de Sitter with length $\sqrt{3/\Lambda}$.

We will soon derive the values of M and Q for such black holes that lead to extremal solutions. Fig. A.1 shows the space of extremal solutions. There are three horizons: the inner black hole horizon, the outher black hole horizon, and the cosmological horizon [108, 109]. The upper red line connected to the origin, or the *upper branch*, represents the cases in which the inner black hole horizon and outer black hole horizon meet. The cosmological horizon is not in contact with these two, except at the tip of the shark fin diagram. We may view this system as an extremal Reissner-Nordstrom black hole in a de Sitter universe. On the black dotted line, $\sqrt{G_{\rm N}}M = Q$. This line would represent extremal black holes if the action had vanishing cosmological constant. Indeed, in that case, there would be no limit to how large an extremal Reissner-Nordstrom black holes could be, but here, if we were to make the black hole larger and larger, eventually the black hole would become large enough to reach the cosmological horizon. This is the ultracold point, which is the tip of the shark fin diagram.

Furthermore, the red right branch respresents the case in which the black hole outer horizon is coincident with the cosmological horizon but the inner horizon is

not, except at the tip. This is the *Nariai branch*. The tip of the shark fin diagram itself represents the values of parameters for which the three horizons coincide. This point is called the *ultracold point*. We outline below where the numerical values of the particular points originate.

While points on the shark fin represent extremal solutions, points interior represent subextremal solutions, and points exterior represent superextremal solutions. In particular, note that starting on any point on the Nariai branch, if we reduce the charge/electric field, we transition to a superextremal state; this behavior is in stark contrast to the upper branch, or Reissner-Nordstrom black holes in flat backgrounds. It is precisely this feature that allows for the Festina Lente conjecture [44, 45] to hold.

A.1 Horizon Structure

Let us return to the line element,

$$ds^2 = -h(r)dt^2 + h(r)^{-1}dr^2 + r^2 d\sigma^2 + r^2 \sin^2\sigma d\phi^2, \tag{A.7}$$

with lapse function

$$h(r) = 1 - \frac{2G_{\mathrm{N}}M}{r} + \frac{G_{\mathrm{N}}Q^2}{r^2} - \frac{r^2}{l^2}, \text{ where } l^2 = \frac{3}{\Lambda}. \tag{A.8}$$

It is helpful to write $h(r) = -u(r)/(lr)^2$ where we have defined

$$u(r) = r^4 - l^2r^2 + 2G_{\mathrm{N}}Ml^2r - G_{\mathrm{N}}Q^2l^2, \tag{A.9}$$

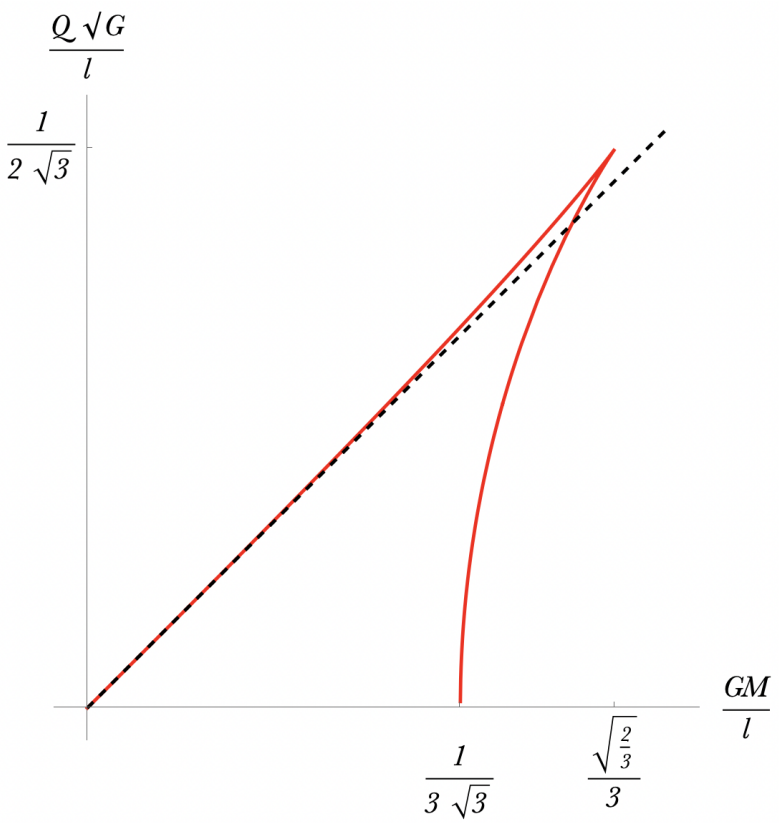

Figure A.1: The *shark fin* diagram depicting in red the lines of extremal black holes solutions, where atleast two horizons meet. The ultracold point is at the tip of the shark fin. The black dashed line represents $\sqrt{G_{\rm N}}M = Q$.

which is a quartic polynomial in r. In particular, since the coefficient of the cubic term is vanishing, it follows that the sum of roots of $u(r)$ is vanishing. The polynomial $u(r)$ factorizes, so that for general values of parameters (M, Q, l):

$$h(r) = -\frac{1}{(lr)^2}(r-\alpha)(r-\beta)(r-\gamma)(r+\alpha+\beta+\gamma). \tag{A.10}$$

The roots give the radial coordinates of the horizon, asssuming the root is a positive real number. If the first three roots are positive, then the final root is negative. We therefore see that we have at most three horizons corresponding to the three positive roots at which $h(r)$ vanishes. The outermost root with largest r gives the cosmological horizon, the middle root gives the black hole outer horizon, and the

smallest root gives the black hole inner horizon. We are most interested in extremal solutions, which are solutions that arise when at least two roots are degenerate.

First consider the special case in which all three horizons are coincident. This is the ultracold point. Then call all the positive roots α. We find

$$h(r) = -\frac{1}{(lr)^2}(r-\alpha)^3(r+3\alpha). \tag{A.11}$$

Expanding the above, and equating with eq. (A.8) gives $\alpha = l/\sqrt{6}$. This parameter is the radial coordinate of the three coincident horizons.

Second, we will consider the theory of two degenerate roots for general values of (M, Q, l), before classifying spacetimes of special interest that occur from particular choices of these parameters. We may express the degeneracy of two roots by taking $\gamma \to \beta$ in eq. (A.10), so that β is the radial coordinate of the two coincident horizons. Then,

$$h(r) = -\frac{1}{(lr)^2}(r-\alpha)(r-\beta)^2(r+\alpha+2\beta), \tag{A.12}$$

which, upon expanding out and collecting terms in powers of r, simplifies to the expression

$$h(r) = -\frac{1}{(lr)^2}\Big(r^4 - r^2((\alpha+\beta)^2+2\beta^2) + r(2\beta(\alpha+\beta)^2) - \alpha\beta^2(\alpha+2\beta)\Big). \tag{A.13}$$

Comparing this result with eq. (A.8), we may eliminate α and obtain a parametric system of equations in β,

$$\frac{G_{\rm N}M}{l} = \frac{\beta}{l}\left(1 - 2\Big(\frac{\beta}{l}\Big)^2\right), \quad \frac{\sqrt{G_{\rm N}}Q}{l} = \frac{\beta}{l}\left(1 - 3\Big(\frac{\beta}{l}\Big)^2\right)^{1/2}. \tag{A.14}$$

This is precisely the parametric plot Fig.A.1. We see that $0 \leq \beta/l \leq 1/\sqrt{3}$ since we keep the charge real. Note that as $l \to \infty$ (i.e. $\Lambda \to 0$), we find that $\sqrt{G_{\rm N}}M = Q$, indicating a Reissner-Nordstrom solution in Minkowski background, as expected. Furthermore, when $0 \leq \beta/l < 1/\sqrt{6}$, we are on the upper branch, when $1/\sqrt{6} < \beta/l \leq 1/\sqrt{3}$, and when $\beta/l = 1/\sqrt{6}$, we are at the ultracold point.

A.2 Near-Horizon Geometry

We are interested in the near-horizon geometry of observers in extremal spacetime configurations for charged black holes in de Sitter in $(3+1)d$. Since $h(r)$ contains at least a double zero on either the upper or Nariai branch[1], the $h'(r) = 0$ on the radial coordinate of the coincident horizons. Defining $x = r - u$, we may expand

$$h(r)dt^2 \approx \left(dt\sqrt{h(u)}\right)^2 \left(1 + \frac{x^2}{2h(u)/h''(u)} + \cdots\right), \tag{A.15}$$

and

$$h(r)^{-1}dr^2 \approx \left(\frac{dr}{\sqrt{h(u)}}\right)^2 \left(1 + \frac{x^2}{2h(u)/h''(u)} + \cdots\right)^{-1}. \tag{A.16}$$

Defining new coordinates,

$$y = \frac{x}{\sqrt{h(u)}}, \text{ and, } \tau = t\sqrt{h(u)}, \tag{A.17}$$

we see that

$$h(r)dt^2 \approx d\tau^2 \left(1 + \frac{h''(u)}{2}y^2\right) \text{ and, } \frac{dr^2}{h(r)} \approx dy^2 \left(1 + \frac{h''(u)}{2}y^2\right)^{-1}, \tag{A.18}$$

where we have truncated the expressions to quadratic powers of y. Taking $r = u$ to be the radial coordinate of the coincident horizons, we see that the sign of $h''(u)$

[1] And a triple zero at the ultracold point.

determines whether the near horizon geometry is $AdS_2 \times S^2$ (on the upper branch)[2] or $dS_2 \times S^2$ on the Nariai branch, in the $\{\tau, x, \sigma, \phi\}$ coordinate system. It is merely a tedious algebraic exercise to check that this sign is positive on the upper branch and negative on the Nariai branch.

However, one thing is clear without any further calculation at all: since the ultracold point has a triple zero, $h''(u) = 0$ there and so the near horizon geometry becomes $\text{Mink}_2 \times S^2$. We see clearly now via explicit redefinition of coordinates that the singularities of the metric stemming from the zeros of $h(r)$ corresponding to horizons were entirely coordinate singularities, except the singularity at $r = 0$, which is a physical singularity. One point to mention is that just as in extremal Reissner-Nordstrom, in addition to the near horizon metric being $AdS_2 \times S^2$, there was also a uniform background electric field in the radial direction, here to we have a uniform background electric field $E = Q/r^2$ where r is the S^2 radius. Near the ultracold point, $E \sim M_{\text{Pl}}H$.

The results above generalize to higher dimensions (for instance, see [110, 111, 112, 113]) which have a similar shark fin shaped (sub-)extremal region.

[2]This outcome is expected since the near horizon geometry of an extremal Reissner-Nordstrom black hole is precisely $AdS_2 \times S^2$, with a background electric field.

Bibliography

[1] Steven Weinberg. "A New Light Boson?" In: *Phys. Rev. Lett.* 40 (1978), pp. 223–226. DOI: 10.1103/PhysRevLett.40.223.

[2] Frank Wilczek. "Problem of Strong P and T Invariance in the Presence of Instantons". In: *Phys. Rev. Lett.* 40 (1978), pp. 279–282. DOI: 10.1103/PhysRevLett.40.279.

[3] R. D. Peccei and Helen R. Quinn. "CP Conservation in the Presence of Instantons". In: *Phys. Rev. Lett.* 38 (1977), pp. 1440–1443. DOI: 10.1103/PhysRevLett.38.1440.

[4] John Preskill, Mark B. Wise, and Frank Wilczek. "Cosmology of the Invisible Axion". In: *Phys. Lett. B* 120 (1983). Ed. by M. A. Srednicki, pp. 127–132. DOI: 10.1016/0370-2693(83)90637-8.

[5] Leanne D. Duffy and Karl van Bibber. "Axions as Dark Matter Particles". In: *New J. Phys.* 11 (2009), p. 105008. DOI: 10.1088/1367-2630/11/10/105008. arXiv: 0904.3346 [hep-ph].

[6] Edward Witten. "Dyons of Charge $e\theta/2\pi$". In: *Phys. Lett. B* 86 (1979), pp. 283–287. DOI: 10.1016/0370-2693(79)90838-4.

[7] Willy Fischler and John Preskill. "Dyon-Axion Dynamics". In: *Phys. Lett. B* 125 (1983), pp. 165–170. DOI: 10.1016/0370-2693(83)91260-1.

[8] Sidney Coleman. "The Fate of the False Vacuum 1: Semiclassical Theory". In: *Phys. Rev. D* 15 (1977). [Erratum: Phys.Rev.D 16, 1248 (1977)], pp. 2929–2936. DOI: 10.1103/PhysRevD.16.1248.

[9] Curtis G. Callan Jr. and Sidney R. Coleman. "The Fate of the False Vacuum. 2. First Quantum Corrections". In: *Phys. Rev. D* 16 (1977), pp. 1762–1768. DOI: 10.1103/PhysRevD.16.1762.

[10] Sidney R. Coleman, V. Glaser, and Andre Martin. "Action Minima Among Solutions to a Class of Euclidean Scalar Field Equations". In: *Commun. Math. Phys.* 58 (1978), pp. 211–221. DOI: 10.1007/BF01609421.

[11] Sidney Coleman. *Aspects of Symmetry: Selected Erice Lectures*. Cambridge, U.K.: Cambridge University Press, 1985. ISBN: 978-0-521-31827-3. DOI: 10.1017/CBO9780511565045.

[12] Ki-Myeong Lee and Erick J. Weinberg. "TUNNELING WITHOUT BARRIERS". In: *Nucl. Phys. B* 267 (1986), pp. 181–202. DOI: 10.1016/0550-3213(86)90150-1.

[13] Malcolm J. Duncan and Lars Gerhard Jensen. "Exact tunneling solutions in scalar field theory". In: *Phys. Lett. B* 291 (1992), pp. 109–114. DOI: 10.1016/0370-2693(92)90128-Q.

[14] J. David Brown and C. Teitelboim. "Neutralization of the Cosmological Constant by Membrane Creation". In: *Nucl. Phys. B* 297 (1988), pp. 787–836. DOI: 10.1016/0550-3213(88)90559-7.

[15] Jonathan L. Feng et al. "Saltatory relaxation of the cosmological constant". In: *Nucl. Phys. B* 602 (2001), pp. 307–328. DOI: 10.1016/S0550-3213(01)00097-9. arXiv: hep-th/0005276.

[16] Prateek Agrawal et al. "Electroweak Phase Transition with a Double Well Done Doubly Well". In: (Dec. 2023). arXiv: 2312.06749 [hep-ph].

[17] Prateek Agrawal and Michael Nee. "The Boring Monopole". In: *SciPost Phys.* 13.3 (2022), p. 049. DOI: 10.21468/SciPostPhys.13.3.049. arXiv: 2202.11102 [hep-ph].

[18] Michael Nee. "Phase transitions in the early universe". PhD thesis. Oxford University, Oxford U., 2023.

[19] Julian S. Schwinger. "On gauge invariance and vacuum polarization". In: *Phys. Rev.* 82 (1951). Ed. by K. A. Milton, pp. 664–679. DOI: 10.1103/PhysRev.82.664.

[20] W. Heisenberg and H. Euler. "Consequences of Dirac's theory of positrons". In: *Z. Phys.* 98.11-12 (1936), pp. 714–732. DOI: 10.1007/BF01343663. arXiv: physics/0605038.

[21] Saquib Hassan, John March-Russell, and Georges Obied. "Chern-Simons bubbles: Lopsided false vacuum decay in axion electrodynamics". In: (Jan. 2024). arXiv: 2402.00119 [hep-th].

[22] M. Shifman. *Advanced Topics in Quantum Field Theory: A Lecture Course*. Cambridge University Press, 2022. ISBN: 9781108882088. URL: https://books.google.co.uk/books?id=AVxqEAAAQBAJ.

[23] E.J. Weinberg. *Classical Solutions in Quantum Field Theory: Solitons and Instantons in High Energy Physics*. Cambridge Monographs on Mathematical Physics. Cambridge University Press, 2012. ISBN: 9780521114639. URL: https://books.google.co.uk/books?id=rfvFNI2C7i8C.

[24] V. Rubakov and S.S. Wilson. *Classical Theory of Gauge Fields*. Princeton University Press, 2009. ISBN: 9781400825097. URL: https://books.google.co.uk/books?id=BxjL6EkIpfUC.

[25] Adam R Brown. "Schwinger pair production at nonzero temperatures or in compact directions". In: *Physical Review D* 98.3 (2018), p. 036008.

[26] Wen-Yuan Ai and Marco Drewes. "Schwinger effect and false vacuum decay as quantum-mechanical tunneling of a relativistic particle". In: *Phys. Rev. D* 102.7 (2020), p. 076015. DOI: 10.1103/PhysRevD.102.076015. arXiv: 2005.14163 [hep-th].

[27] Markus B. Fröb et al. "Schwinger effect in de Sitter space". In: *JCAP* 04 (2014), p. 009. DOI: 10.1088/1475-7516/2014/04/009. arXiv: 1401.4137 [hep-th].

[28] Prasant Samantray and Suprit Singh. "Schwinger Effect in Compact Space". In: *Phys. Rev. D* 103.12 (2021), p. 125012. DOI: 10.1103/PhysRevD.103.125012. arXiv: 2010.13453 [hep-th].

[29] Yue Qiu and Lorenzo Sorbo. "Schwinger effect in compact space: a real time calculation". In: *Phys. Rev. D* 102.4 (2020), p. 045010. DOI: 10.1103/PhysRevD.102.045010. arXiv: 2005.10121 [hep-th].

[30] Oliver Gould et al. "Observing Thermal Schwinger Pair Production". In: *Phys. Rev. A* 99.5 (2019), p. 052120. DOI: 10.1103/PhysRevA.99.052120. arXiv: 1812.04089 [hep-ph].

[31] Patrick Draper. "Virtual and Thermal Schwinger Processes". In: *Phys. Rev. D* 98.12 (2018), p. 125014. DOI: 10.1103/PhysRevD.98.125014. arXiv: 1809.10768 [hep-th].

[32] Oliver Gould and Arttu Rajantie. "Thermal Schwinger pair production at arbitrary coupling". In: *Phys. Rev. D* 96.7 (2017), p. 076002. DOI: 10.1103/PhysRevD.96.076002. arXiv: 1704.04801 [hep-th].

[33] Marieke van Beest et al. "Lectures on the Swampland Program in String Compactifications". In: *Phys. Rept.* 989 (2022), pp. 1–50. DOI: 10.1016/j.physrep.2022.09.002. arXiv: 2102.01111 [hep-th].

[34] Eran Palti. "The Swampland: Introduction and Review". In: *Fortsch. Phys.* 67.6 (2019), p. 1900037. DOI: 10.1002/prop.201900037. arXiv: 1903.06239 [hep-th].

[35] Mariana Grana and Alvaro Herráez. "The swampland conjectures: a bridge from quantum gravity to particle physics". In: *Universe* 7.8 (2021), p. 273.

[36] Daniel Harlow et al. "Weak gravity conjecture". In: *Reviews of Modern Physics* 95.3 (Sept. 2023). ISSN: 1539-0756. DOI: 10.1103/revmodphys.95.035003. URL: http://dx.doi.org/10.1103/RevModPhys.95.035003.

[37] Alek Bedroya and Cumrun Vafa. "Trans-Planckian Censorship and the Swampland". In: *JHEP* 09 (2020), p. 123. DOI: 10.1007/JHEP09(2020)123. arXiv: 1909.11063 [hep-th].

[38] Georges Obied et al. "De Sitter Space and the Swampland". In: (June 2018). arXiv: 1806.08362 [hep-th].

[39] John March-Russell and Rudin Petrossian-Byrne. "QCD, Flavor, and the de Sitter Swampland". In: (June 2020). arXiv: 2006.01144 [hep-th].

[40] Sylvain Fichet and Prashant Saraswat. "Approximate Symmetries and Gravity". In: *JHEP* 01 (2020), p. 088. DOI: 10.1007/JHEP01(2020)088. arXiv: 1909.02002 [hep-th].

[41] Rudin Petrossian-Byrne. "Aspects of the Standard Model Landscape and Post Vacuum Transition Dynamics". Other thesis.

[42] Clay Cordova, Kantaro Ohmori, and Tom Rudelius. "Generalized symmetry breaking scales and weak gravity conjectures". In: *JHEP* 11 (2022), p. 154. DOI: 10.1007/JHEP11(2022)154. arXiv: 2202.05866 [hep-th].

[43] Miguel Montero, Julian B. Muñoz, and Georges Obied. "Swampland bounds on dark sectors". In: *JHEP* 11 (2022), p. 121. DOI: 10.1007/JHEP11(2022)121. arXiv: 2207.09448 [hep-ph].

[44] Miguel Montero, Thomas Van Riet, and Gerben Venken. "Festina Lente: EFT Constraints from Charged Black Hole Evaporation in de Sitter". In: *JHEP* 01 (2020), p. 039. DOI: 10.1007/JHEP01(2020)039. arXiv: 1910.01648 [hep-th].

[45] Miguel Montero et al. "The FL bound and its phenomenological implications". In: *JHEP* 10 (2021), p. 009. DOI: 10.1007/JHEP10(2021)009. arXiv: 2106.07650 [hep-th].

[46] Richard Phillips Feynman and Albert Roach Hibbs. *Quantum mechanics and path integrals*. International series in pure and applied physics. New York, NY: McGraw-Hill, 1965. URL: https://cds.cern.ch/record/100771.

[47] Cesim K. Dumlu and Gerald V. Dunne. "Complex Worldline Instantons and Quantum Interference in Vacuum Pair Production". In: *Phys. Rev. D* 84 (2011), p. 125023. DOI: 10.1103/PhysRevD.84.125023. arXiv: 1110.1657 [hep-th].

[48] R. Penrose. "Gravitational collapse: The role of general relativity". In: *Riv. Nuovo Cim.* 1 (1969), pp. 252–276. DOI: 10.1023/A:1016578408204.

[49] David G. Boulware. "Naked Singularities, Thin Shells, and the Reissner-Nordström Metric". In: *Phys. Rev. D* 8.8 (1973), p. 2363. DOI: 10.1103/PhysRevD.8.2363.

[50] Tom Banks and Nathan Seiberg. "Symmetries and Strings in Field Theory and Gravity". In: *Phys. Rev. D* 83 (2011), p. 084019. DOI: 10.1103/PhysRevD.83.084019. arXiv: 1011.5120 [hep-th].

[51] S. W. Hawking. "Black hole explosions". In: *Nature* 248 (1974), pp. 30–31. DOI: 10.1038/248030a0.

[52] S. W. Hawking. "Particle Creation by Black Holes". In: *Commun. Math. Phys.* 43 (1975). Ed. by G. W. Gibbons and S. W. Hawking. [Erratum: Commun.Math.Phys. 46, 206 (1976)], pp. 199–220. DOI: 10.1007/BF02345020.

[53] N. D. Birrell and P. C. W. Davies. *Quantum Fields in Curved Space*. Cambridge Monographs on Mathematical Physics. Cambridge, UK: Cambridge Univ. Press, Feb. 1984. ISBN: 978-0-521-27858-4, 978-0-521-27858-4. DOI: 10.1017/CBO9780511622632.

[54] Ted Jacobson. *Introduction to Quantum Fields in Curved Spacetime and the Hawking Effect*. 2004. arXiv: gr-qc/0308048 [gr-qc].

[55] Werner Israel. "Event horizons in static vacuum space-times". In: *Phys. Rev.* 164 (1967), pp. 1776–1779. DOI: 10.1103/PhysRev.164.1776.

[56] C.W. Misner et al. *Gravitation*. Princeton University Press, 2017. ISBN: 9781400889099. URL: https://books.google.co.uk/books?id=zAAuDwAAQBAJ.

[57] Don N. Page. "Particle Emission Rates from a Black Hole. 3. Charged Leptons from a Nonrotating Hole". In: *Phys. Rev. D* 16 (1977), pp. 2402–2411. DOI: 10.1103/PhysRevD.16.2402.

[58] Leonard Susskind. "Trouble for remnants". In: (Jan. 1995). arXiv: hep-th/9501106.

[59] Nima Arkani-Hamed et al. "The String landscape, black holes and gravity as the weakest force". In: *JHEP* 06 (2007), p. 060. DOI: 10.1088/1126-6708/2007/06/060. arXiv: hep-th/0601001.

[60] Ben Heidenreich and Matteo Lotito. "Proving the Weak Gravity Conjecture in Perturbative String Theory, Part I: The Bosonic String". In: (Jan. 2024). arXiv: 2401.14449 [hep-th].

[61] G. W. Gibbons. "Vacuum Polarization and the Spontaneous Loss of Charge by Black Holes". In: *Commun. Math. Phys.* 44 (1975), pp. 245–264. DOI: 10.1007/BF01609829.

[62] George Johnson. "Tunnelling of Charged Particles from Black Holes". In: *JHEP* 03 (2020), p. 038. DOI: 10.1007/JHEP03(2020)038. arXiv: 1911.12379 [hep-th].

[63] Nima Arkani-Hamed et al. "Causality, unitarity, and the weak gravity conjecture". In: *JHEP* 03 (2022), p. 083. DOI: 10.1007/JHEP03(2022)083. arXiv: 2109.13937 [hep-th].

[64] Jens C. Niemeyer and Raphael Bousso. "The Nonlinear evolution of de Sitter space instabilities". In: *Phys. Rev. D* 62 (2000), p. 023503. DOI: 10.1103/PhysRevD.62.023503. arXiv: gr-qc/0004004.

[65] Yoichiro Nambu. "DUALITY AND HADRODYNAMICS". In: *Winter School in Theoretical Particle Physics*. 1986, pp. 573–596.

[66] Tetsuo Goto. "Relativistic quantum mechanics of one-dimensional mechanical continuum and subsidiary condition of dual resonance model". In: *Prog. Theor. Phys.* 46 (1971), pp. 1560–1569. DOI: 10.1143/PTP.46.1560.

[67] Michael B. Green, John H. Schwarz, and Edward Witten. *Superstring Theory Vol. 1: 25th Anniversary Edition*. Cambridge Monographs on Mathematical Physics. Cambridge University Press, Nov. 2012. ISBN: 978-1-139-53477-2, 978-1-107-02911-8. DOI: 10.1017/CBO9781139248563.

[68] Michael B. Green, John H. Schwarz, and Edward Witten. *Superstring Theory Vol. 2: 25th Anniversary Edition*. Cambridge Monographs on Mathematical Physics. Cambridge University Press, Nov. 2012. ISBN: 978-1-139-53478-9, 978-1-107-02913-2. DOI: 10.1017/CBO9781139248570.

[69] Joseph Polchinski. "Tasi lectures on D-branes". In: *Theoretical Advanced Study Institute in Elementary Particle Physics (TASI 96): Fields, Strings, and Duality*. Nov. 1996, pp. 293–356. arXiv: hep-th/9611050.

[70] J. Polchinski. *String theory. Vol. 1: An introduction to the bosonic string*. Cambridge Monographs on Mathematical Physics. Cambridge University Press, Dec. 2007. ISBN: 978-0-511-25227-3, 978-0-521-67227-6, 978-0-521-63303-1. DOI: 10.1017/CBO9780511816079.

[71] J. Polchinski. *String theory. Vol. 2: Superstring theory and beyond*. Cambridge Monographs on Mathematical Physics. Cambridge University Press, Dec. 2007. ISBN: 978-0-511-25228-0, 978-0-521-63304-8, 978-0-521-67228-3. DOI: 10.1017/CBO9780511618123.

[72] Elias Kiritsis. *String Theory in a Nutshell: Second Edition*. USA: Princeton University Press, Apr. 2019. ISBN: 978-0-691-15579-1, 978-0-691-18896-6.

[73] K. Becker, M. Becker, and J. H. Schwarz. *String theory and M-theory: A modern introduction*. Cambridge University Press, Dec. 2006. ISBN: 978-0-511-25486-4, 978-0-521-86069-7, 978-0-511-81608-6. DOI: 10.1017/CBO9780511816086.

[74] Constantin P. Bachas. "Lectures on D-branes". In: *A Newton Institute Euroconference on Duality and Supersymmetric Theories*. June 1998, pp. 414–473. arXiv: hep-th/9806199.

[75] Clifford V. Johnson. "D-brane primer". In: *Theoretical Advanced Study Institute in Elementary Particle Physics (TASI 99): Strings, Branes, and Gravity*. July 2000, pp. 129–350. DOI: 10.1142/9789812799630_0002. arXiv: hep-th/0007170.

[76] David Tong. "String Theory". In: (Jan. 2009). arXiv: 0908.0333 [hep-th].

[77] Horatiu Nastase. *Introduction to the ADS/CFT Correspondence*. Cambridge University Press, Sept. 2015. ISBN: 978-1-107-08585-5, 978-1-316-35530-5.

[78] Joseph Polchinski. "Dirichlet Branes and Ramond-Ramond charges". In: *Phys. Rev. Lett.* 75 (1995), pp. 4724–4727. DOI: 10.1103/PhysRevLett.75.4724. arXiv: hep-th/9510017.

[79] M. Stone. "Semiclassical Methods for Unstable States". In: *Phys. Lett. B* 67 (1977), pp. 186–188. DOI: 10.1016/0370-2693(77)90099-5.

[80] Giovanni Grilli di Cortona et al. "The QCD axion, precisely". In: *JHEP* 01 (2016), p. 034. DOI: 10.1007/JHEP01(2016)034. arXiv: 1511.02867 [hep-ph].

[81] Luca Di Luzio et al. "The landscape of QCD axion models". In: *Phys. Rept.* 870 (2020), pp. 1–117. DOI: 10.1016/j.physrep.2020.06.002. arXiv: 2003.01100 [hep-ph].

[82] Liam McAllister et al. "The Powers of Monodromy". In: *JHEP* 09 (2014), p. 123. DOI: 10.1007/JHEP09(2014)123. arXiv: 1405.3652 [hep-th].

[83] P. Sikivie. "On the Interaction of Magnetic Monopoles With Axionic Domain Walls". In: *Phys. Lett. B* 137 (1984), pp. 353–356. DOI: 10.1016/0370-2693(84)91731-3.

[84] P. Sikivie. "Axions in Astrophysics and Cosmology". In: *Inner Space/ Outer Space: Conference on Physics at the Interface of Astrophysics / Cosmology and Particle Physics*. July 1984.

[85] Lawrence M. Widrow. "The Collapse of Nearly Spherical Domain Walls". In: *Phys. Rev. D* 39 (1989), p. 3576. DOI: 10.1103/PhysRevD.39.3576.

[86] David I. Dunsky and Marius Kongsore. "Primordial black holes from axion domain wall collapse". In: *JHEP* 06 (2024), p. 198. DOI: 10.1007/JHEP06(2024)198. arXiv: 2402.03426 [hep-ph].

[87] Jaume Garriga and Alexander Vilenkin. "Quantum fluctuations on domain walls, strings and vacuum bubbles". In: *Phys. Rev. D* 45 (1992), pp. 3469–3486. DOI: 10.1103/PhysRevD.45.3469.

[88] E. Poisson. *A Relativist's Toolkit: The Mathematics of Black-Hole Mechanics*. Cambridge University Press, 2004. ISBN: 9780521830911. URL: https://books.google.co.uk/books?id=FKg3mAEACAAJ.

[89] R.M. Wald. *General Relativity*. University of Chicago Press, 2010. ISBN: 9780226870373. URL: https://books.google.co.uk/books?id=9S-hzg6-moYC.

[90] T. Padmanabhan. *Gravitation: Foundations and Frontiers*. Cambridge University Press, 2010. ISBN: 9781139485395. URL: https://books.google.co.uk/books?id=BSfe2MjbQ3gC.

[91] T. Needham. *Visual Differential Geometry and Forms: A Mathematical Drama in Five Acts*. Princeton University Press, 2021. ISBN: 9780691203690. URL: https://books.google.co.uk/books?id=L8OQEAAAQBAJ.

[92] M. Spivak. *Calculus On Manifolds: A Modern Approach To Classical Theorems Of Advanced Calculus*. Avalon Publishing, 1965. ISBN: 9780805390216. URL: https://books.google.co.uk/books?id=g_EXJtkz7PYC.

[93] M. Spivak. *A Comprehensive Introduction to Differential Geometry*. A Comprehensive Introduction to Differential Geometry v. 1. Publish or Perish, Incorporated, 1999. ISBN: 9780914098706. URL: https://books.google.co.uk/books?id=ahSWQgAACAAJ.

[94] W. Rudin. *Principles of Mathematical Analysis*. International series in pure and applied mathematics. McGraw-Hill, 1976. ISBN: 9780070856134. URL: https://books.google.co.uk/books?id=kwqzPAAACAAJ.

[95] C.C. Pugh. *Real Mathematical Analysis*. Undergraduate Texts in Mathematics. Springer New York, 2003. ISBN: 9780387952970. URL: https://books.google.co.uk/books?id=R_ZetzxFHVwC.

[96] Sidney R. Coleman and Frank De Luccia. "Gravitational Effects on and of Vacuum Decay". In: *Phys. Rev. D* 21 (1980), p. 3305. DOI: 10.1103/PhysRevD.21.3305.

[97] Djuna Croon. "TASI lectures on Phase Transitions, Baryogenesis, and Gravitational Waves". In: *PoS* TASI2022 (2024), p. 003. DOI: 10.22323/1.439.0003. arXiv: 2307.00068 [hep-ph].

[98] J. Antoniadis et al. "The International Pulsar Timing Array second data release: Search for an isotropic gravitational wave background". In: *Mon. Not. Roy. Astron. Soc.* 510.4 (2022), pp. 4873–4887. DOI: 10.1093/mnras/stab3418. arXiv: 2201.03980 [astro-ph.HE].

[99] B. P. Abbott et al. "GW150914: The Advanced LIGO Detectors in the Era of First Discoveries". In: *Phys. Rev. Lett.* 116.13 (2016), p. 131103. DOI: 10.1103/PhysRevLett.116.131103. arXiv: 1602.03838 [gr-qc].

[100] T. Accadia et al. "Status of the Virgo project". In: *Class. Quant. Grav.* 28 (2011). Ed. by Donald Marolf and Daniel Sudarsky, p. 114002. DOI: 10.1088/0264-9381/28/11/114002.

[101] J. Aasi et al. "Advanced LIGO". In: *Class. Quant. Grav.* 32 (2015), p. 074001. DOI: 10.1088/0264-9381/32/7/074001. arXiv: 1411.4547 [gr-qc].

[102] Pau Amaro-Seoane et al. "Laser Interferometer Space Antenna". In: (Feb. 2017). arXiv: 1702.00786 [astro-ph.IM].

[103] L. Badurina et al. "AION: An Atom Interferometer Observatory and Network". In: *JCAP* 05 (2020), p. 011. DOI: 10.1088/1475-7516/2020/05/011. arXiv: 1911.11755 [astro-ph.CO].

[104] Peter W. Graham et al. "Mid-band gravitational wave detection with precision atomic sensors". In: (Nov. 2017). arXiv: 1711.02225 [astro-ph.IM].

[105] Mahiro Abe et al. "Matter-wave Atomic Gradiometer Interferometric Sensor (MAGIS-100)". In: *Quantum Sci. Technol.* 6.4 (2021), p. 044003. DOI: 10.1088/2058-9565/abf719. arXiv: 2104.02835 [physics.atom-ph].

[106] Zhong-Chao Wu. "Gravitational Effects in Bubble Collisions". In: *Phys. Rev. D* 28 (1983), pp. 1898–1906. DOI: 10.1103/PhysRevD.28.1898.

[107] S. W. Hawking, I. G. Moss, and J. M. Stewart. "Bubble Collisions in the Very Early Universe". In: *Phys. Rev. D* 26 (1982), p. 2681. DOI: 10.1103/PhysRevD.26.2681.

[108] Hidekazu Nariai. "On some static solutions of Einstein's gravitational field equations in a spherically symmetric case". In: *Sci. Rep. Tohoku Univ. Eighth Ser.* 34 (Jan. 1950), p. 160.

[109] Hidekazu Nariai. "On a New Cosmological Solution of Einstein's Field Equations of Gravitation". In: *General Relativity and Gravitation* 31 (1951), pp. 963–971. URL: https://api.semanticscholar.org/CorpusID:116125316.

[110] F. R. Tangherlini. "Schwarzschild field in n dimensions and the dimensionality of space problem". In: *Nuovo Cim.* 27 (1963), pp. 636–651. DOI: 10.1007/BF02784569.

[111] Oscar J. C. Dias and Jose' P. S. Lemos. "Pair creation of higher dimensional black holes on a de Sitter background". In: *Phys. Rev. D* 70 (2004), p. 124023. DOI: 10.1103/PhysRevD.70.124023. arXiv: hep-th/0410279.

[112] Robert C. Myers and M. J. Perry. "Black Holes in Higher Dimensional Space-Times". In: *Annals Phys.* 172 (1986), p. 304. DOI: 10.1016/0003-4916(86)90186-7.

[113] Dumitru Astefanesei, Robert B. Mann, and Eugen Radu. "Reissner-Nordstrom-de Sitter black hole, planar coordinates and dS / CFT". In: *JHEP* 01 (2004), p. 029. DOI: 10.1088/1126-6708/2004/01/029. arXiv: hep-th/0310273.